DESIGN OF FLUORESCENT PROBES FOR BIOORTHOGONAL LABELING OF CARBONYLATION IN LIVE CANCER CELLS

by
Hazel Erkan

Submitted to Graduate School of Natural and Applied Sciences
in Partial Fulfillment of the Requirements
for the Degree of Master of Science in
Biotechnology

Yeditepe University
2018

DESIGN OF FLUORESCENT PROBES FOR BIOORTHOGONAL LABELING OF CARBONYLATION IN LIVE CANCER CELLS

APPROVED BY:

Prof. Dr. Dilek Telci
(Thesis Supervisor) .....

Assoc. Prof. Dr. Özlem Dilek
(Thesis Co-supervisor) .....

Assoc. Prof. Dr. Damla Arısan .....

Assoc. Prof. Dr. Mustafa Güzel .....

Assist. Prof. Dr. Hüseyin Çimen .....

DATE OF APPROVAL: ..../..../2018

ACKNOWLEDGEMENTS

First of all, I would like to thank to my supervisors Assoc. Dr. Özlem Dilek and Prof. Dr. Dilek Telci for their support, encouragement and giving a chance to be part of their team throughout my master period. They helped me in every trouble I have faced during experimental and writing phase of my thesis.

I am also grateful to work at COST CM1004 and TUBITAK 3501 project (project no: 113s812) entitled as "Design of Azacoumarin Based Bioorthogonal Fluorescent Probe For Bioorthogonal Click Chemistry In Live Cancer Cells' Under the supervision of Assoc. Dr. Özlem Dilek in collaboration with Prof. Dr. Dilek Telci, which was given me time management and team work skills.

Furthermore, I am deeply grateful to Assist. Prof. Dr. Hüseyin Çimen for his permission to use his laboratory facilities.

I am so thankful my research group İnci Kurt Celep, Halime İlhan Sığınç, Zeynep Bolat, Hande Nayman, Ece Nezir and Kaan Öztürk and to my dear friends Cansu Atılgan, Zeynep Dalar, Fulya Cankurt and Tutku Aksoy for their understanding and assistance during my thesis and for their endless support and patience during my master period.

Lastly but most importantly, this thesis would not have been possible without the loving support of my dear parents Songül Erkan and Ali Rıza Erkan and my sister Hande Erkan and my brother Barış Erkan. I owe my profound gratitude to my family for their endless encouragement, patience and unconditional love. Without their encouragement and understanding it would have been impossible for me to be here.

ABSTRACT

DESIGN OF FLUORESCENT PROBES FOR BIOORTHOGONAL LABELING OF CARBONYLATION IN LIVE CANCER CELLS

Oxidative stress is known as the steady state level of oxidative damage in live cell, tissue, or organ, caused by the reactive oxygen species (ROS) such as free radicals. Along with neurodegenerative diseases and diabetes, high levels of reactive oxygen species have been noticed in almost all cancers, where they promote many aspects of tumor development and progression. Bioorthogonal labeling of oxidative stress-induced carbonylation of biomolecules have a critical role in the identification of cancer aggressiveness. Hydrazine or amine-based fluorophores act as strong nucleophiles that react rapidly with carbonyl sections in live cells. In this study, hydrazine and amine derivatives were synthesized in order to detect ROS induced protein carbonylation in various cancer cell lines. 2-Hydrazine-5-nitrophenol was utilized as a novel bioorthogonal fluorescent probes to demonstrate labeling of carbonylated biomolecules. Reaction between carbonyl group and hydrazine containing fluorophore yielded in hydrazone which maintained a spectroscopic alteration. Microscopic and fluorometric analyses were used to distinguish the exogenous and endogenous ROS induced carbonylation profile in A498 primary site and ACHN metastatic site renal cell carcinoma (RRC) cell lines. When cells were treated with H_2O_2 as an exogenous ROS inducer, A498 cell line demonstrated higher carbonylation level. On the other hand, serum starvation as an endogenous ROS inducer resulted in higher carbonylation level in ACHN metastatic site RCC cell line. The probe developed here may be used as a small molecule in the development of new diagnostics approach in the molecular staging of cancer.

ÖZET

CANLI KANSER HÜCRELERINDE KARBONILASYON İŞARETLENMESİ İÇİN BİYOORTOGONAL FLORESAN PROBE SENTEZİ

Oksidatif stres, reaktif oksijen türlerinin canlı hücreler, dokular ve organlarda oluşturduğu hasar olarak bilinir. Nörodejeneratif hastalıklar ve diyabetle birlikte, tümör gelişim ve ilerlemesine neden olan serbest radikaller hemen hemen tüm kanser türlerinde yüksek düzeyde bulunmaktadır. Reaktif oksijen türleri kanser hücrelerinde çoğalma, gelişim ve ölüm gibi durumları kontrol eder, bu nedenle serbest radikallerin özgün hedef olarak kullanılması kanser hücrelerinin ölümünü tetikleyebilir. Bu tezde, oksidatif stresse bağlı gelişen protein karbonilasyonunun, hücre içerisine verilen özgün biyoortogonal floresan moleküller ile görüntülenmesi amaçlanmıştır.

Oksidatif stres sonucu biyomoleküllerde oluşan karbonilasyonun, biyoortogonal işaretlenmesi, kanserin agresifliğinin belirlenmesinde önemli bir yere sahiptir. Bu bağlamda sentezlenen hidrazin ve amin bazlı moleküllülerin spektroskopik özellikleri karakterize edilmiştir. Nükleofilik yapıları nedeniyle hidrazin veya amin bazlı floroforlar, canlı hücrelerde bulunan karbonil gruplar ile hızlı hydrazone veya imin reaksiyonu gerçekleştirirler ve bu reaksiyon hızı, kanser hücre hatlarına göre farklılık göstermektedir. Buna bağlı olarak hidrazin bazlı 2-Hidrazin 5-Nitrofenol molekülünün karbonil gruplar ile reaksiyona girmesiyle spektroskopik değişime uğrayarak hidrazon oluşturur. Bu çalışmada, oksidatif stres düzeyine bağlı olarak hücre içerisinde değişiklik gösteren floresan yoğunluk miktarları, ACHN ve A498 kanser hücre hatlarının metastatik özelliklerinin ayırt edilmesinde kullanılmıştır. Hücrelerde oksidatif stres H_2O_2 ile indüklendiğinde, A498 hücresinde ACHN hücresine kıyasla daha fazla protein karbonilasyonu gerçekleştiği tespit edilmiştir. Diğer yandan, hücreler serum açlığına sokularak oksidatif stres uyarıldığında protein karbonilasyonu seviyesinin metastatik ACHN hücrelerinde daha yüksek olduğu bulunmuştur. Tez kapsamına geliştirilen 2-Hidrazin 5-Nitrofenol molekülü kanserin tespitinde ve kanserin moleküler evrelerinin belirlenmesinde kullanılabilecek belirteç boya niteliği taşımaktadır.

TABLE OF CONTENTS

LIST OF FIGURES

LIST OF TABLES

LIST OF SYMBOLS/ABBREVIATIONS

Cu(I)	Copper (I) salt
2Hzin5np	2-Hydrazine-5-nitrophenol HCl
AcOH	Acetic acid
BSA	Bovine serum albumin
c-MET	Mesenchymal-epithelial transition factor
DCFH-DA	2',7' – dichlorofluorescein diacetate
EAA	Ethyl acetoacetate
EGFR	epidermal growth factor receptor
ETC	Electron transport chain
EtOAc	Ethyl acetate
EtOH	Ethanol
GLUT	Glucose transporters
Hex	Hexane
HGF	Hepatocyte growth factor receptor
HRE	Hypoxia-response elements
LC	Liquid chromatography
MeOH	Methanol
MS	Mass spectrometry
OCT	Cyclooctyne
PMSF	Phenylmethylsulphonyl fluoride
ROS	Reactive oxygen species
SAL	Salicylaldehyde
TFA	Trifluoroacetic acid
TGF-a	Transforming growth factor alpha
VEGF	Vascular endothelial growth factor

1. INTRODUCTION

1.1. BIOORTHOGONAL CHEMISTRY

Chemical probes have been used for site-specific biomolecule labeling in order to clarify molecular mechanisms of biological systems. Bioconjugational strategies are based on selectively attachment of one chemical probe to a biological molecule with covalent bond in appropriate conditions. With an understanding of the concepts of bioorthogonal chemistry, these molecules' ligation should generate new complex molecules which have different chemical and biological properties from its constituent molecules. Bioorthogonal reactions are fast and selective ligation under biological conditions have found comprehensive applications in the development of new bioconjugational strategies [1].

Todays, many alternative bioconjugational techniques have been utilized for elucidating the functions and dynamics of biomolecules in live systems such as antibodies and fluorescent fusion proteins. However, usage of these tools has some limitations for biomolecule labeling. Especially, large molecular size of fusion proteins or low cell membrane permeability of antibodies cause restriction with studying of these biomolecules. In addition, fusion proteins are not interpretable to examination for non-protein biomolecules just as carbohydrates, lipids and other small molecule metabolites. Because of these limitations as shown in Table 1.1, studies of bioorthogonal chemistry have been accelerated in last century [2, 3].

Table 1.1. Comparison of fluorescent fusion proteins and chemical fluorescent probes [4].

Properties	**Fluorescent Fusion Proteins**	**Chemical Fluorescent Probes**
Molecular size	Large	Small
Transgene Expression	Essential	Nonessential
Labeling time	During Translation	Any Time
Labeling position	Basically C/N-Terminus	Reactive Chemical Reporters or C/N-Terminus
Labeling efficiency	High	Case Dependent
Labeling variety	Narrow	Wide

Bioorthogonal click chemistry can be applied with two-step strategy when it is used on biomolecules. The first step is placement of an appropriate chemical reporter that is an affinity tag on biomolecule. Then, the second step is the ligation between the chemical reporter and site-specific bioorthogonal probe via biochemical reactions in living biosystems as shown in Figure 1.1 (a). This covalent ligation must be stable, site-specific and non-toxic in aqueous environments. Another strategy of click chemistry is based on bioorthogonal reaction activated fluorescence probe. Incorporation between biomolecule and probe produce successful labeling as shown in Figure 1.1 (b). Another application of bioorthogonal chemistry is based on the reaction between target biomolecule and bioorthogonal probe which is enriched with a drug as a cargo molecule. The cargo molecule is released for targeted drug delivery as shown in Figure 1.1 (c) [5].

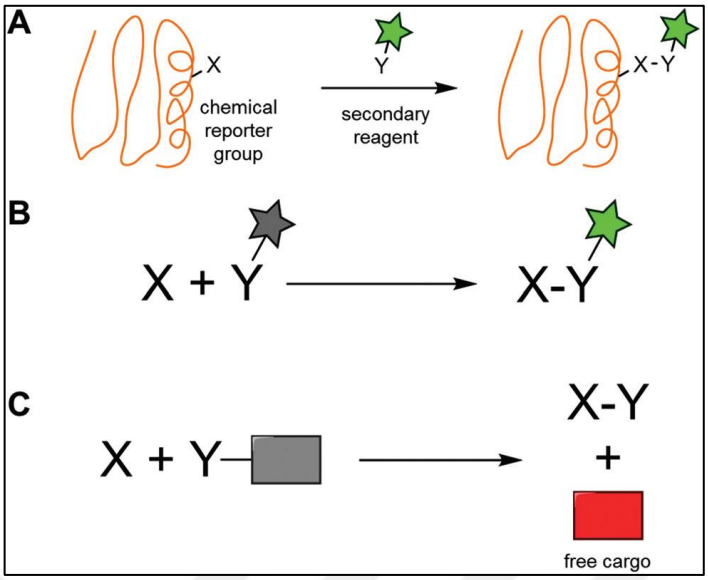

Figure 1.1. Strategies of bioorthogonal labeling. (a) site-specific labeling of chemical reporter tagged biomolecule, (b) bioorthogonal reaction activated turn-on fluorescent probe, (c) bioorthogonal probe as a cargo molecule container [5].

The bioorthogonal reactions can be categorized depending on their ligation systems such as click reaction, photo-click reactions, tetrazine ligation and Staudinger-Bertozzi ligation which are utilized for site-specific labeling and selectivity of biomolecules [6].

1.1.1. Click Reactions

Click reaction requires acceptable unsaturated carbon and hydrogen moieties on reactant and target molecules [7]. The first click reaction was introduced by Huisgen with the design of cycloaddition reactions [8]. Azide – alkyne reactions are milestone of click reactions in bioorthogonal chemistry. Azide is a small, non-polar reactive structure with weak hydrogen bonds. Azides have been used to modify the biomolecules like glycans, proteins, lipids or nucleic acids. Correspondingly, alkyne is an unsaturated hydrocarbon containing non-biological molecule which is used for biomolecule labeling. Reaction between azide and alkyne, the azide electron pairs are delocalized and a stable triazole is formed as a fluorescent chemical reporter in bioorthogonal labeling [9].

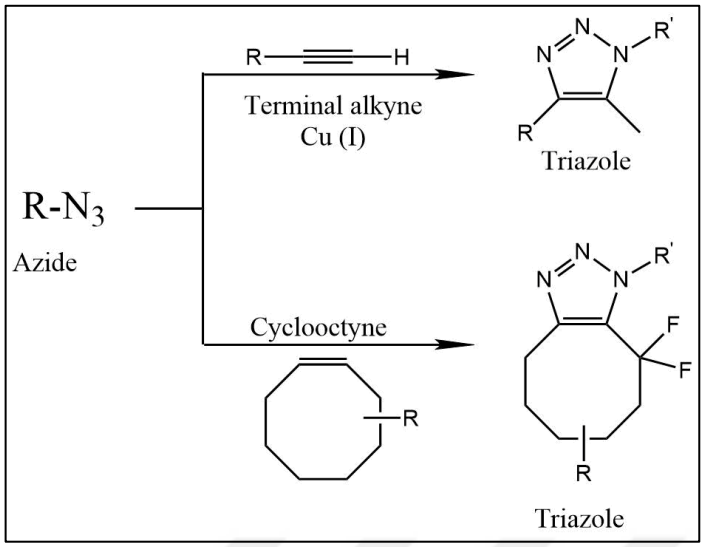

Figure 1.2. Click reactions. (a) copper-catalyzed cycloaddition reaction, (b) strain-promoted cycloaddition reaction [10].

Cycloaddition of azide and alkynes reactions are the most common click reactions for biomolecule labeling because of their kinetic stability [4]. Copper-catalyzed and strain-promoted cycloaddition reactions create the baseline of click reactions as shown in Figure 1.2.

1.1.1.1. Copper – Catalyzed Azide-Alkyne Cycloaddition Reaction (CUAAC)

Azide-Alkyne cycloaddition is highly selective reaction for bioorthogonal live cell labeling. Azide compounds do not exist in biological systems so its incorporation between biomolecules is site specific. Because of high stability and no cytotoxicity effect, azide is preferred for bio-imaging. The most popular azide-alkyne copper catalyzed cycloaddition reactions were introduced by Sharpless [11] and Meldal [12]. When the regioselective reaction between azide and alkyne is catalyzed with Copper (I) salt, 1,4 disubstituted 1,2,3 triazoles is yielded with 6-7 times faster the reaction rate than without Cu(I) catalysis [13]. Cu(III) metallacycle intermediate is a reaction rate accelerator which is formed by the reaction between copper acetylide activated alkyne and azide as shown in Figure 1.3 [14]. With the formation of triazole, bioorthogonal chemical reporter is quenched and fluorescence is emitted.

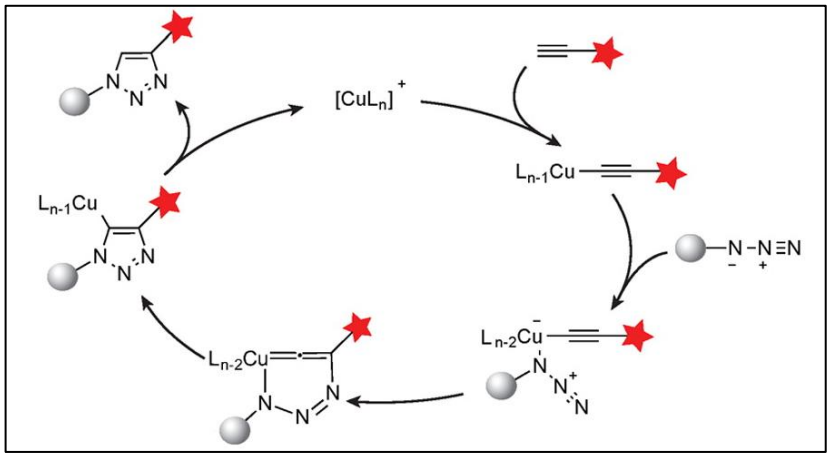

Figure 1.3. Mechanism of CUAAC [15].

CUAAC is one of the most popular click reaction due to accelerated reaction rate in live cell imaging. However, the main limitation of this reaction is cytotoxicity of Cu (I) salt in living systems. Presence of Cu (I) salt leads to metal-induced oxidative stress via reactive oxygen species generation in live cells [16]. In order to eliminate the cytotoxic effect, water soluble ligands are designed for labeling of cell surface [17, 18] also, azide groups are modified with addition of copper-chelating moiety on the biomolecules [19, 20].

1.1.1.2. Strain – Promoted Azide-Alkyne Cycloaddition Reaction (SPAAC)

Because of toxic effect of copper catalyzed azide-alkyne cycloaddition reaction, catalyst free reactions have been demonstrated in 2004. Bertozzi group demonstrated a bioorthogonal reaction between azide and cyclooctyne (OCT) which is alkyne introduced strain structure [21]. Different derivatives of cyclooctyne and azine groups have enriched the click reactions while reaction rate is also increased, and cytotoxicity effects are diminished. For example, difluoro cyclooctyne (DIFO) reaction with benzyl azide gives 63-fold increase in reaction rate [22].

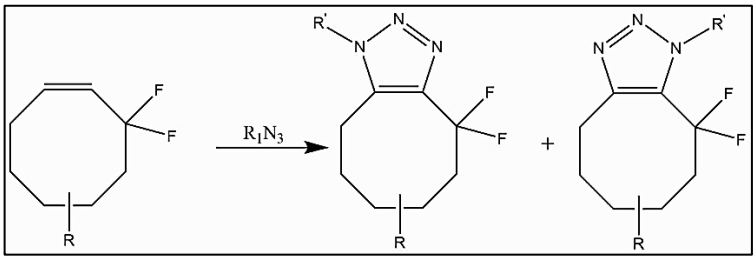

Figure 1.4. Illustration of DIFO-azide cycloaddition.

Release of the free energy in C≡C−C bonds encourages the reaction between azide and alkyne without catalyst [2]. In addition, delocalization of azide nitrogen into the triazole alkyne induces the incorporation between chemical reporter and fluorescent probe [5]. Design and synthesis of azide probes can derivate with the usage of different fluorophores. Azidocoumarin is one of the first smart fluorescent azido probes which is described by Wang group in 2004. In that study, the researcher demonstrated that the click reaction was completed in mild conditions at pH:7 in PBS with high fluorescence intensity [23]. In biological applications, azidocoumarin is one of the common bioorthogonal probes for site-specific biotarget labeling in vitro and in vivo because of its water solubility and cell permeability [24, 25]. Organic and biological chemists have maintained to develop novel scaffolds which are modified with azide functional group as shown in Figure 1.5 for instance, 1,8-naphthalimide [26], carbazole [27], benzothiazole [28], and BODIPY [29].

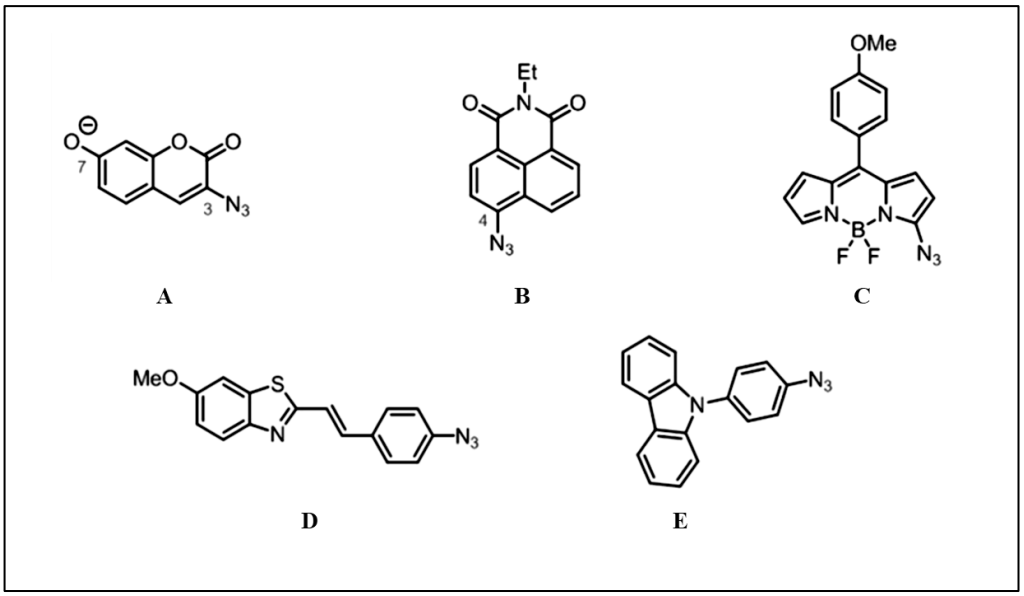

Figure 1.5. Azide containing scaffolds (a) Azidocoumarin, (b) Naphthylamide, (c) BODIPY, (d) Benzothiazole, (e) Carbazole [5].

1.1.2. Photo – Click Reaction

Photo-click reactions are performed for site-specific and spatiotemporal biomolecule labeling. Although the first photo-click cycloaddition strategies have been developed by Huisgen et al [30], the first biological application of 1,3-dipolar cycloaddition reaction has been introduced by Lin and coworkers in order to apply in systems. The fluorogenic pyrazoline is obtained by incorporation between alkene and nitrile imine which is an intermediate product from photoactivation of diaryl tetrazole by ultraviolet (UV) light at 302 nm as shown in Figure 1.6. Only N_2 is exposed as a byproduct of the reaction [9]. Besides, photoactivated azirine is yielded nitrile ylide which can conjugate with PEG modified lysosome [31].

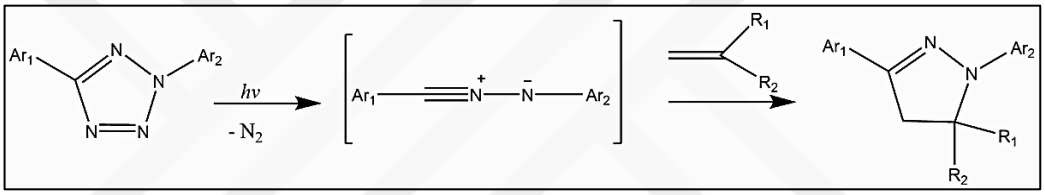

Figure 1.6. Photo induced click reaction.

The main limitation of photo-click reaction is phototoxicity of UV light in biological systems. Lin and coworkers alternate the tetrazole scaffold with substations of oligothiophene which is photoinducible at 405 nm [32]. In addition, naphthalene contained tetrazole has been designed as a fluorescent probe which is activated at 700 nm laser light in order to diminish photocytotoxicity of UV light in vivo imaging [33].

1.1.3. Tetrazine Ligation

Reaction between electron-poor tetrazine and electron-rich alkyne or strained alkene is called inverse electron-demand Diels – Alder reaction. Cycloaddition reaction between tetrazine and trans-cyclooctyne (TCO) is yielded with fluorogenic dihydropyridazine and nitrogen gas as only byproduct as shown in Figure 1.7 (a) [34, 35]. Second-order rate of tetrazine ligation is higher than 10^4 $M^{-1}s^{-1}$, so inverse electron-demand Diels – Alder reactions are faster than SPAAC and photo-click reactions. Reactivity and selectivity of tetrazine depend on substitutions of the tetrazine scaffold. Monosubstitutions of tetrazine

with aryl and H groups either increase its reactivity or decrease its stability in the presence of water. In order to eliminate this limitation, the tetrazine is substituted with electron donating groups like 2-pyridyl to maintain high stability and reactivity of tetrazine for bioconjugational labeling in biological systems [36].

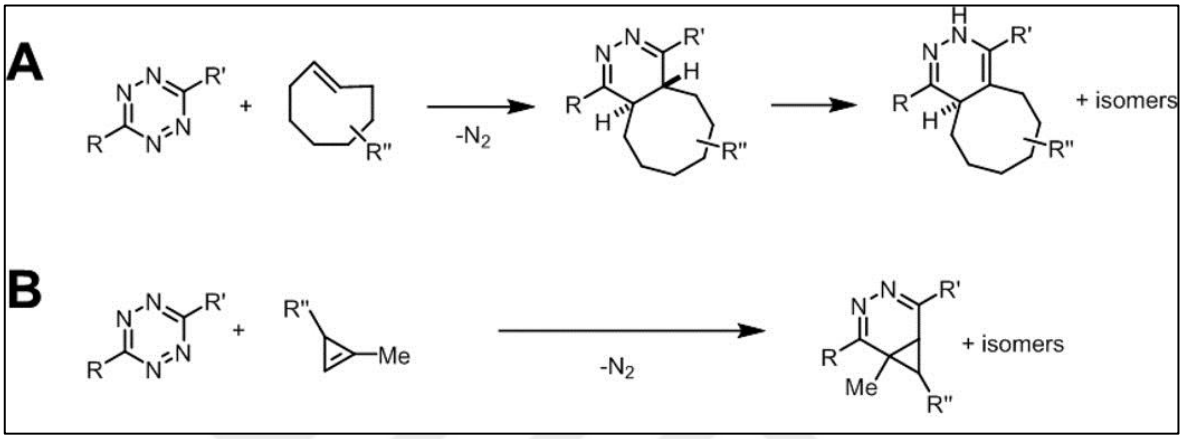

Figure 1.7. Tetrazine reaction [5].

Devaraj's and Prescher's research groups demonstrated that tetrazine could react with cyclopropene which is small strained alkene as shown in Figure 1.7 (b) [37, 38]. With the help of small cyclopropene structure, it has an advantage of application and labeling of mammalian cells and eukaryotes [39], especially labeling of nucleic acids [40] and cell surface glycan [41].

1.1.4. Staudinger – Bertozzi Ligation

Most of the bioorthogonal reactions had been derived from classical organic chemistry which were discovered before their biological applications were accomplished. Staudinger ligation is also one of these organic reactions which is rely on Staudinger reduction of azide with triphenylphosphine. In 1919, Staudinger and co-workers demonstrated that electrophilic nitrogen of azide is reduced by nucleophilic phosphorus atom that leads to formation of an aza-ylide intermediate by molecular nitrogen ejection. Following of the reaction the intermediate is hydrolyzed to primary imine and phosphine oxide under aqueous condition as shown in Figure 1.8 (a) [42].

In 2000, Bertozzi and co-workers modified the Staudinger Reduction to Staudinger Ligation. An electrophilic ester carbonyl group is introduced to phosphine to form stable amide bond after hydrolysis of five-membered ring intermediate as shown in Figure 1.8 (b) [43, 44].

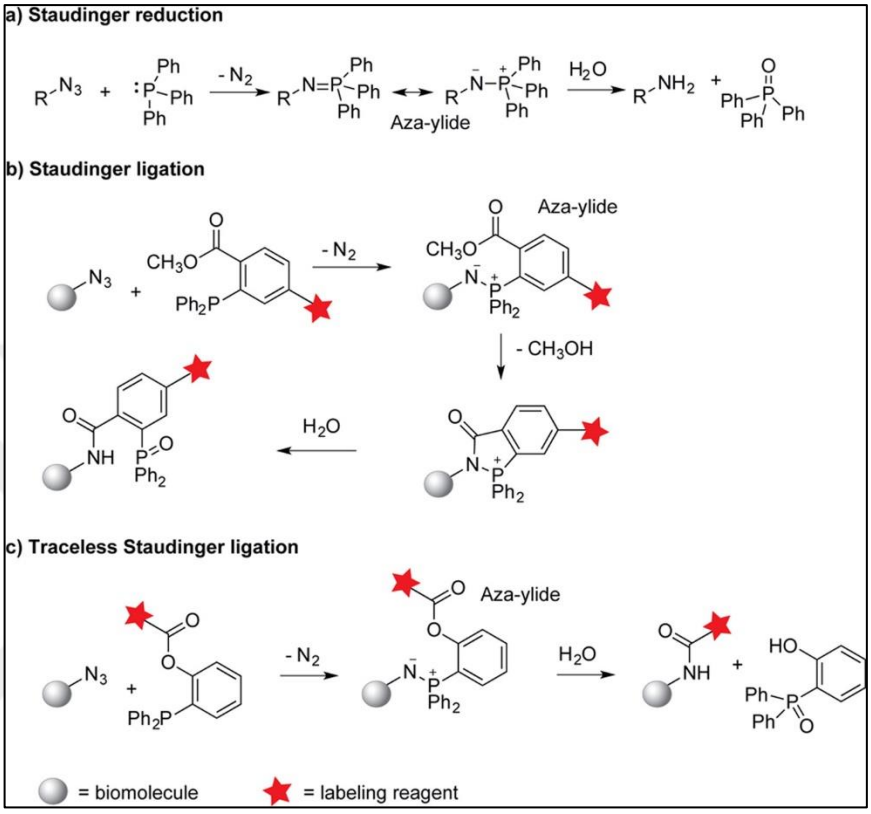

Figure 1.8. Reaction mechanism of staudinger ligation. (a) Staudinger reduction, (b) Staudinger ligation, (c) Traceless staudinger ligation [15]

After a few months from initial Staudinger ligation publish, Bertozzi and Raines research groups simultaneously advanced the Staudinger ligation to 'Traceless Staudinger Ligation' via modification within tagging a cleavable acyl group on phosphide. Hydrolysis of intermedia aza-ylide is yielded in a stable amide-bonded product which conjugates target and chemical reporter and phosphine oxide moiety as a byproduct as shown in Figure 1.8 (c) [45, 46].

Staudinger reactions do not have byproduct toxicity and catalyst requirement for biological application. In addition, Staudinger ligation has high chemoselectivity between biomolecule target and chemical reagent that expands its usage capabilities *in vitro* and *in vivo* [47]. Applications of Staudinger ligation have two main limitations for bioorthogonal chemistry. First of them is low second-order-reaction rate in 10^{-3} M^{-1} s^{-1} even in the presence of high

target and reagent concentrations [43]. The second limitation is non-specific phosphine oxidation. Either increasing in nucleophilicity of phosphine reagent [48] or designing fluorescence resonance energy transfer (FRET)-based phosphine probes [49] are applied to eliminate undesired phosphine oxidation. Another limitation of Staudinger ligation is Phosphines reactivity on proteinogenic disulfide bonds, so its usage in cell surface labeling is the best bioorthogonal application of Staudinger ligation [50].

1.1.5. Transition Metal – Catalyzed Reaction

The key reactions of transition-metal catalyzed bioorthogonal chemistry can be listed as olefin metathesis, Suzuki-Miyaura reaction and Sonogashira reaction. These reactions are responsible from new C-C bond formation under biological conditions and become new affordable approaches as chemical protein modifications especially designing unnatural amino acids for bioorthogonal labeling strategies [51]. Olefin metathesis is based on forming C-C bond by deconstruction of alkenes. In 2008, Davis and co-workers introduced an allyl sulfide group on cysteine under catalysis of Ruthenium as metal catalyzed as shown in Figure1.9 [52].

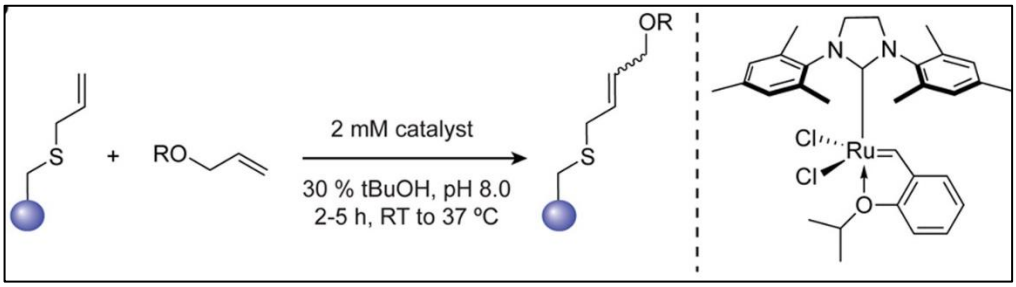

Figure 1.9. Olefin metathesis [15].

Suzuki-Miyaura and Sonogashira reactions are Palladium-catalyzed coupling reactions which are commonly used in bioorthogonal labeling. The Suzuki-Miyaura reaction is achieved in presence of iodophenyl group and Pd catalyst [53]. The first study was reported in 2006 by Yokoyama and co-workers, the researchers demonstrated the usage of Pd-TPPTS (Palladium-2-triphenylphosphine-3,3,3-trisulfonate) as a catalyst for labeling of iodophenyl alanine amino acid modified Ras protein [54]. In 2009, Davis research group established a water soluble complex that includes Pd catalyst and 2-amino-4,6-dihydroxypyrimidine sodium salt [$Pd(OAc)_2(ADHP)_2$] for ligation of iodobenzyl group and boronic acid under

biological conditions as shown in Figure 1.10 [55]. The Sonogashira reaction was developed for incorporation between alkyne group labeled proteins and iodophenyl chemical probes in de presence of Pd catalysis [56].

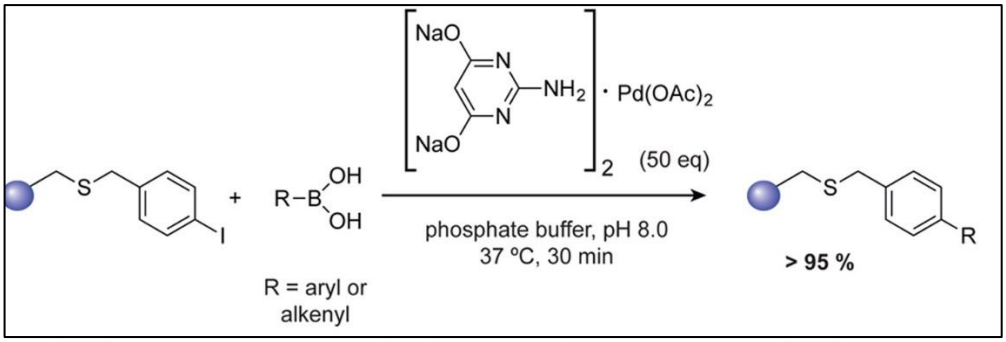

Figure 1.10. Palladium (Pd)-catalyzed cross-coupling reaction [15].

1.1.6. Aldehyde/Ketone – Hydrazide/Alkoxyamine Pair

Aldehyde and ketone groups are the most common chemical reporters in bioorthogonal labeling. Chemoselective and reversible reactions between aldehyde/ketone (carbonyl functional group) and hydrazide/alkoxyamine (α-effect amine) provide stable hydrazone or oxime product [57]. Under acidic conditions (pH 4-6), protonated carbonyl groups react with primary and secondary amine-based nucleophiles to form carbinolamine intermediate that is dehydrated into imine, oxime or hydrazone adducts as a reversible Schiff base as shown in Figure 1.11 (a) [58]. In 1986, Rideout and co-workers firstly demonstrated a drug combined aldehyde/hydrazide reaction in cancer cells [59]. Hydrazine-based fluorophores quench fluorescence by intramolecular charge transfer mechanism [60]. Different scaffolds as coumarins, BODIPYs can composed with hydrazine moiety to develop fluorescence probe derivatives for usage in bioorthogonal labeling strategies [61, 62]. Small size of aldehyde and ketones can furnish easy incorporation into target biomolecules via biosynthesis mechanisms such as periodate oxidation of exogenous membranes [63] or enzymatic oxidation of endogenous membranes in living systems [64]. The reaction between ketone and hydrazide form hydrazone linkage that is more stable than the linkage between aldehyde and hydrazide. On the other hand, aldehyde condensation is faster than ketone condensation with hydrazide [65]. In additionally, double bond of imine linkage between aldehyde and amine can be reduced by cyanoborohydride to form more stable covalent bonding [66]. Even

though, aldehyde/ketone condensation is a favorable bioorthogonal labeling strategy, it has also three main application restrictions on living systems. First of all, requirement of acidic condition limits targeting the endogenous biomolecules, so the reaction is notably appropriate for cell surface or extracellular membrane labeling [67, 68]. Another limitation is that the formation of carbinolamine intermediate play a role for reaction rate limiting step to cause slow kinetics and low reaction rate in the range of 10^{-5}-10^{-4} M^{-1} s^{-1} [59, 69]. With the participation of nucleophilic catalysts into the formation of hydrazone and imine, the limitations as low reaction rate and slow kinetics are eliminated. In 2006, Dawson and co-workers introduced an oxime reaction which is catalyzed with aniline [70, 71] and the research group demonstrated the second order reaction rate constants as 170 M^{-1} s^{-1} for hydrazone formation and 8.2 M^{-1} s^{-1} for oxime formation as shown in Figure 1.11 (b) [72]. So far, derivatives of aniline as nucleophilic catalyst of hydrazone - oxime reaction were introduced. For instance, 4-aminophenylalanine (4a-Phe) and m-phenylenediamine (m-PDA) were investigated to alternate the aldehyde and ketone condensation catalysts which are also water soluble and have higher an increase in reaction rate than aniline [73, 74].

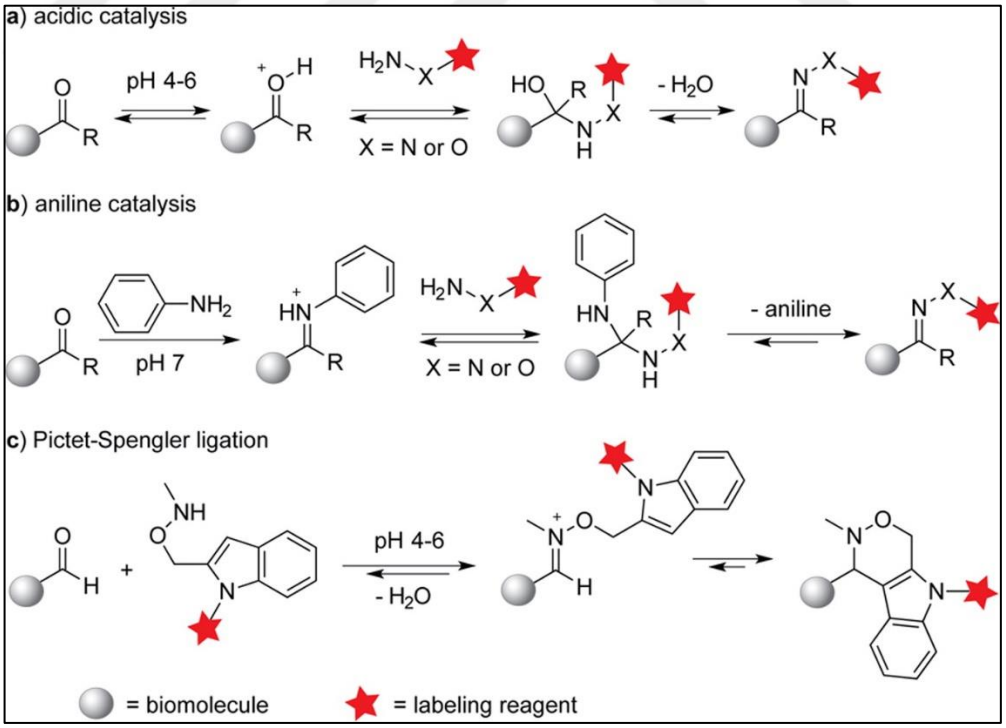

Figure 1.11. Reaction mechanism between aldehyde/ketone and hydrazine/alkoxyamine. (a) acid-catalyzed reaction, (b) aniline-catalyzed reaction, (c) pictet-spengler ligation [15].

The third limitation factor is abundancy of carbonyl-containing endogenous metabolites like pyruvate, oxaloacetate and glucose. Intracellular aldehydes and ketones can react with hydrazide/alkoxyamine. This undesired cross-reaction obstructs the aldehyde/ketone condensation-based bioorthogonal labeling in living systems [2]. Bertozzi and co-workers developed a different aldehyde-ketone condensation variant which is based on Pictet-Spengler Reaction. The Pictet-Spengler ligation authorize the reaction between aldehyde and tryptamine at 10.5-0.26 M^{-1} s^{-1} reaction rate under range of 4.5-7 pH [75]. The reaction between carbonyl-tagged biomolecule and tryptamine yields in intermediate oxyiminium ion which forms oxacarboline product by the nucleophilic attraction of indole moiety as shown in Figure 1.11 (c). The reaction can be modified like Hydrazino-Pictet-Spengler ligation that provide usage in antibody-drug ligation strategies [76].

1.2. APPLICATIONS OF BIOORTHOGONAL CHEMISTRY

1.2.1. Protein Labeling

Bioorthogonal chemistry is an excellent approach to clarify the questions about protein chemistry, localization, dynamics, activation and protein-protein interaction in living systems. The target proteins are incorporated with unnatural amino acids via translational mechanism of central dogma. In addition, post-translational modifications also play an influential role for chemical reporter tagging into proteins. The concept of residue-specific incorporation predicates on introduction of unnatural amino acid via translational machinery. In 2003, Tirrell and co-workers demonstrated that unnatural amino acids are incorporated by natural amino acid specific aminoacyl-tRNA synthetase (AARS) to target protein as shown in Figure1.12 (a) [77]. Auxotrophic bacterial strains are responsible from synthesis of unnatural amino acid synthesis. Methionine and phenylalanine analogues which are modified with chemical reporters as azide, alkyne or carbonyl group, synthesized by auxotrophic E. Coli with the mutant methionyl-tRNA synthetase and phenylalanyl-tRNA synthetase [78, 79]. In order to prevent competition between natural and unnatural amino acid synthesis, auxotrophic bacteria require minimal medium which is lack of natural amino acid [80]. Residue-specific protein labeling permits multiple site conjugation to a chemical

reporter bearing unnatural amino acid. Although, a genetical modification is not required, proteins are manipulated with their chemical and physical properties [81].

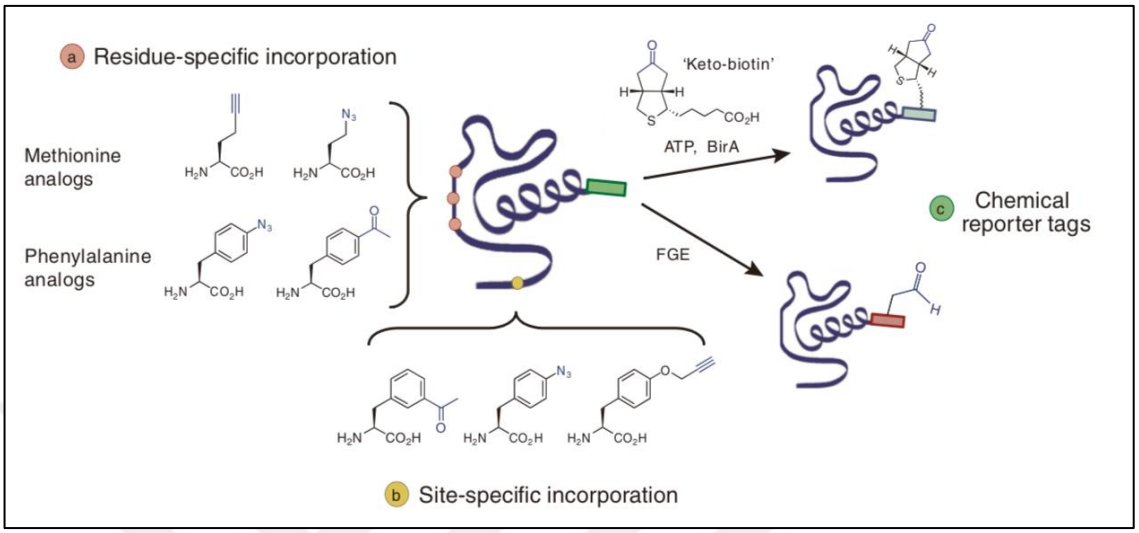

Figure 1.12. Methods of protein labeling. (a) residue specific incorporation, (b) site specific incorporation, (c) chemical reporter tag incorporation. Adapted from Ref. [80].

Site-specific incorporation allows a genetic code expansion for introduction of an unnatural amino acid into only one position of target protein as shown in Figure 1.12 (b). In 2004, Shultz and co-workers demonstrate that the unnatural amino acid is introduced to amber suppressor tRNA via aminoacyl tRNA synthetase. The mutant tRNA is conjugated to nonsense UAG amber codon on mRNA which codes the target protein. When translation is completed, unnatural amino acid is introduced site-specifically to the amino acid chain as shown in Figure1.13 [82].

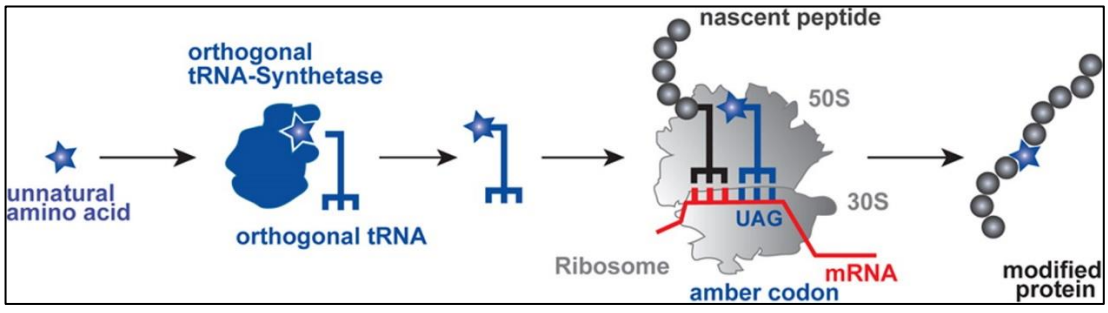

Figure 1.13. Genetic code expansion for site-specific incorporation [15].

The concept of site-specific incorporation has a field-wide application to bioorthogonal protein labeling in both bacterial [83, 84] and mammalian live cells [85, 86] via combining

with Pd-catalyzed click reaction and tetrazine ligation. The concept of site-specific genetic code expansion is authorized for many amino acids for bioorthogonal protein labeling, even though, low yield of aminoacylated tRNA synthesis limits the its applicability [87]. In addition to translational machinery of central dogma for site specific protein labeling, post-translational modifications (PTM) also have an important role for site-specific protein labeling [88]. A keto-biotin as a biotin analogue is utilized to conjugate with residue of 15 amino acid sequence of protein by the agency of biotin ligase (BirA) as shown in Figure 1.12 (c) [89]. Bane and co-workers demonstrated a site specific tyrosine C-terminus labeling with the usage of tubulin tyrosine ligase (TTL) which provides a post-transitional modification on tubulin by incorporation of formyltyrosine [90].

1.2.2. Glycan Labeling

Glycans have many vital roles in cellular processes [91] and cell surface facilities [92]. In addition, dynamic level of glycosylation is correlated with cancer metabolism and immune system [93]. Bioorthogonal labeling of glycans is different from the protein labeling since, glycans do not encoded in the genome so genetical modifications or translational machinery could not applied for glycan labeling. Glycan labeling strategies based on glycosylation as post-transitional modification which is responsible from glycan biosynthesis mechanism.

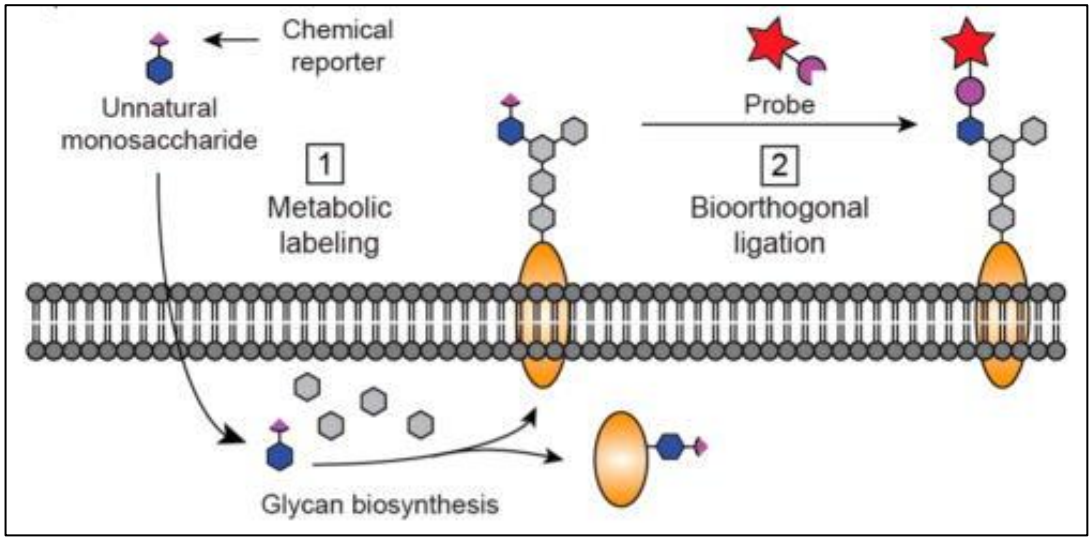

Figure 1.14. Bioorthogonal labeling of exogenous and endogenous glycans [94].

Bioorthogonal glycan labeling requires a two-step labeling concept. In first step, a chemical reporter tagged unnatural monosaccharide is introduced to cell and permitted insertion to glycan backbone via glycan biosynthesis. Metabolic labeled glycans are utilized in cell surface or intracellular processes. The second step is based on click chemistry that is provided by incorporation between chemical reporter and bioorthogonal labeling probes as shown in Figure 1.14 [95]. Bertozzi and coworkers investigated an unnatural monosaccharide, N-azidoacetylmannosamine (Ac4ManNAz) which is incorporated to cell surface for glycan labeling via Staudinger ligation in vivo and ex vivo [44, 96].

1.2.3. Nucleic Acid Labeling

Click chemistry serves a new perspective on bioorthogonal nucleic acid labeling. Site-specific DNA and RNA labeling strategies are achieved by metabolic labeling in the presence of active endogenous enzymes. During replication of genome or post-transcriptional machineries, nucleic acids are incorporated with chemical reporter introduced nucleotide analogs [1]. Mitchison and coworkers developed an unnatural nucleotide 5-ethynyl-2-deoxyuridine (EdU) (Figure 1.15, a) is incorporated with DNA during DNA replication. Conjugation between ethynyl group and fluorescent probe (Figure 1.15, b) yields in fluorescence labeled DNA in vivo [97]. Similar concept of DNA labeling can be applied for bioorthogonal RNA labeling in the presence of RNA polymerase enzyme [98].

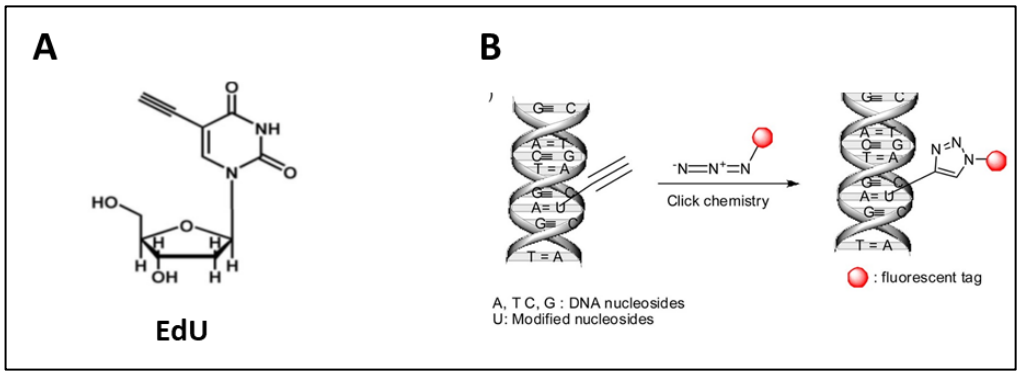

Figure 1.15. Bioorthogonal DNA labeling via azide-alkyne reaction (a) EdU, (b) illustration of DNA labeling [99].

1.2.4. Lipid Labeling

Lipids have critical missions in cellular processes especially participating in cell trafficking and signaling [100]. Furthermore, lipidation of glycans and proteins regulates metabolic activation of biomolecules. Lipids cannot be labeled with genetic modifications like glycans, not encoded genetically. Lipids are labeled during co-translational or post-translational machineries. Myristylation and palmitoylation are main post-translational modification for fatty acid acylation which provides chemical tagging to lipids [101]. Phospholipids are the most abundant lipids in cellular systems. In 2009, Schultz and co-workers modified the phospholipids with alkyne-tagging phosphatidic acid for labeling with azidocoumarin, this concept was demonstrated as the first bioorthogonally labeling of lipid bilayer in live cells [102].

1.2.5. Click Chemistry in Drug Discovery

Drug discovery aims chemical library screening in order to identify the target of biomolecules in living systems. Click chemistry provides with collecting novel chemicals to create a library and find the best reactive chemical tool for target molecule of disease metabolism [103]. Click chemistry has three main application concepts on drug discovery, these are high throughput screening, fragment-based drug discovery and dynamic template assisted strategies in fragment-based drug discovery. Lead-prodrugs are determined via high throughput screening, is that chemical collections are examined by click reactions for selecting active drug targets on biomolecules. Automated microarray assays let easy application to click reactions with large chemical libraries and target molecules [104]. Fragment-based drug discovery is based on free binding energy of chemically labeled protein fragments to the active site of target biomolecules [105]. Dynamic template assisted strategies in fragment-based drug discovery is desired by combining the concepts of high throughput screening and fragment-based drug discovery because of deficiency binding of low affinity fragments [106]. Fragment combinations as prodrug are incubated with reactive target biomolecule, then click reaction is achieved between selected fragments on target biomolecule [107]. Click chemistry diversify the bioorthogonal prodrug combinations to interact with targets and these approaches provide the personalized medicine development.

1.2.6. Live - Cell Imaging via Bioorthogonal Chemistry

Live cell imaging is one of the essential approaches of click chemistry with design and synthesis of site-specific fluorescent probes for visualization of the target molecule in biological systems. Bioorthogonal labeling makes concessions for both quantitative measurements of fluorescent-labeled biomolecules also, live cell imaging in vitro and in vivo.

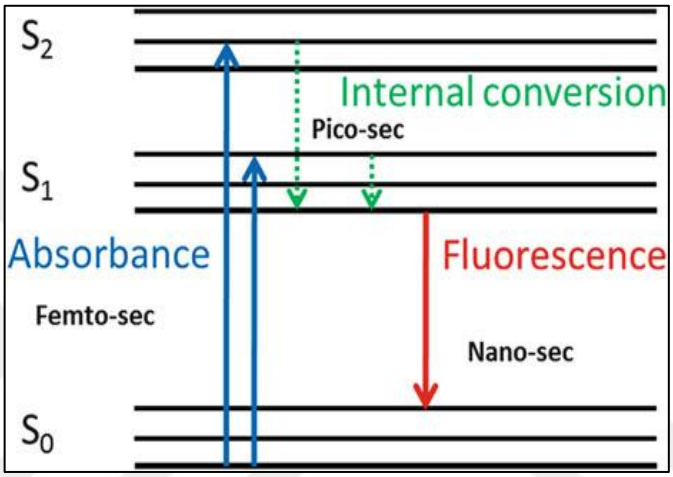

Figure 1.16. Jablonski diagram: excitation and emission of fluorophore [108].

According to fluorescence mechanism, a fluorophore absorbs maximum photon energy and, it is excited to S_1 or S_2 singlet states. Then, the excess energy of fluorophore is released from S_1 state to S_0 ground state with fluorescence emission as shown in Figure 1.16 Jablonski Diagram [109].

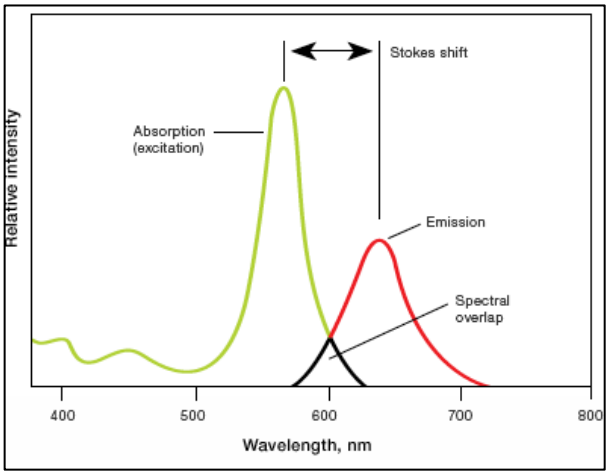

Figure 1.17. Stoke's shift diagram.

When the energy is released from singlet state, emission maximum peak of fluorophore has lower energy than excitation maximum peak therefore this energy differences provide with higher wavelength for emission maximum. The differences between excitation and emission wavelength is called as Stoke's Shift as shown in Figure 1.17 [108]. Range of the shift is dependent on molecular structure of the fluorophore hence, bioorthogonal fluorescent probes are designed to have larger Stoke's Shift to prevent self-quenching of the fluorophore during live-cell imaging processes [110]. To prevent phototoxicity of fluorescence emission and autofluorescence, near infrared (NIR) fluorescent probes are designed to utilize in live cell imaging [111].

1.3. OXIDATIVE STRESS IN CANCER

1.3.1. ROS Mechanism and Cancer

'Oxidative stress' is correlated with imbalance in the level of reactive oxygens species (ROS) and antioxidants in cellular metabolism. Low level of ROS not only induces the activation of transcription factors for oxidative stress adaptation [112] but also acts as a signaling molecule in cellular processes [113], the main research topic in the field of redox biology. High level of ROS causes oxidative stress-induced cell death. Reduced molecular forms of oxygen are mainly consist of hydroxyl radical (OH^-), superoxide anion (O_2^-) and hydrogen peroxide (H_2O_2). Mitochondria, cell membrane and endoplasmic reticulum are the main ROS generating cellular compartments [114]. ROS equilibrium is maintained by the enzymatic ROS scavengers such as superoxide dismutase (SOD), glutathione reductase-peroxidase, thioredoxins and the non-enzymatic antioxidants such as vitamin C, E [115]. The most reactive molecule O_2^-, is reduced by the metalloenzyme SOD to less reactive H_2O_2, which is then reduced by antioxidants to H_2O and O_2 [116]. Nicotinamide Adenine Dinucleotide Phosphate (NADPH)-oxidase (NOX) in cell membrane [117] and electron transport chain in mitochondria [118] are the major H_2O_2 generators.

Cancer cells prone to the aerobic glycolysis that is referred as Warburg Effect, which leads to ROS accumulation and high level of oxidative stress [119]. Increased level of H_2O_2 acts as a tumorigenesis promoter via activation of the Nuclear Factor-κB (NF-κB),

Phosphoinositide 3-Kinase (PI3K), Hypoxia Inducible Factor-1 (HIF) and Mitogen-Activated Protein Kinase (MAPK) pathways as shown in Figure 1.18.

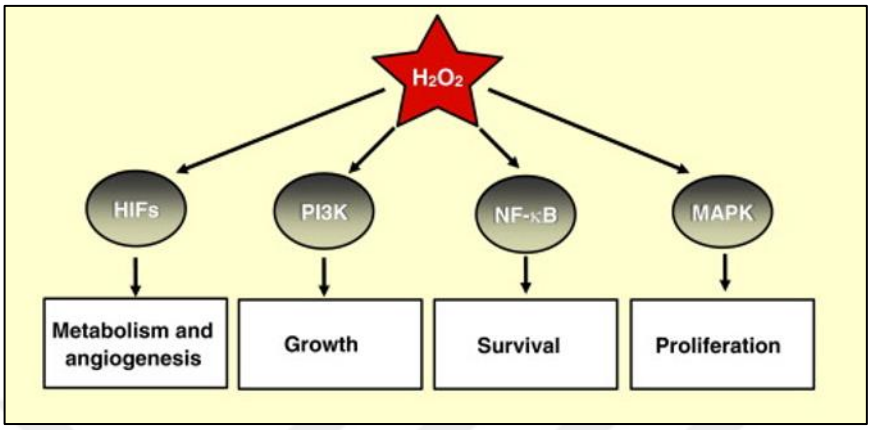

Figure 1.18. H_2O_2-regulated signaling pathways [120].

NF-κB is a H_2O_2-regulated transcription factor that is related with cancer cell survival. During estrogen metabolism, ROS concentration activates PI3K/Akt pathway which deals with the cell growth via phosphorylation and activation of mTOR kinase responsible from the activation of protein translation [121]. Under high level of ROS conditions, HIF transcription factor is induced, which promotes angiogenesis and tumorigenesis [122].

MAPK/Erk1/2 pathway activation is responsible for the activation of cell proliferation [123]. Erk1/2 is activated in the presence of H_2O_2 and MAPK pathway Myc-cyclin D, RB. On the other hand, H_2O_2 treatment of cells mimics the high endogenous ROS conditions and leads to the activation of p38 MAPK resulting in cell death induction in glioma cells [124].

In living systems, ROS have a very short lifetime as nanoseconds to seconds depending on reactivity of the species. Hence, detection methods of ROS are quite challenging and must be performed within the specified durations [125]. Spin-trapping is the oldest ROS detection method which has limitations such as slow rate constant, non-specificity and toxicity [126]. Therefore, chemiluminescent [127] and fluorescent probes [128] are designed, these probes provide more specific and fast detection of ROS in the biological systems. Dichlorodihydrofluorescein (DCFH-DA) is one of the common commercial fluorescent probe specific for the intracellular H_2O_2 detection [129]. Dihydroethidium and mitoSOX probes are preferred for the mitochondrial and intracellular O_2^- detection [130].

1.3.2. Biomarkers of Oxidative stress

The increased level of ROS and disturbed redox signaling results in the oxidative damage on biomolecules in living systems. Many diseases such as cancer and neurodegenerative diseases are closely correlated with the oxidative stress [131, 132]. ROS causes the oxidation of biomolecules, which could be used as biomarkers in order to determine oxidative stress-induced diseases.

One of the major ROS-induced oxidation process is the lipid peroxidation. Lipid oxidation causes membrane decomposition, enzyme inactivation and cell function defects. Bis-allylic hydrogen of unsaturated lipids is abstracted by free radicals to form lipid radical. The unreactive lipid radicals are oxidized to reactive lipid peroxyl radicals. Reaction between unsaturated lipids and lipid peroxyl radicals either yield lipid peroxide products (LPP) or enter propagation to yield lipid radicals as shown in Figure 1.19 [133]. Lipid oxidation products as malondialdehyde [134], isoprostanes [135] and 4-hydroxynonenal [136] are the most common oxidative stress biomarkers which are used for the determination of oxidative stress mediated diseases. The biomarkers can then be detected by the immunocytochemistry or proteomic analysis [137].

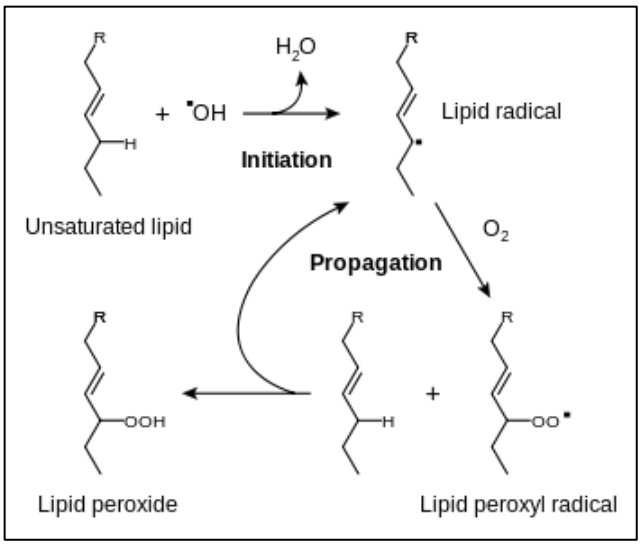

Figure 1.19. Lipid peroxidation mechanism [138].

Another detrimental effect of oxidative stress is observed on nucleic acids that promotes aging and mutagenesis [139]. ROS causes double or single strand breakage [140], nucleic acid modification and base sugar disruption [141]. Guanine is one of the most oxidative

damaged nucleic acid base due to its low redox potential [142], therefore it is easily either oxidized into 8-oxo-7,8-dihydroguanine (8-oxo-G) as shown in Figure 1.20 [142] or hydroxylated into 8-hydroxyguanosine (8-OHG) and 8-hydroxy-2′-deoxyguanosine (8-OHdG) [143] which are considered as oxidative stress biomarkers. Presence of 8-oxo-G in DNA template results in GC→TA transversions and nucleotide mispairing during the DNA replication, which later on may lead to the cellular transformation [144].

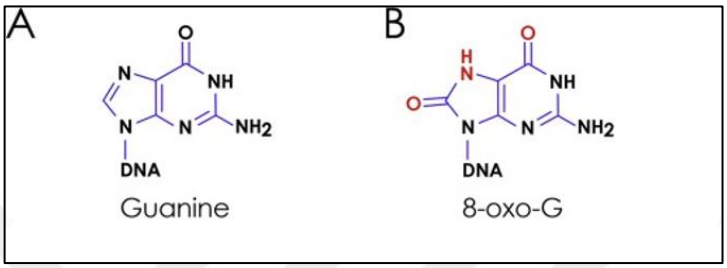

Figure 1.20. Structure of (a) Guanine, (b) 8-oxo-G [145].

ROS production is directly correlated with the glucose consumption due to the increased glycation of proteins [137]. Advanced glycation end product (AGE) formation is stimulated with high-glucose-induced ROS generation [146]. AGE not only participate oxygen free radical generation but also has toxic effects to the cell metabolism. Because of these reasons, glycation and AGE are used as biomarkers for the oxidative damage to carbohydrates.

Oxidation of proteins may cause loss of function and hence alter metabolic activity of the cell associated with many diseases especially neurodegenerative disorders and carcinogenesis [147]. Accumulation of oxidized protein lead to the formation of protein aggregates seen in diabetes, atherosclerosis and rheumatic arthritis [148]. ROS-mediated posttranslational modifications can be used as oxidative stress biomarkers. Hydroxylation of aromatic group-containing amino acids, the oxidization of cysteine and methionine residues, the nitration of tyrosine [149] and metal catalyzed oxidation of positively charged amino acids (Arginine, Lysine, Proline and Threonine) [150] are utilized as the biomarkers of oxidative stress modifications on proteins. Carbonylation and nitration modifications are the most common used biomarkers due to their stability [151]. When aliphatic side chains on the amino acid residues are removed using β-scission reaction, carbonyl groups remained can serve as a selective biomarker for the oxidative stress-mediated protein carbonylation [148].

1.3.3. Chemistry of Protein Carbonylation

Under oxidative stress conditions, micro and macromolecules are exposed to many different modifications like oxidation, nitration, hydroxylation and carbonylation. Protein carbonylation is the major modification affecting the stability of on biomolecules. Carbonylation is an irreversible post-translation modification which introduces reactive aldehyde, ketone or lactam moieties into proteins [152]. Protein carbonylation consists of primary and secondary protein carbonylation mechanisms [153]. Primary protein carbonylation mechanism comprises metal catalyzed oxidation (MCO) and direct oxidation of side chain of amino acids, while secondary protein carbonylation involves the glycoxidation and lipid peroxidation.

H_2O_2 is reduced to OH^- radical in the presence of metal catalysts such as Fe (III), Fe(II), Cu(I) and Mn(II), which is called Fenton reaction [154]. Free OH^- radical leads the oxidation of amino acids side chains such as lysine, proline, arginine and threonine. Another primary protein carbonylation occurs on tryptophan with seven different oxidized analogs such as N-formyl kynurenine and kynurenine [155].

One of the major protein carbonylation mechanism is based on lipid peroxidation. Lipid peroxidation products are obtained by Michael addition that requires the abstraction of hydrogen and addition of oxygen to form carbonyl moiety into the unsaturated side of fatty acid [156]. Electrophilic carbonylated-lipid products react with the nucleophilic side chain of amino acids as cysteine, histidine and lysine to yield Michael adducts. In addition to lipid peroxidation, glycoxidation, which is also called as glycation, plays a critical role in protein carbonylation mechanism by catalyzing the reaction between reducing sugars and positively charged amino acids as lysine and arginine. Glycation products are reduced by ROS to form AGE which carries a reactive carbonyl group. For instance, AGE form of lysine and arginine yields in pyrraline and imidazolone [155].

Lack of decarbonylation mechanism causes aggregation of carbonylated proteins due to high level of carbonyl moiety on proteins [157]. Such as carbonylated proteins must be degraded by proteasome in order to eliminate toxicity effects' of excess carbonylation in cellular mechanisms [155]. 20S and 26S proteasomes are responsible from the recognition of carbonyl moieties on proteins and their degradation. While 26S proteasome activity is

inhibited by oxidative stress byproducts, 20S proteasome is more effective to degrade carbonylated proteins [158].

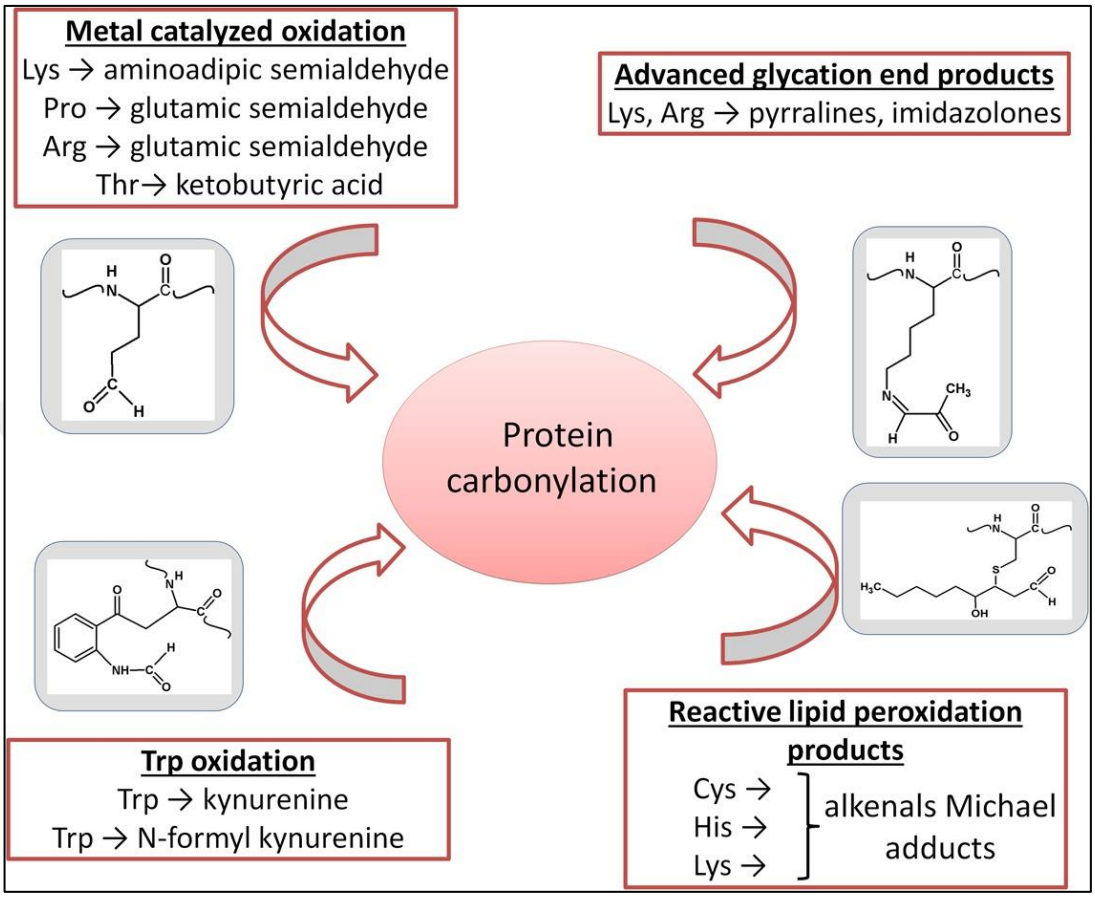

Figure 1.21. Protein carbonylation mechanisms [155].

1.3.4. Induction and Inhibition of Protein Carbonylation

Level of protein carbonylation depend on the anabolism and catabolism of carbonylated proteins, which relies on the reduction of carbonyl moiety on proteins. Inhibition of ROS scavengers induces protein carbonylation for example, the inhibition of thioredoxin reductase both stimulates the protein carbonylation and inhibits the decarbonylation processes. While the oxidation of carbonyl groups yields in carboxylic acid, reduction of carbonyl moiety results in the formation of alcohol [159]. Another enzymatic induction of protein carbonylation based on activation of Lon protease, which is activated under the stress condition such as high level of H_2O_2 participates in the degradation of carbonylated proteins [160]. It is well known that lipid peroxidation and glycoxidation widely provide protein

carbonylation, so that, detoxification of LPP and AGE leads to a decrease in the formation of carbonylated proteins [161]. The non-enzymatic endogenous protection of carbonylation is provided by the presence of pyruvate as a free radical scavenger [162]. Increase in the pyruvate concentration relieves the oxidative stress on biomolecules [163]. In addition, serum deprivation induces generation of ROS [62], while lack of growth factors may cause apoptotic cell death [164].

1.4. DETECTION METHODS OF PROTEIN CARBONYLATION

Carbonylation is an oxidative stress biomarker which is allowed to detect within different biochemical and analytical methodologies. Mass spectrometry (MS) is an analytical detection method which could characterized the carbonyl-modified site chain of proteins with quantitative measurements for carbonylation level. As well as, MS determines the source of the carbonylation which belongs to either primary carbonylation or secondary carbonylation mechanisms [165]. As mentioned section 1.1.16, carbonyl groups can bioorthogonally labeled with hydrazide/alkoxyamine based probes. 2,4-Dinitrophenyl hydrazine (DNPH) is a fluorescent probe which is specific for carbonyl moiety on aldehydes and ketones. Usage of DNPH is modified with application in both biochemical and spectrophotometric detection methods of biomolecule carbonylation. Immunocytochemistry is a biochemical technique that allows to detect only protein carbonylation via immunoblotting. Anti-DNP antibodies may readily utilized to perform OXYblot which is a commercial application on western blot for oxidative stress induced protein carbonylation [166]. Biotin hydrazide probes are designed as DNPH alternative which permit the application in immunoblotting, spectrophotometric and MS analysis to detect carbonylation both of proteins, lipids and glycans [155]. Recently, hydrazine-tagged coumarin or BODPY scaffolds are used as fluorescent probes which operate the detection of carbonylation via bioorthogonal labeling in live cells [62, 167].

1.5. RENAL CELL CARCINOMA

Renal cell carcinoma (RCC) is a renal parenchyma originated kidney cancer which is the eighth most common cancer in the worldwide. Appearance of RCC elucidates 80 per cent of

all kidney cancer types [168]. RCC is classified by different histological subtypes such as clear cell renal cell carcinoma (ccRCC), papillary renal carcinoma, and chromophobe renal cell carcinoma which have higher prevalence in the subtypes of RCC [169]. Active and passive smoking [170], obesity [171] and hypertension [172] are qualified risk factors of RCC.

1.6. AIM OF THE STUDY

Oxidative stress is characterized by the imbalance between level of pro-oxidants and antioxidants in live cells. Increased level of ROS overwhelms the cells' buffering system which is known as the redox biology. The major consequence of high ROS level is the carbonylation of biomolecules. Carbonylation is an irreversible post translational modification on biomolecules, which can also serve as an oxidative stress biomarker. Determination of carbonylation level of biomolecules may provide the information about cancer staging due to the distortion of redox biology in cancer cells. Bioorthogonal chemistry provides labeling strategies with the designing of site-specific fluorescent probes to target biomolecules. Aldehyde - hydrazine reactions are well suited for the detection of carbonylation in live cells. Starting from this point of view, there are two main purposes of this study. Design and synthesis of novel hydrazine based bioorthogonal fluorescent probes is aimed in order to label oxidative stress induced carbonylated biomolecules in live cells.

2. MATERIALS

2.1. INSTRUMENTS

- -80 °C Freezer (Thermo Forma -86 C ULT Freezer, USA)
- Bruker Avance III 500 MHz Spectrometry (Germany)
- Centrifuge (Hettich Mikro 22r And Sigma 2-5 Centrifuge, Germany)
- CO_2 Incubator (Nuaire Nu5510/E/G, USA)
- Confocal Microscope (Zeiss Lsm 800)
- Fluorescence Microscope (Nikon 80i Eclipse Fluorescence Microscope)
- Fume Hood (Greenlab, Turkey)
- Heater (Bioer, Mb102, China)
- Laminar flow cabinet (ESCO Lab culture Class II Biohazard Safety Cabinet 2A, Singapore)
- Light Microscope (Nikon Eclipse #Ts100, Japan)
- Magnetic Stirrer (Heidolph Mr 3004, Germany)
- Ph Meter (Hanna Instruments Ph211, Germany)
- Rotary evaporator (Heidolph, Hei-VAP Silver Packages, Germany)
- UV lamb - cabinet (CAMAG, Swiss)
- Varioskan Lux Multimode Microplate Reader (Thermo Fisher, USA)
- Vortex (Stuart Sa8, Up)
- Water bath (Stuart, Sb540, UK)

2.2. EQUIPMENTS

- Bright-Line™ Hemocytometer (Sigma Aldrich, Z359629, USA)
- Cover Slip (Sigma Aldrich, Z375357, USA)
- Electronic Pipette (CAPP Aid, Denmark)
- Filter 0.22 mm (TPP, Switzerland), 0.45 mm (Santorium Stedim Biotech, Germany)
- Graduated Cylinder 50,250,500,1000 ml (Isolab, Germany),

- Micropipettes 10µl, 20µl, 100µl, 200µl, 1000µl (Eppendorf Research, Germany)
- Pipette Tips 10,100, 200, 1000 µl (Capp Expell Plus, Denmark)
- Polypropylene Centrifuge Tubes 0.5, 1.5, 2, 15, 50 ml, (Isolab, Germany)
- Serological Pipettes 2, 5, 10, 25 ml (Grenier Bio or Axygen, USA)
- Tissue Culture Flasks, T-25, T-75, T-150, Multiple-Well Cell Culture Plates, And Cryovials (TPP Switzerland Or Grenier-Bio, Germany)
- Whatman Paper (Isolab, Germany)

2.3. Chemicals

The chemicals used in this study were as follows:

2.3.1. Chemical Synthesis

- Silica Gel (Silica Gel 60-200 Mesh)-2.5 Kg Merck 107734
- Hexane (2,5 Lt, Merck 104368)
- Ethanol (100 per cent, Cat No: M.100986.2500)
- Chloroform (Cat No: SC.CL.0200.2500)
- Dichloromethane (2,5 Lt. Cat No: M.106050.2500)
- Acetone (2,5lt. Cat No: M.100013.2500)
- Hydrochloric Acid (2,5lt, Cat No: Merck 100317)
- Sodium Hydroxide Pellets (Merck 106498)
- Sodium Chloride (SC.SO.0227.1000)
- Dioxane per cent 99 (2,5 Lt. Merck 103115)
- Methanol (Spectral Grade, Anhydrous Cat No: Merck 106009, 2,5 Lt)
- Dioxane (Spectrophotometric, Cat No: 154822, 1 Lt)
- Methanol (Normal, 2,5 Lt, Cat No: 34885,)
- Sodium Nitrite (1 Kg, Merck 106544)
- Palladium Carbon 10 per cent (10 g, Cat No: 804107)
- 3-Aminophenol (500 g, Cat No: 100242)
- Ethyl Pyruvate (100 g, Cat No: E47808)
- Tin (II) Chloride (100 g, Cat No: 31669)

- Acetic Acid (500 ml, 100056.2500)
- 2,5-Diaminophenol Dihydrochloride (25 mg, Cat No: S579009)
- 2-Amino-5-Nitrophenol (100 g, Sigma, Cat No: 303585)
- Toluene (Anhydrous 98 per cent), (2,5 L, Merck, Cat No: 108325)
- Hydrazine Hydrate (100 ml, Cat No: 225819)
- Methyl Pyruvate (100 g, Cat No: 371173)
- Methyl Benzoyl Formate (25 g, Cat No: M30507,)
- Ethyl Chloroformate (100 g Cat No: 185892),
- Diethyl Ether (1 L)-Merck 100921
- TLC Aluminum Sheets (Merck, Cat No: 105554)

2.3.2. Cell Culture Media

- Dulbecco's Modified Eagle's Medium, High Glucose (Gibco 41966)
- Fetal Bovine Serum (FBS) – Cell Culture Tested (Sigma F9665) (Gibco #10082, USA),

2.3.3. Other Reagents for Cell Culture

- Acrylamide/ Bis-Acrylamide (29:1) (Sigma A3574)
- Bovine Serum Albumin, Protein Standard (Sigma P0834)
- Dimethyl Sulfoxide (Santa Cruz Sc-202581, USA)
- Dulbecco's Phosphate Buffered Saline (DPBS) (Pan Biotech P04-53500, Germany)
- Glycerol 99 Per Cent (HPLC Grade) (Sigma #G2025, Germany)
- H_2O_2 (50 wt. per cent in H_2O Sigma, 519813, Germany)
- L-Glutamine (Invitrogen 25030, USA)
- Methanol 99 per Cent (Sigma, 34885, USA)
- Phenylmethanesulfonylfluoride (PMSF) (Sigma 78830, USA)
- Protease Inhibitor (Pi) (Sigma, P8340, USA)
- Penicillin-Streptomycin (Thermo Scientific Sv30010 Or Biochrom A2213, Germany)

- Trypsin-EDTA (Biochrom L2153, Germany)

2.4. KITS

- Cell Proliferation Reagent Wst-1 (Roche 05015944001, Germany)
- Protein Assay Reagent A (Bio-Rad, 5000113)
- Protein Assay Reagent B (Bio-Rad, 5000114)
- DCFDA - Cellular Reactive Oxygen Species Detection Assay Kit (Abcam Ab113851, USA)

2.5. CELL LINES

- A-498, Primary Human Kidney Epithelial Carcinoma, Adherent (ATCC Number: Htb-44)
- ACHN, Metastatic Renal Cell Adenocarcinoma, Adherent (ATCC Number: Crl-1611)
- HDF, Human Dermal Fibroblast, Adherent (ATCC Number: PCS 201-012)

3. METHODS

3.1. ORGANIC SYNTHESIS

Synthesis of azacoumarin based 3-Methyl-7-aminoazacoumarin and 3-Methyl-7-hydrazine azacoumarin fluorescent probes were shown in Sec.3.1.1-Sec.3.1.5.

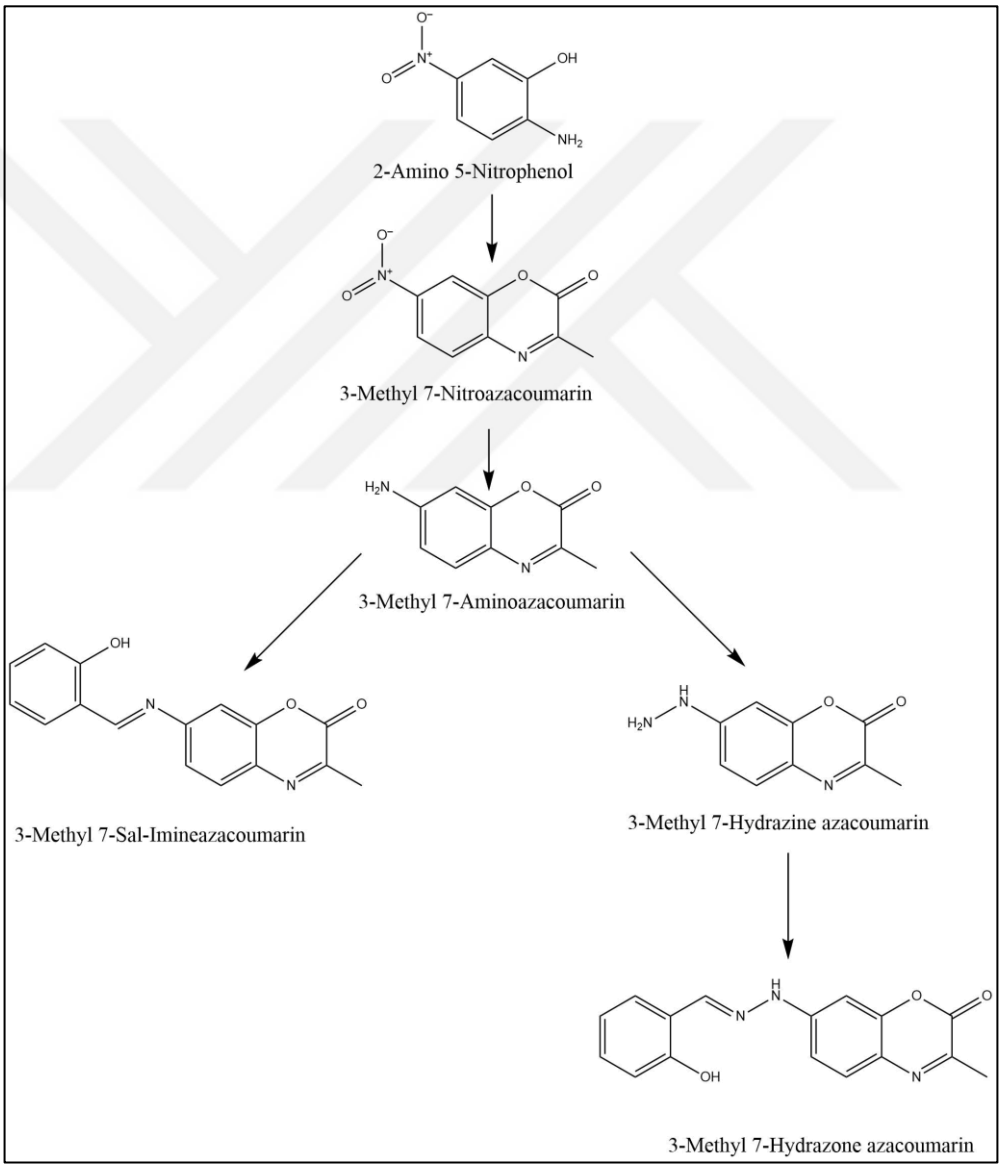

Figure 3.1. Reaction schema of 3-Methyl azacoumarin based fluorescent probes

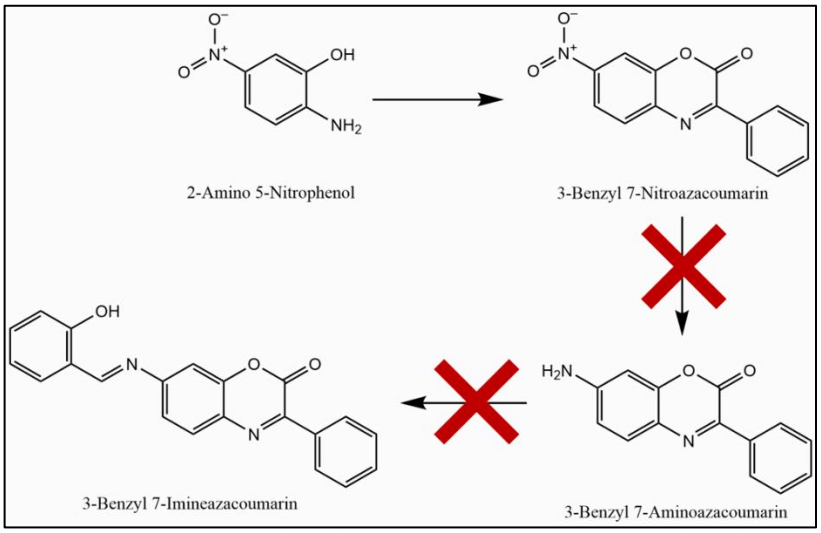

Figure 3.2. Reaction schema of 3-Phenyl azacoumarins

Synthesis of azacoumarin based 3-Phenyl-7-aminoazacoumarin as a fluorescent probe were shown in Sec.3.1.6-Sec.3.1.8.

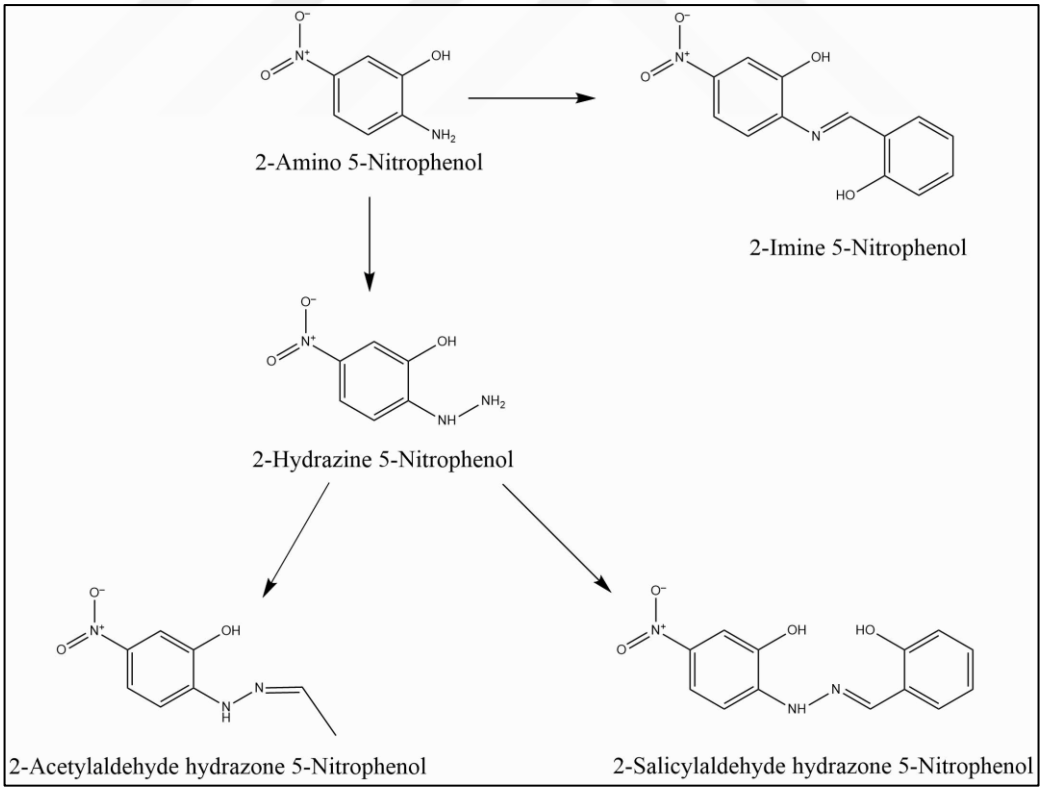

Figure 3.3. Reaction schema of 2-Hydrazine-5-nitrophenol

Synthesis of 2-Hydrazine-5-nitrophenol and derivatives of fluorescent products were shown in Sec.3.1.10-Sec.3.1.12.

3.1.1. Synthesis of 3-Methyl-7-nitro azacoumarin

2-Amino-5-nitrophenol (15.41 g, 0.1 mmol) was stirred with 18 ml methyl pyruvate for 65 minutes at 115˚C [173]. The reaction was monitored by TLC with using different solvent systems as 7:3 Hex: EtOAc and 10:1 CH_2Cl_2: MeOH. Because of wet clay form of product, the reaction yield could not be calculated. The product was chromatographed with 100 per cent CH_2Cl_2 as a mobile phase and 100 per cent Hex as a stationary phase.

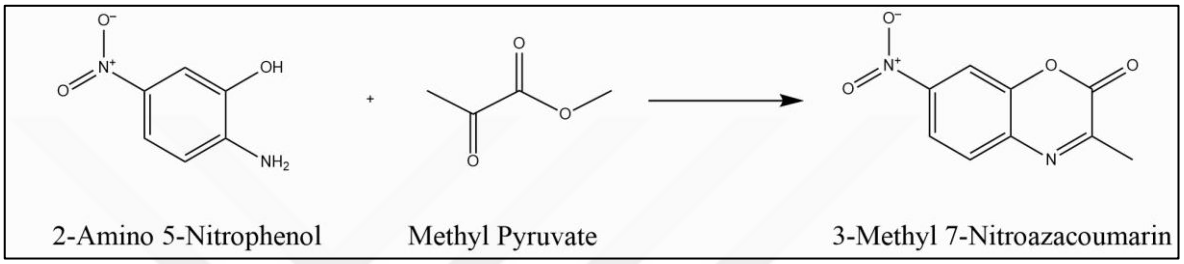

Figure 3.4. Synthesis of 3-Methyl-7-nitro azacoumarin.

3.1.2. Synthesis of 3-Methyl-7-amino azacoumarin

3-Methyl-7-nitro azacoumarin (100 mg, 0.37 mmol) was dissolved in 10.5 ml ethanol. Hydrazine hydrate (211 µl) and 10 per cent Pd/C (39 mg) were added in the mixture. The reaction was stirred for 6 hours at RT [174]. Wet clay product (240 mg) was obtained and stored at -20˚C.

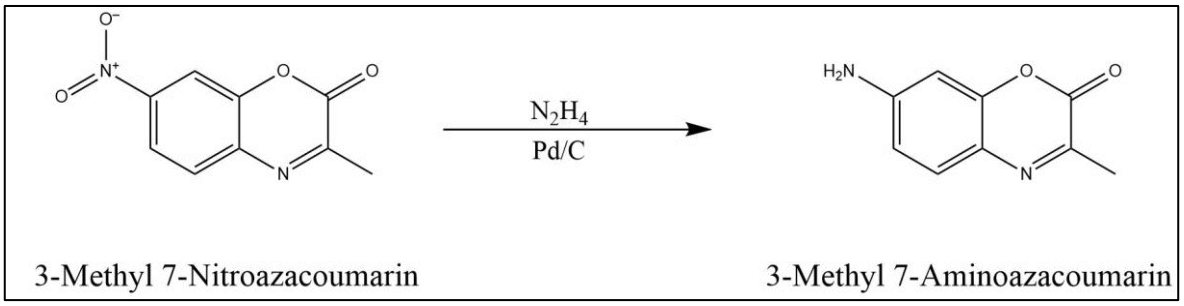

Figure 3.5. Synthesis of 3-Methyl-7-amino azacoumarin.

3.1.3. Synthesis of 3-Methyl-7-salicylaldehyde imine azacoumarin

TLC scale Amino-Imine reaction was achieved. 3-Methyl-7-amino azacoumarin (20 mg, 0.08 mmol) was mixed with SAL (80 µl, 0.8 mmol) in 640 ml methanol. A drop of TFA was added and reaction was stirred for 30 minutes at RT [90]. 20 mg 3-Methyl-7-salicylaldehyde imine aza coumarin.

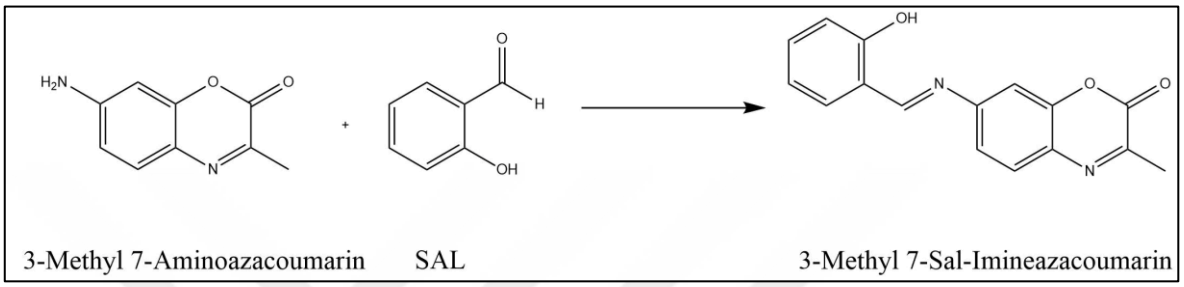

Figure 3.6. Synthesis of 3-Methyl-7-salicylaldehyde imine azacoumarin

3.1.4. Synthesis of 3-Methyl-7-hydrazine azacoumarin

3-Methyl-7-amino azacoumarin (80 mg, 0.33 mmol) was dissolved in cold 1 ml HCl and reaction was placed on ice bath at -10˚C. A solution of sodium nitrate (0.22 mg, 0.33 mmol) in 99 µl cold water was dropwise added on the reaction. The mixture was stirred for 1 hour at -5˚C. The mixture was filtered, and filtrate was added drop by drop on a cold solution of stannous chloride dihydrate (0.37 mg, 1.65 mol) in 1.98 ml HCl. The reaction was mixed for 1 hour at -5˚C. The mixture was filtered, and precipitate was washed with water and ethanol. While 3-Methyl-7-hydrazine azacoumarin HCl salt was washed, the precipitate was solved in ethanol and water, so all mixture was evaporated with rotary evaporator [175]. The product was obtained with impurities (270 mg)

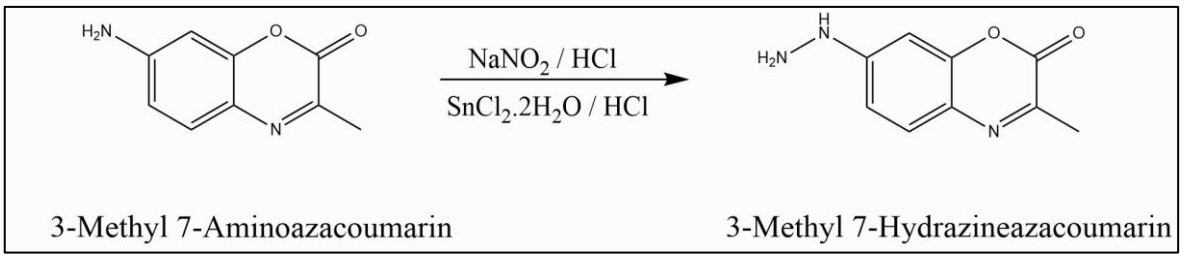

Figure 3.7. Synthesis of 3-Methyl-7-hydrazine azacoumarin

3.1.5. Synthesis of 3-Methyl- 7-hydrazone azacoumarin

3-Methyl-7-hydrazine azacoumarin (270 mg, 1 mmol) was dissolved in 5 ml MeOH. A solution of salicylaldehyde (1 ml, 10 mmol) in 3ml methanol was added on the mixture. After addition of 2 drops of Trifluoroacetic acid, the reaction was stirred for 30 minutes at RT conditions. Precipitate was vacuum filtered and washed with MeOH then dried with vacuum [90]. The reaction gave 57 mg 3-Methyl-7-hydrazone azacoumarin with 20 per cent reaction yield.

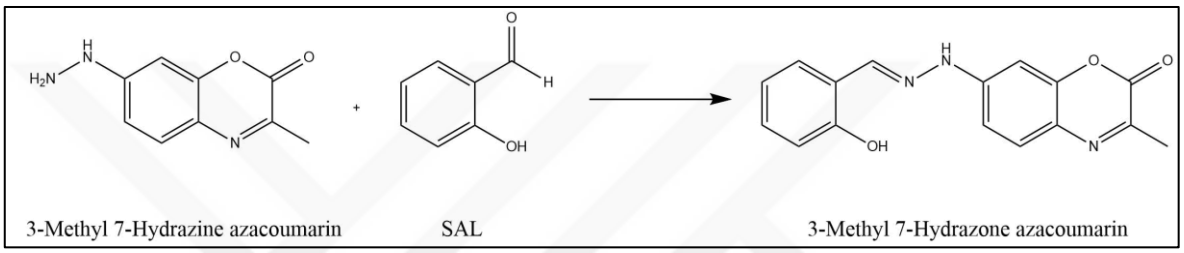

Figure 3.8. Synthesis of 3-Methyl-7-hydrazone azacoumarin

3.1.6. Synthesis of 3-Phenyl-7-nitro azacoumarin

2-Amino-5-nitrophenol (4.3 g, 28 mmol) was mixed with Methyl Benzoylformate (8 ml, 56 mmol) in a rounded bottom flask and reaction was stirred for 1 hour at 130˚C. The product formation was checked with TLC in 7: 4 Hex: EtOAc solvent system. Wet clay crude product was recrystallized with ethanol twice. Most of the impurities were eliminated in the product. Excess starting compound which was 2-Amino-5-nitrophenol was clarified via silica gel colon chromatography with 8:1 Hex: EtOAc eluents [173]. Solvent evaporation gave 4.2 g product (52 per cent yield).

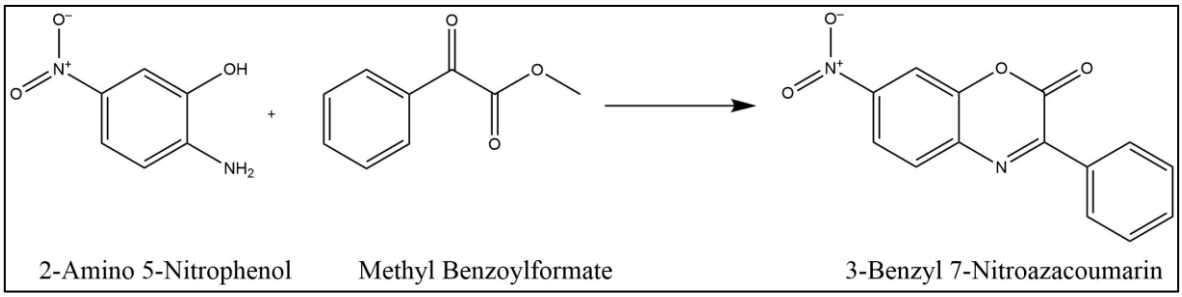

Figure 3.9. Synthesis of 3-Phenyl-7-nitro azacoumarin

3.1.7. Synthesis of 3-Phenyl-7-amino azacoumarin

3-Phenyl-7-nitro azacoumarin (95 mg, 0.35 mmol) was dissolved in 10 ml MeOH. After addition of Hydrazine hydrate (0.2 ml) and 10 per cent Pd/C (37 mg), reaction was stirred for 90 minutes at room temperature. Pd/C was discarded with vacuum filtration [174]. The solution was evaporated, and wet clay product was obtained.

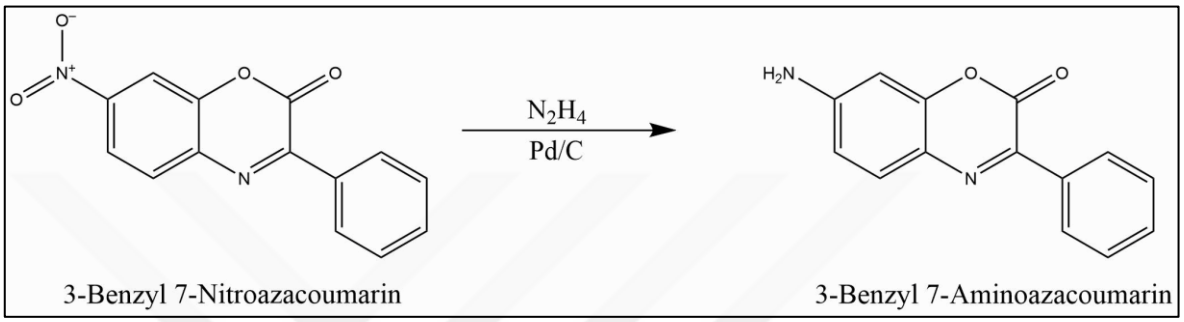

Figure 3.10. Synthesis of 3-Phenyl-7-amino azacoumarin

3.1.8. Synthesis of 3-Phenyl-7-imine azacoumarin

3-Phenyl-7-amino azacoumarin (60 mg, 0.25 mmol) was dissolved in 80 µl MeOH. A solution of SAL (26.6 µl, 0.25 mmol) in 125 µl MeOH was added on the reaction. The mixture was stirred for 1 hour at room temperature. Solvent was evaporated, and reaction gave 90 mg impure 3-Phenyl 7-Imineazacoumarin. The product was clarified with silica gel colon chromatography with dichloromethane eluent [90]. Purification gave 35 mg pure product (41 per cent yield).

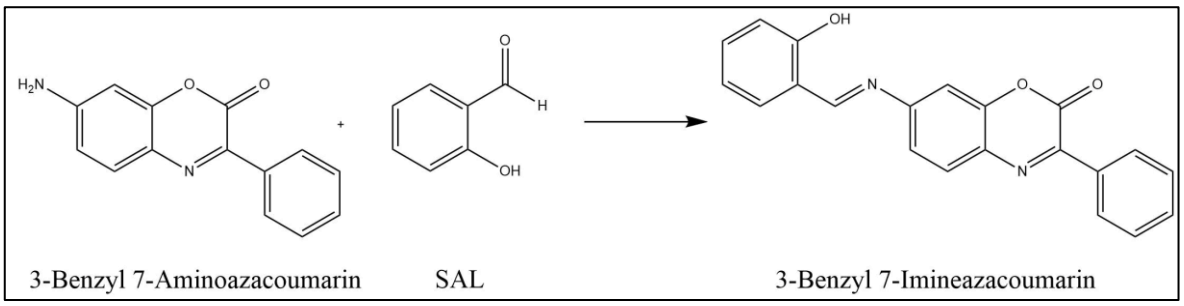

Figure 3.11. Synthesis of 3-Phenyl-7-imine azacoumarin

3.1.9. Synthesis of 2-Imine-5-nitrophenol

2-Amino-5-nitrophenol (1 g, 635 mmol) and Salicylaldehyde (0.75 ml, 6.5 mmol) were mixed in 10 ml EtOH. The mixture was refluxed for 2 hours. The reaction mixture was cooled in ice bath and bright red precipitate was formed. The mixture was filtered, and solid product was washed with cold EtOH and dried under vacuum. The reaction gave 1 g fluorescent product (63 per cent yield). The reaction was checked with TLC in Hex: EtOAc (7: 4) eluents Rf:0.72.

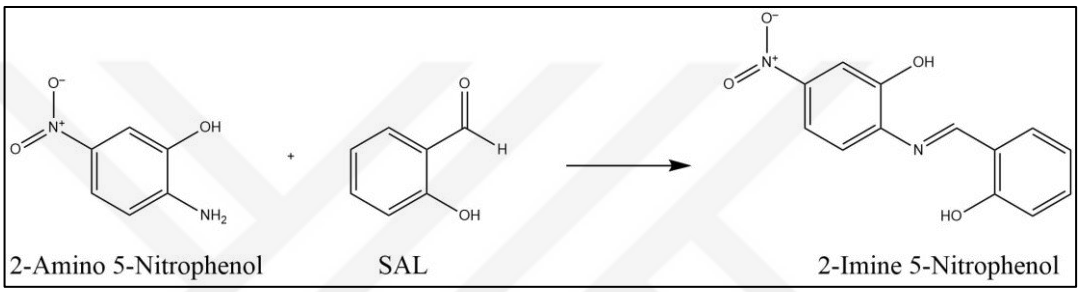

Figure 3.12. Synthesis of 2-Imine-5-nitrophenol.

3.1.10. Synthesis of 2-Hydrazine-5-nitrophenol HCl Salt

A cold solution of sodium nitrate (106 mg, 1.5 mmol) in 385 µl water was dropwise added on a cold solution of 2-Amino-5-nitrophenol (200 mg, 1.3 mmol) in 648 µl HCl. The mixture was stirred for 1 hour at -5 ˚C. Stannous tin chloride (931 mg, 4.1 mmol) was dissolved in 927 µl cold HCl and slowly added on the reaction mixture. The reaction was mixed for 1 hour at -5 ˚C. The mixture was vacuum filtered, precipitate was washed with cold MeOH and ether [90]. The reaction gave 177 mg (66 per cent yield) dried 2-Hydrazine-5-nitrophenol HCl (2Hzin5np) Salt.

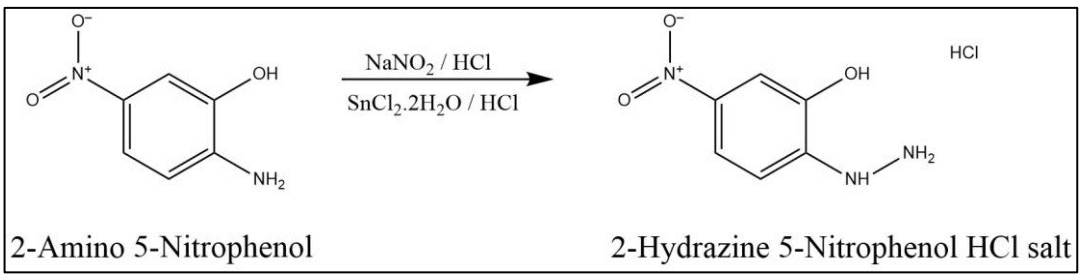

Figure 3.13. Synthesis of 2-Hydrazine-5-nitrophenol HCl salt.

3.1.11. Synthesis of 2-Salicylaldehyde hydrazone-5-nitrophenol

2-Hydrazine 5-Nitrophenol (400 mg, 2.36 mmol) and Salicylaldehyde (0.75 ml, 6.5 mmol) were stirred in 19 ml MeOH for 1 hour at room temperature. The reaction mixture was cooled in ice bath and the mixture was filtered. Solid product was washed with cold MeOH and dried under vacuum. The reaction gave 155 mg fluorescent product (24 per cent yield). The product has Rf:0.39 value within TLC in Hex: EtOAc (7: 4) eluents.

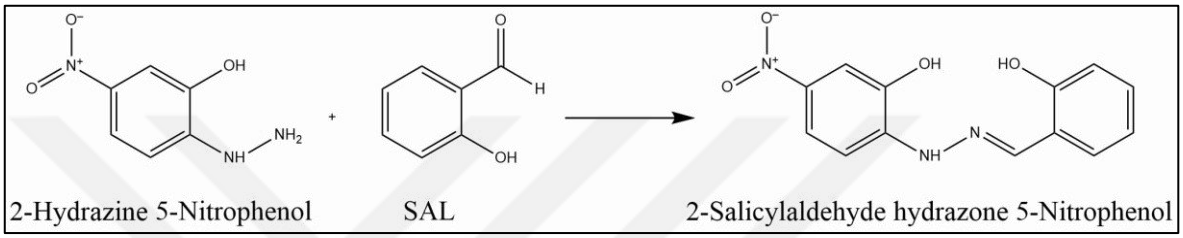

Figure 3.14. Synthesis of 2-Salicylaldehyde hydrazone-5-nitrophenol.

3.1.12. Synthesis of 2-Acetaldehyde hydrazone-5-nitrophenol

2-Hydrazine-5-nitrophenol (400 mg, 2.36 mmol) and Salicylaldehyde (0.75 ml, 6.5 mmol) were stirred in 19 ml MeOH for 1 hour at room temperature. The reaction mixture was cooled in ice bath and the mixture was filtered. Solid product was washed with cold MeOH and dried under vacuum. The reaction gave 155 mg fluorescent product (24 per cent yield).

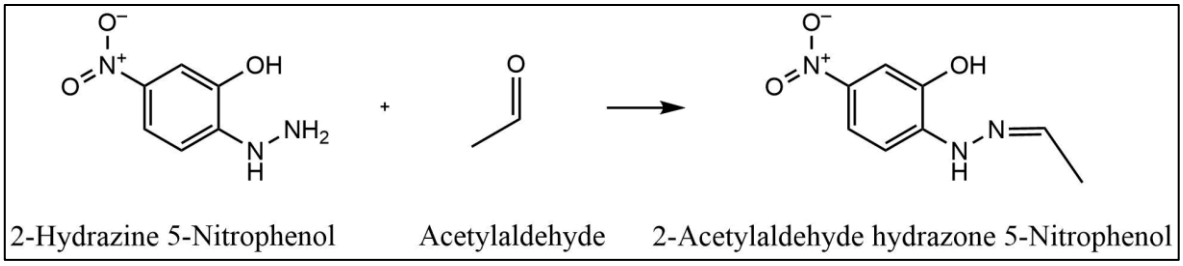

Figure 3.15. Synthesis of 2-Acetylaldehyde hydrazone-5-nitrophenol.

3.2. CELL CULTURE

A498, ACHN, and HDF cell lines were cultured in standard Dulbecco's Modified Essential Medium (DMEM) containing 4.5 g/L glucose, 1 mmol/L sodium pyruvate and 200 mM L-glutamine. The medium was completed with 10 per cent (v/v) Fetal Bovine Serum (FBS) and 1 per cent pen strep (100 units/ml Penicillin and 100 µg/ml Streptomycin). All cell lines were incubated at 37˚C and 5 per cent (v/v) CO_2 conditions.

3.2.1. Passage of Cell Lines

A498, ACHN, and HDF cells were subcultured when cells reached to almost 80 per cent cell confluency. After the media was discarded, cell monolayer was rinsed with PBS (Dulbecco's Phosphate-Buffered Saline pH 7.4). Cells were then incubated with 25 per cent Trypsin / 5 mM EDTA solution in PBS (pH 7.4) at 37˚C for 5 minutes. Detached cell suspension was mixed with 10 per cent FBS (v/v) complete DMEM in two times the volume of trypsin to inhibit trypsin activity. Cell suspension was centrifuged at 300 *x g* for 5 minutes. Supernatant was discarded, and cell pellet was resuspended in complete growth medium and seeded in a new tissue culture flask.

3.2.2. Determination of Cell Number

Hemocytometer was used for cell counting. 10 µl aliquot of cell suspension was loaded into the square of hemocytometer. The cells were counted in three times, into the middle of square under the inverted light microscope with using 20x objective. Cell concentration was calculated with the equation as:

"Cell Number/ml = Number of Counted Cell *X* Dilution Factor/mm^2 *X* Chamber Depth".

3.2.3. Cryopreservation of Cell Lines

After cell trypsinization and cell counting, cells were suspended with freezing mixture. Freezing mixture was composed of 10 per cent (v/v) Dimethyl Sulfoxide (DMSO) in heat

inactivated FBS. Approximately $1x10^6$ cell pellet was suspended with 1ml freezing mixture and transferred into the cryovial. Firstly, cryovials were placed in -80˚C freezer for at least 16 hours then transferred into the liquid nitrogen tank for long term storage.

3.2.4. Thawing of Cell Lines

Cryopreserved cells in cryovial were taken from the liquid nitrogen or -80˚C freezer and rapidly warmed up to 37˚C. Cell suspension was added into the complete DMEM dropwise with to prevent cell disruption due to osmatic pressure difference between freezing mixture and medium. Cell suspension was centrifuged at 300 *x g* for 5 minutes. Supernatant was discarded, and cell pellet was suspended in complete DMEM and cells were seeded in a tissue culture flask. After the cells attached to the flask approximately 12-24 hours, the medium was exchanged with fresh complete DMEM to remove excess DMSO in the medium.

3.3. BIOCHEMICAL ANALYSIS

3.3.1. Cell Cytotoxicity Assay

In order to determine the cellular toxicity of H_2O_2 treatment and 2-Hydrazine 5-Nitrophenol labeling, WST-1 cell cytotoxicity assay was applied to A498, ACHN, and HDF cells.

3.3.1.1. Cytotoxicity of H_2O_2 Treatment

A498, ACHN and HDF cells were seeded at a density of 10.000 cell/well and HDF cells were seeded at a density of 5000 cell/well into 96-well plate, then the cells were incubated for 9 hours. The cells were treated with 0.5, 1, 1.5, 2, and 2.5 mM H_2O_2 in FBS free standard DMEM for 120 minutes. Following H_20_2 treatment, the medium was changed with standard complete DMEM and cells were incubated at 37˚C for 24 hours. In standard complete DMEM, 10 per cent WST-1 reagent was dissolved and 50 µl of the WST-1 mix was placed into the cells to be incubated for 1 hour at 37˚C. Absorbance values were measured at 450

nm and 650 nm. Background absorbance at 650 nm was subtracted from formazan absorbance at 450 nm by Varioskan Lux Multimode Microplate Reader.

3.3.1.2. Cytotoxicity of 2-Hydrazine 5-Nitrophenol Labeling

A498, ACHN and HDF cells were plated at a density of 10.000 cell/well and HDF cells were plated at a density of 5000 cell/well into 96-well plate, then the cells were incubated for 9 hours. The cells were treated with 5, 10, 15, 20, 25, and 50 µM 2Hzin5np in PBS (pH 7.4) for 30 minutes at 37°C. Labeling reagent was then discarded, and cells were washed with PBS (pH 7.4). The cells were incubated with standard complete DMEM at 37˚C for 24 hours. In order to measure cell viability, 50 µl of standard complete DMEM containing 10 per cent WST-1 reagent was placed into each well for 1 hour at 37˚C. The cell viability was determined using WST-1 reagent as described in Section 3.3.4.1.

3.3.2. Hydrogen Peroxide Concentration Optimization

A498 and ACHN cells were seeded into 96 well plate ($10x10^3$ cell/well) and incubated for 24h. After 24 hours later, the medium was discarded, and cells were rinsed with PBS (pH 7.4), then treatment mediums in different concentration were added on the cells. A498 and ACHN cells were treated with 1, 2, 2.5, 3, 3.5 and 4 mM H_2O_2 in FBS free standard DMEM with incubation for 120, 180, 210, and 240 minutes. The cells were imaged with inverted light microscope at room temperature within 10 minutes after treatment was completed.

3.3.3. Reactive Oxygen Species Detection Assay

Detection of ROS level after hydrogen peroxide treatment, cells were labeled with DCFDA (2′, 7′-Dichlorofluorescin Diacetate) which is a cellular reactive oxygen species detection assay kit. A498 and ACHN cells were counted and seeded in to 96 well plate ($10x10^3$ cell/well) and incubated for 24 hours. While A498 cells were incubated with 2.5 mM H_2O_2, ACHN cells were incubated with 2 mM H_2O_2 in FBS free standard DMEM for 120 minutes. After treatment, the medium was discarded, and cells were washed with PBS (pH 7.4). 50 µl of 20 µM DCFDA in PBS (pH 7.4) was loaded into each well and the cells were incubated

for 3 minutes in dark at room temperature. Then, cells were washed with PBS (pH 7.4) and the cells were immediately imaged with fluorescence microscope by using green fluorescence filter.

3.3.4. Optimization of 2-Hydrazine-5-nitrophenol Labeling Concentration

A498 cells were seeded 96-well plate (7500 cells/well) and incubated for 48 hours. Cells were then treated with 2.5 mM H_2O_2 in FBS free standard DMEM for 2 hours at 37˚C. After the removal of H_2O_2 containing medium, cells were rinsed with PBS (pH 7.4). Both H_2O_2 treated and control A498 cells were then labeled with 10 µM, 15 µM and 20 µM 2-Hydrazine-5-nitrophenol in FBS free DMEM for 30, 60, 90 and 120 minutes at 37˚C. Finally, cells were imaged under fluorescence microscope using green fluorescence filter at each incubation period.

ACHN cells were seeded 96-well plate (7000 cells/well) and incubated for 48 hours. The cells were then incubated in FBS free standard DMEM treated with and without 2.5 mM H_2O_2 for 2 hours at 37˚C. After the treatment medium was discarded, the cells were rinsed with PBS (pH 7.4). Cells were labeled with 10, 15, 20, and 25 µM 2-Hydrazine 5-Nitrophenol in FBS free DMEM for 15, 30, 45, 60, 75, 90, 105 and 120 minutes in CO_2 incubator at 37˚C.

3.3.5. Inhibition of Hydrogen Peroxide Induced Carbonylation

A498, ACHN, and HDF cells were seeded on cover glasses in 6 well plate ($5x10^5$ cell/well) and allowed to rest overnight. Following wash of the monolayers using PBS (pH 7.4), cells were incubated with 0 mM, 1 mM, 2 mM sodium pyruvate in complete DMEM for 1 hour at 37˚C. After incubation, cells were treated with H_2O_2 in FBS free DMEM containing 0 mM, 1 mM, 2 mM sodium pyruvate at 37˚C for 2 hours. After H_20_2 treatment, the medium was discarded, and cells were washed once with PBS (pH 7.4). A498 cells were labeled with 20 µM 2Hzin5nitrophenol, ACHN and HDF cells were labeled with 15 µM, in PBS (pH 7.4) for 30 minutes. Wells were washed with PBS (pH 7.4) and cover slides were placed onto the glass slide and mounted with a drop of ClearMount medium. Samples were imaged by

confocal microscopy and fluorescence intensity of cell lysate was measured with Varioskan Lux Multimode Microplate Reader.

3.3.6. Serum Starvation Induced Carbonylation

A498, ACHN and HDF cells were seeded on cover slide in 6well plate ($5x10^5$ cell/well) and incubated overnight. Cells were incubated in standard DMEM in the presence or absence of 10 per cent FBS for 16 hours. After 16 hours incubation, while A498 cells were labeled with 20 µM, ACHN and HDF cells were labeled with 15 µM 2-Hydrazine-5-nitrophenol in PBS (pH 7.4) for 30 minutes. Specimens were prepared as mentioned in Section 3.3.5 in order to capture the confocal images and measure the fluorescence intensity of the labeled cells.

3.3.7. DAPI Staining

A498 ($5x10^5$ cells/well) cells were seeded onto cover glasses that were placed into 6-well-plate. After overnight incubation, the cells were treated and labeled as described below (Section 3.3.4). End of the treatment and labeling steps, the cells were washed with PBS (pH 7.4) and cells nuclei were labeled with 50 µg/ml DAPI in PBS (pH 7.4) at room temperature for 30 minutes in dark. To remove the excess stain, cells were washed with PBS (pH 7.4) for 3 times and the cover glasses were placed onto a drop of mounting media placed onto the glass slides. Specimens' images were captured using Zeiss LSM 800 confocal microscope.

3.3.8. DETECTION OF CARBONYLATED PROTEINS

Cell pellets of A498, ACHN, and HDF cells were collected after trypsinization step as described above (Section 3.2.1). Cell pellets were washed with PBS (pH 7.4) and centrifuged at 300 x g for 5 minutes. The supernatant was discarded as before and pellets were suspended in the distilled water containing 0.05 mM Phenylmethanesulfonylfluoride Fluoride (PMSF) and one per cent Protease Inhibitor Cocktail (PI). Cells were lysed by six freeze-thaw cycles in liquid nitrogen and water bath at 37°C. If samples were not used immediately for analysis, they were stored at -80°C. Protein content was determined with Lowry assay for the whole cell lysates. The standard curve was plotted with Bovine Serum Albumin (BSA) standards

in the range of 0.05 mg/ml and 1 mg/ml. Cell lysates were diluted 1:5 in distilled water and loaded in 96 well plate as duplicate. Following the addition of 25 µl Reagent A and 200 µl Reagent B into the wells, the plate was incubated for 15 minutes at room temperature in dark. Finally, absorbance value at 750 nm was measured by Varioskan Lux Multimode Microplate Reader.

4. RESULTS

4.1. SPECTROSCOPIC DETERMINATION

4.1.1. Spectrophotometric and Spectrofluorometric Analysis of Azacoumarins

Synthesis of azacoumarin derivatives were shown in Section 3.1.1-3.1.8. Spectrophotometric analysis showed that cyclization of 2-Amino-5-nitrophenol into 3-Methyl-7-nitroazacoumarin led to blue shift between 393 nm and 375 nm in the spectra. On the other hand, reduction of nitro group into amino group caused decrease in energy of the molecule with respect to increase in absorption wavelength into 384 nm that was shown as a red shift spectrum for 3-Methyl-7-amino azacoumarin. Reaction between amino group of azacoumarin and SAL yielded in imine formation. Imine formation was showed as black line in the spectra that two absorption maxima peaks at 292 nm-355 nm were observed with the high blue shift towards the amino azacoumarin. Amine-imine reaction is a reversible reaction. Due to oxygen and air sensitivity of imine, spectroscopic analysis of imine is very challenging.

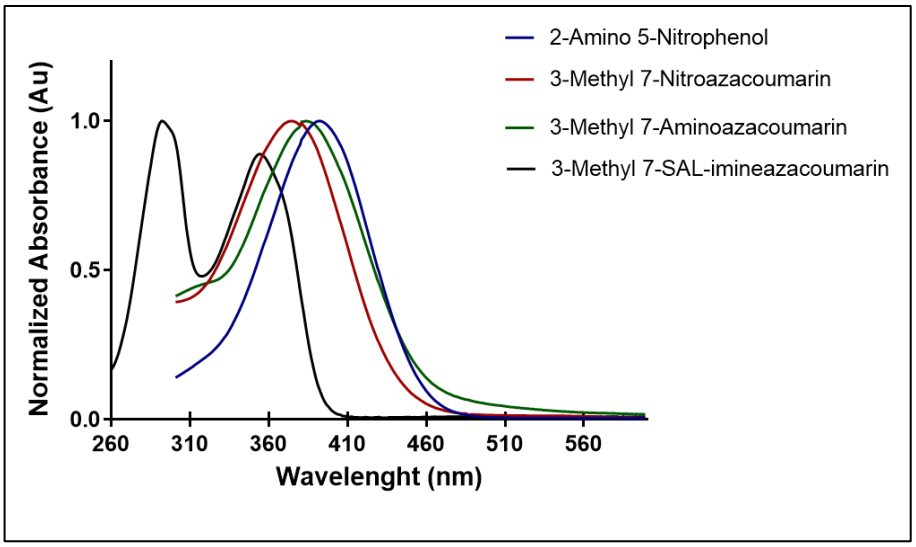

Figure 4.1. Absorption spectra of 3-Methyl 7-SAL-imine azacoumarin synthesis.

Absorption spectra of all products were performed in polar solvent MeOH. It can be seen from the data in Table 4.1 that the absorption spectra of 3-Methyl-7-hydrazine

azacoumarin indicated 132 nm red shift on reaction with salicylaldehyde to form 3-Methyl-7-Hydrazone azacoumarin. Emission spectra of hydrazine indicated 36 nm red shift to yield fluorescent hydrazone which also provided with 2.5-fold increase in fluorescence intensity.

Table 4.1. Absorption and emission maximum of 3-Methyl-7-hydrazine azacoumarin and 3-Methyl-7-hydrazone azacoumarin

Molecule	**Absorption (nm)**	**Emission (nm)**	**Intensity (ϕ) (CPS)**
3-Methyl-7-hydrazine azacoumarin	238	475	$2x10^5$
3-Methyl-7-hydrazone azacoumarin	370	511	$5x10^5$

Figure 4.2. demonstrated that while 3-Methyl-7-amino azacoumarin had a fluorescent maxima peak at 467 nm with $3x10^5$ CPS fluorescent intensity, 3-Methyl 7-SAL-imineazacoumarin indicated a blue Stoke's shift with fluorescent maxima peak at 430 nm for $3x10^6$ CPS fluorescent intensity. Imine formation was provided with 10-fold fluorescent intensity increase towards amino azacoumarin.

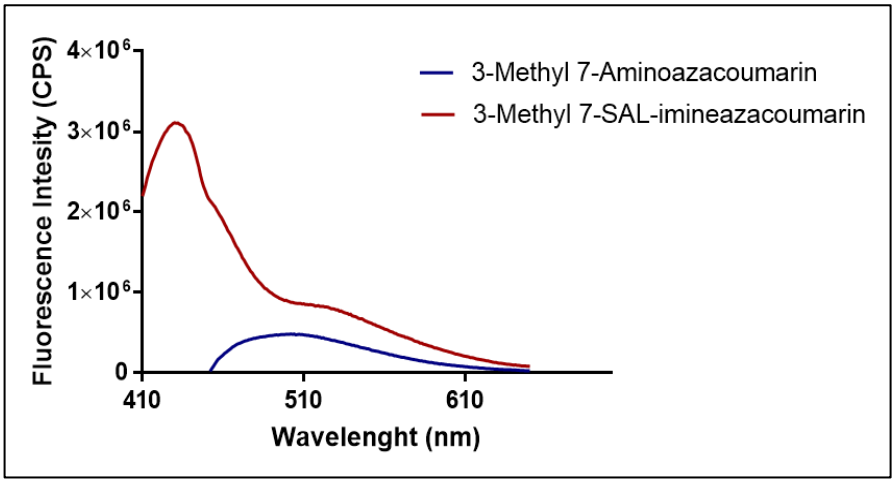

Figure 4.2. Emission spectra of 3-Methyl-7-SAL-imine azacoumarin. 3-Methyl-7-amino azacoumarin was excited at 384 nm and 3-Methyl-7-SAL-imine azacoumarin was excited at 355 nm in MeOH.

Phenyl azacoumarin was a derivative of azacoumarins which had a Phenyl group on third carbon that was shown in Sec.3.1.6-Sec. 3.1.8. According to Figure 4.3, 3-Phenyl-7-nitro azacoumarin had an absorbance maxima peak at 368 nm. Reduction of aromatic nitro group to amine showed an absorption maximum at 382 nm as red shift in the spectrum. 3-Phenyl-7-imine azacoumarin formation was confirmed by high blue shift in the spectrum. Due to reversibility of amine-imine reaction, 3-Phenyl-7-imine azacoumarin had two absorption maxima at 292 nm and 354 nm similar as 3-Methyl-7-imine azacoumarin. Emission spectrum of 3-Phenyl-7-imine azacoumarin was not performed well because of impurities and instability of imine.

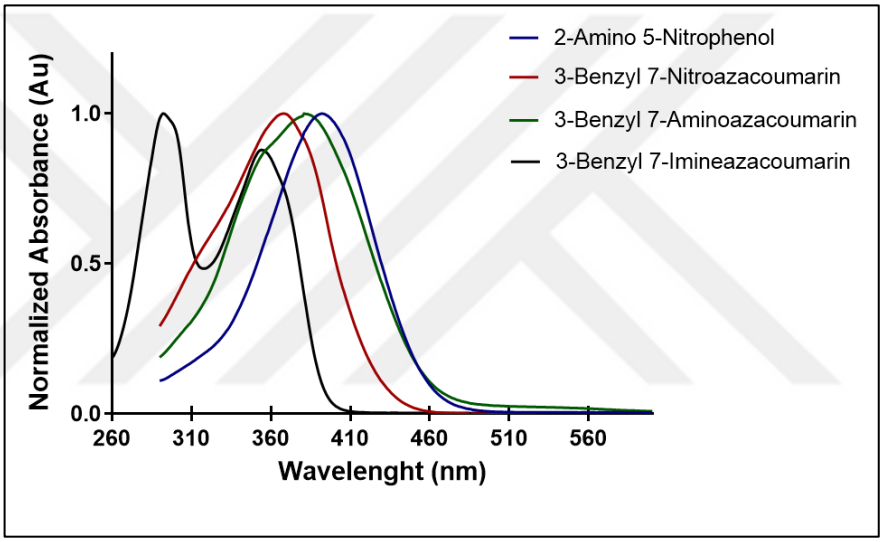

Figure 4.3.Absorption spectra of 3-Phenyl 7-SAL-imine azacoumarin synthesis. Absorption spectra of all products were performed in MeOH. In order to show Stoke's wavelength shift during all reaction steps, normalized absorbance was indicated in the spectra.

4.1.2. Spectroscopic analysis of 2-Hydrazine-5-nitrophenol

2-Hydrazine-5-nitrophenol was synthesized as an alternative of azacoumarins in order to utilize in site-specific labeling of carbonylation in live cells. Due to high dynamic and instability of azacoumarin probes, we focused on designing more stable and applicable probes for live cell labeling.

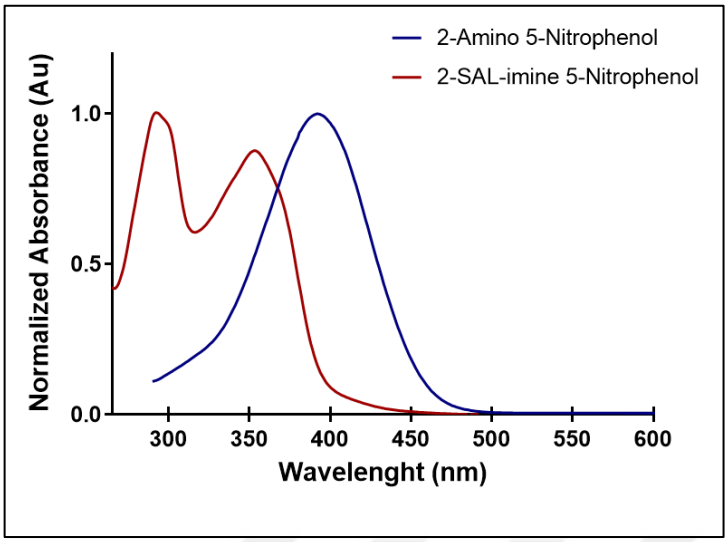

Figure 4.4. Absorption spectrum of 2-SAL-imine-5-nitrophenol formation.

In order to show reaction capability of 2-Amino-5-nitrophenol, imine reaction was examined between amino and salicylaldehyde. 2-SAL-imine-5-nitrophenol had two absorption peaks at 294 nm and 353 nm. Imine nitrophenol was instable like imine form of azacoumarins so its fluorescence emission was not detected clearly.

Diazotization of 2-Amino-5-nitrophenol yielded in 2-Hydrazine-5-nitrophenol which had absorption maximum at 351 nm. Hydrazine was more stable than amine because hydrazine was formed with HCl salt which let dissolving in aqueous solution. Two aldehyde derivatives were reacted with hydrazine to form hydrazone. Acetaldehyde and salicylaldehyde were used as a mimic molecule of carbonyl groups on carbonylated biomolecules. Hydrazine was reacted with acetaldehyde to form 2-Acetyl-hydrazone-5-nitrophenol which showed a red shift to 396 nm. On the other hand, hydrazone reaction between hydrazine and salicylaldehyde showed an absorption maximum at 417 nm that was the highest Stoke’s shift in spectra as shown in Figure 4.5.

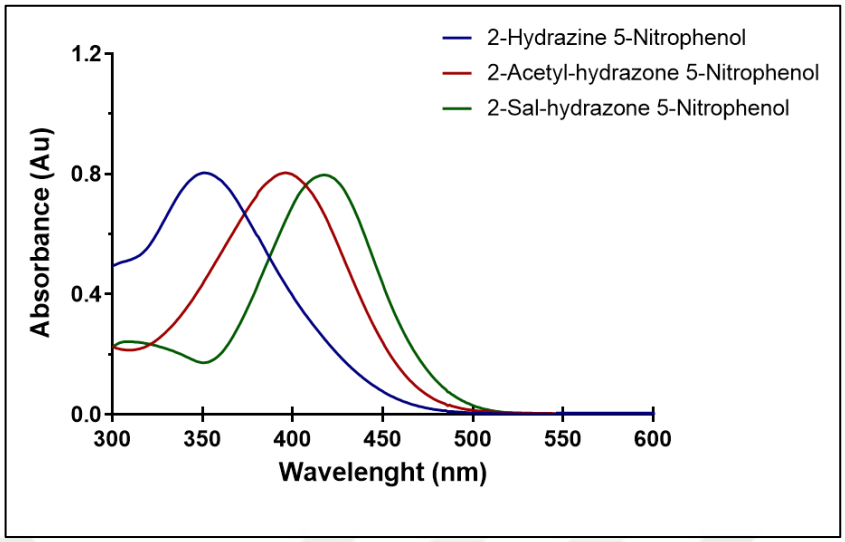

Figure 4.5. Absorbance spectra of hydrazone products. Spectroscopic analyses were performed in MeOH for all samples. Reaction between 2-Hydrazine-5-nitrophenol and acetaldehyde / salicylaldehyde were showed as Red line: 2-Acetyl-hydrazone-5-nitrophenol, Green line: 2-Sal-hydrazone-5-nitrophenol.

Fluorescence emissions of all molecules were detected by Fluoromax 4 Spectrofluorometer with quartz cuvettes in MeOH. 2-Hydrazine-5-nitrophenol was excited at 351 nm and fluorescence emission maximum peak was obtained at 442 nm with $2x10^5$ CPS. 2-SAL-hydrazone 5-Nitrophenol was excited at 417 nm and hydrazone formation was confirmed with fluorescence intensity in to $6x10^5$ CPS at 517 nm. There was 100 nm Stoke's shift on the spectra. When fluorescence intensity of salicylaldehyde hydrazone was compared with hydrazine, there was 3-fold fluorescence intensity increase in MeOH. On the other hand, maximum emission of 2-Acetaldehyde hydrazone-5-nitrophenol was collected from 502 nm. Approximately 106 nm red Stoke's shift was observed for excitation wavelength of 2-Acetylaldehyde hydrazone5-nitrophenol at 396 nm. Figure 4.6 demonstrated that fluorescence intensity of acetyl aldehyde hydrazone was observed as $3.5x10^6$ CPS which provided 12-fold increase in fluorescence intensity of hydrazine.

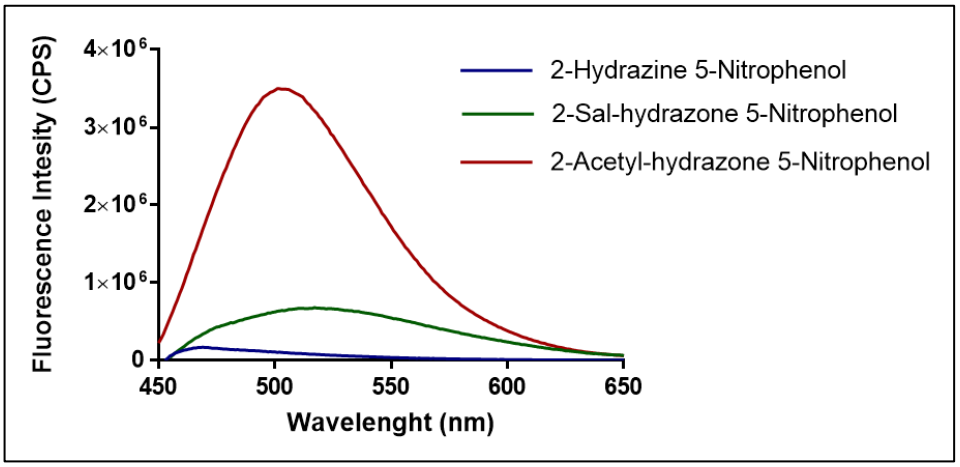

Figure 4.6. Emission spectra of hydrazone derivatives formation. Red line: 2-Acetyl-hydrazone-5-nitrophenol (Ext: 396, Em:502 nm), Green line: 2-Sal-hydrazone-5-nitrophenol (Ext: 417 nm, Em: 517 nm).

4.1.3. Nuclear Magnetic Resonance Spectroscopy of 2-Hydrazine-5-nitrophenol and Its Hydrazone Formations

In section 4.2.1, absorption and emission spectroscopy were applied in order to confirm organic synthesis, however spectrophotometric analyses were not enough to determine the structural formations of molecules. So that, nuclear magnetic resonance (NMR) spectroscopy was employed for the structure confirmation of organic molecules.

Proton NMR (^{1}H NMR) of 2-Hydrazine-5-nitrophenol was showed in Figure 4.7. CH peaks of aromatic structure were observed at a range of 7 ppm and 8 ppm. Hydrazine formation was confirmed with detection of NH and NH_2 peaks in NMR spectrum. While NH protons had a broad peak at 9 ppm, NH_2 had a sharp peak at 3.4 ppm. Proton of OH was indicated at 10 ppm.

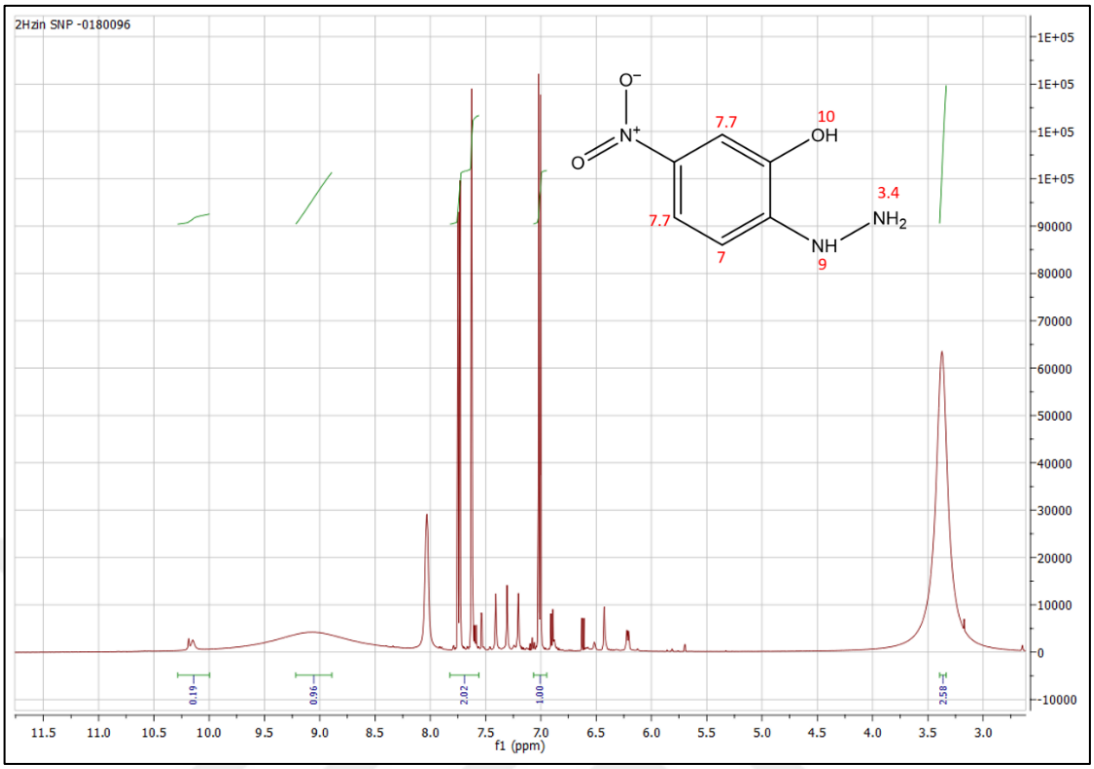

Figure 4.7. ^{1}H NMR spectrum of 2-Hydrazine-5-nitrophenol in DMSO-d_6.

Carbon NMR (^{13}C-NMR) spectrum of 2-Hydrazine-5-nitrophenol was demonstrated in Figure 4.8. Carbon peaks of aromatic structure were observed at a range of 108 ppm 143 ppm.

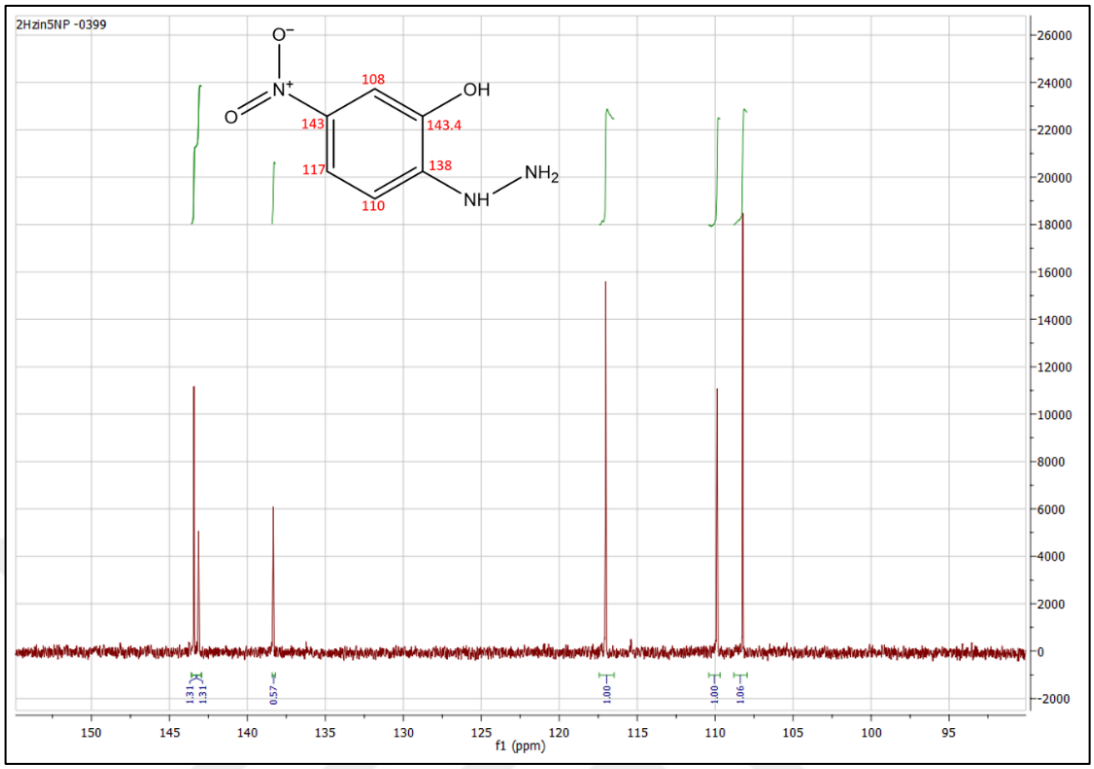

Figure 4.8. ^{13}C NMR spectrum of 2-Hydrazine-5-nitrophenol in DMSO-d_6

The reaction between salicylaldehyde and 2-Hydrazine-5-nitrophenol resulted in deshielding on NH group. Due to decrease in electron density of NH group, NMR peak was downfield shifted to 10.8 ppm. In addition, peak of NH_2 at 3.4 ppm disappeared after the reaction between hydrazine and carbonyl group of aldehydes. When proton NMR spectrums of starting molecule and 2-SAL-hydrazone-5-nitrophenol were compared, presence of the two OH groups on the salicylaldehyde hydrazone led to two similar peaks at 10 ppm and 10.6 ppm as shown in Figure 4.9. As a result of ^{1}H NMR spectrum of 2-SAL-hydrazone-5-nitrophenol, the molecule had been clearly synthesized as mentioned method in Sec.3.1.11.^{13}C NMR spectrum of 2-SAL-hydrazone-5-nitrophenol confirmed the molecule structure with thirteen peaks at between 108 ppm and 156 ppm.

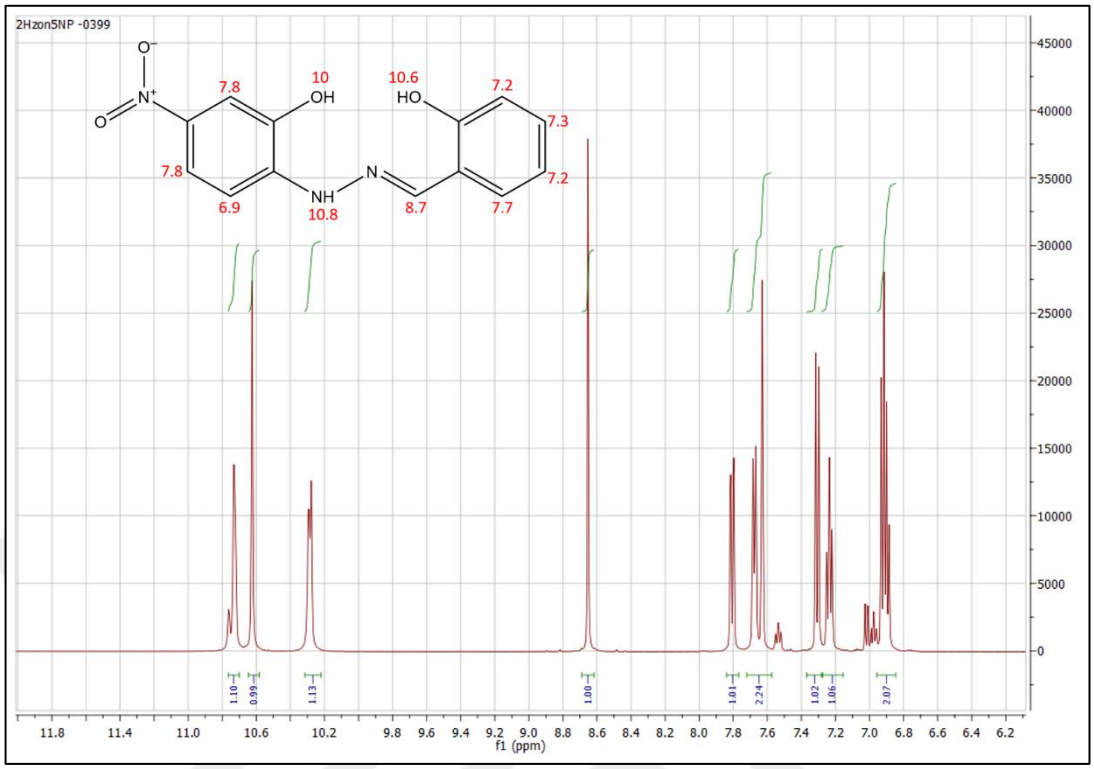

Figure 4.9. ^{1}H NMR spectrum of 2-SAL-hydrazone-5-nitrophenol in DMSO-d_6.

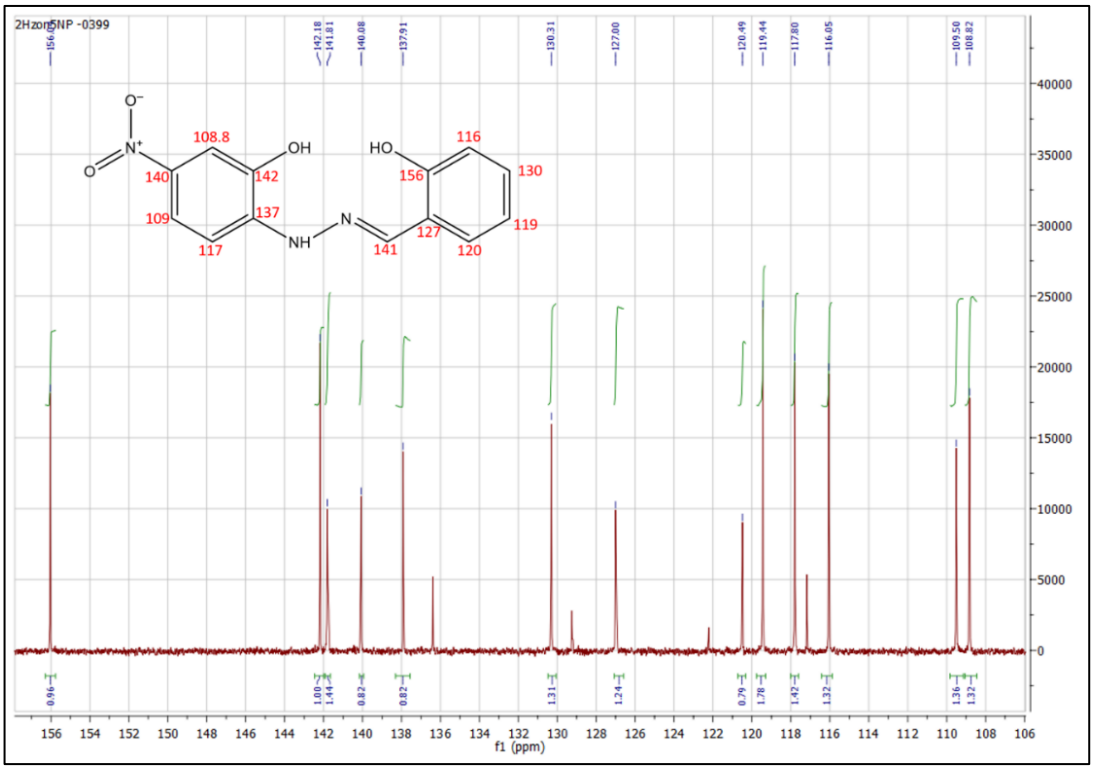

Figure 4.10. ^{1}C NMR spectrum of 2-SAL-hydrazone-5-nitrophenol in DMSO-d_6.

2-Acetyl aldehyde hydrazone-5-nitrophenol formation was approved by NMR spectroscopy. Deshielding of NH peak to 10.83 ppm and appearance of CH_3 peak at 1.31 ppm demonstrated the structural conformation of 2-Acetylaldehyde-hydrazone-5-nitrophenol. However, impurities and solvent peaks were observed in the proton and carbon NMR spectra. According to proton NMR, reaction between hydrazine and acetyl aldehyde had not been completed that was proved by the presence of excess starting materials in the organic molecule. Peak of NH_2 at 4.5 ppm showed the excess hydrazine in the product. Additionally, CH_3 peak of unreacted acetaldehyde was observed at 2 ppm. Furthermore, solvent peak of ethanol was collected from 1 ppm and presence of water was examined with the broad peak at 3.5 ppm.

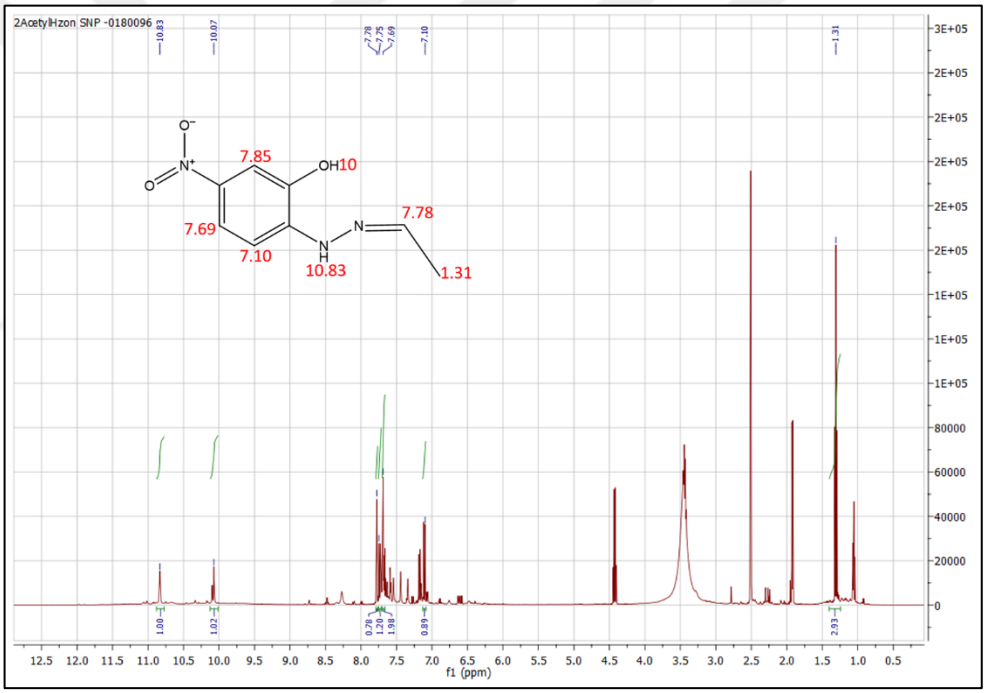

Figure 4.11. ^{1}H NMR spectrum of 2-Acetyl-hydrazone-5-nitro phenol in DMSO-d_6.

^{13}C NMR analysis of 2-Acetyl-hydrazone-5-nitrophenol demonstrated that CH_3 was detected at 13.4 ppm. While starting material acetyl aldehyde has a CH_3 peak at 2 ppm, 2-Acetyl-hydrazone led a downfield shift on CH_3 peak as shown in Figure 4.12.

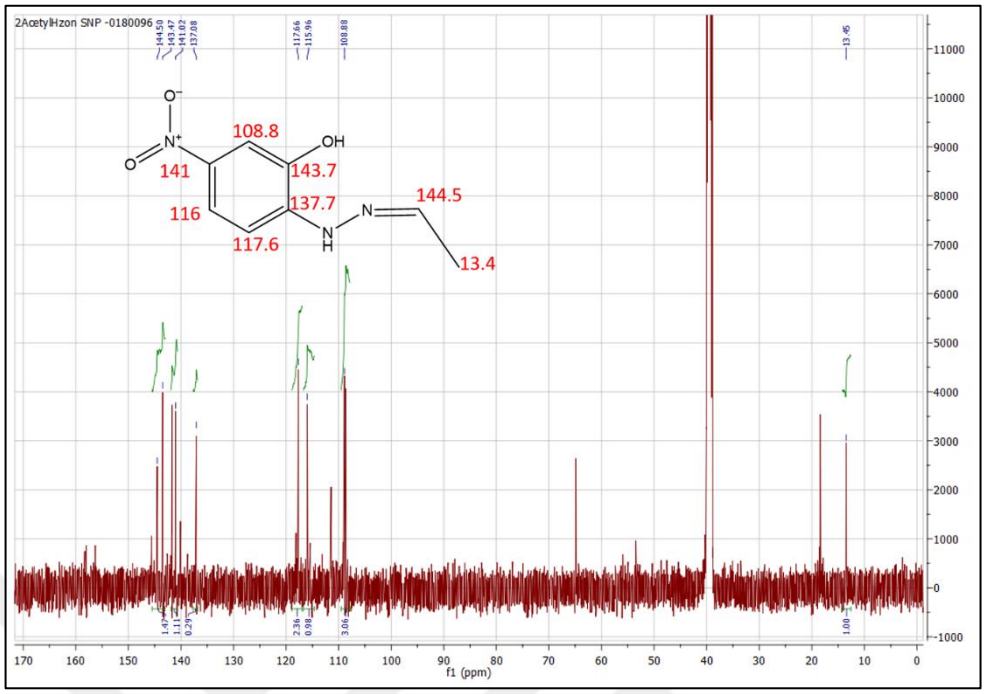

Figure 4.12. ^{1}C NMR spectrum of 2-Acetyl-hydrazone-5-nitrophenol in DMSO-d.

4.2. BIOCHEMICAL ANALYSIS

4.2.1. Cytotoxic Effects of H_2O_2 and 2-Hydrazine-5-nitrophenol

Cytotoxic effects of H_2O_2 and 2Hizn5np on A498, ACHN, and HDF cells were assessed by WST-1 assay (2-[4-Iodophenyl]-3-[4-nitrophenyl]-5-[2,4-disulfophenyl]-2H-tetrazolium). WST-1 is a tetrazolium salt which was reduced to formazan in the presence of mitochondrial dehydrogenases. Cell viability was demonstrated with the colorimetric analysis of formazan formation at 450 nm. A498, ACHN, and HDF cells were treated with H_2O_2 at various concentrations then incubated for 120 minutes. When A498 cells were treated with 0.5 mM, 1 mM and 1.5 mM H_2O_2, the cell viability was decreased to 30 per cent at 24 hours. Likewise, 2.5 mM H_2O_2 treatment inhibited the proliferation of A498 cells with the percentage of 50. While 0.5 mM H_2O_2 treatment did not show any toxic effect on ACHN cells, 1 mM H_2O_2 treatment of ACHN cell decreased the cell viability with the percentage of 20 at 24 hours. 2 mM H_2O_2 and higher concentrations caused a decrease in cell viability up to 60 per cent for ACHN cell line. On the other hand, H_2O_2 treatment of healthy HDF cells with range of 0.5 mM and 2.5 mM resulted in maximum 30 per cent cytotoxicity at 24 hours.

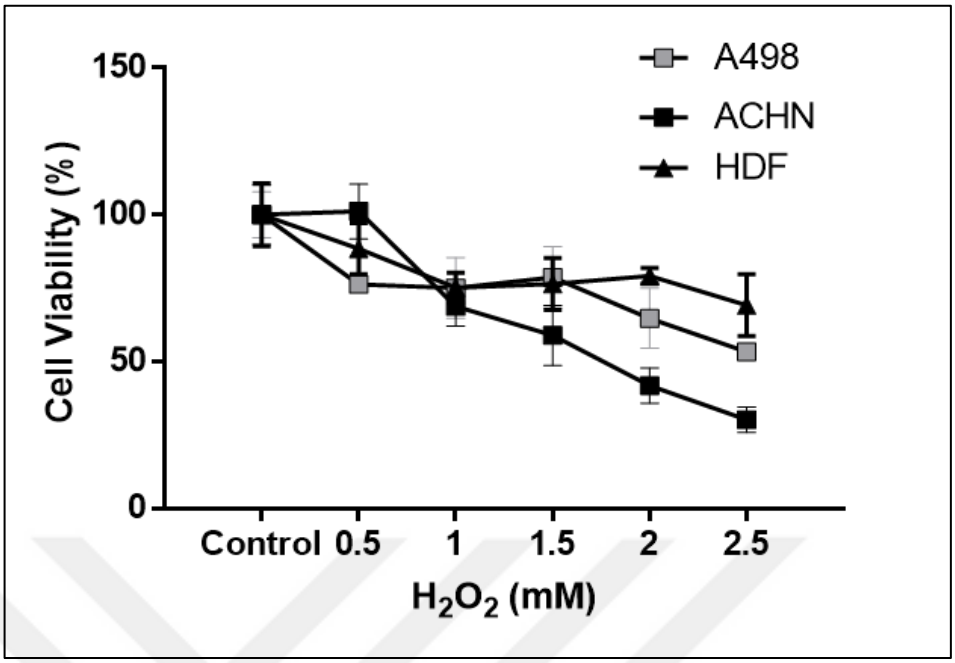

Figure 4.13. Cytotoxic effect of H_2O_2 treatment on cell viability of A498, ACHN, and HDF cell lines. Each data points represents the mean percentage of viable cells after 0.5 mM, 1 mM, 1,5 mM, 2 mM, and 2.5 mM H_2O_2 treatment for 120 minutes. Error bars indicate the standard deviation from a representative experiment in triplicate. Percentage of cell survival was calculated by conversion of absorbance values into percentage of control group.

A498, ACHN, and HDF cells were treated with six different concentrations of 2Hzin5np in PBS (pH 7.4) for 30 minutes to detect the cytotoxic effect of 2-Hydrazine-5-nitrophenol on live cells as shown in Figure 4.14. The 2Hzin5np treated cells were then incubated with standard complete DMEM for 24 hours, then cell viability was detected by WST-1 assay as a colorimetric quantification method of cytotoxicity.

Cytotoxic effect of 5 µM and 10 µM 2Hzin5np on A498 cells was recorded as 10 to 15 per cent, while at 20 µM, cell viability of A498 cell line was decreased by a percentage of 25. 2Hzin5np incubation of A498 cell line at 50 µM caused a highly significant inhibition of cell proliferation by 50 per cent.

When ACHN cells were incubated with 5 to 15 µM 2Hzin5np, there was a slight toxic effect with a decrease in the cell viability by an average of 20 per cent. On the other hand, 2Hzin5np displayed moderate toxicity with an average of 30 per cent at the 20, 25, 35, 50 µM in ACHN cell line.

The treatment of HDF cells with 2Hzin5np resulted in an 20 per cent decrease of cell viability at the concentrations of 5 µM, 20 µM, and 35 µM. Exposure to 2Hzin5np at 10 µM and 15 µM led to an 25 percentage of cytotoxicity in HDF cells, while 50 µM 2Hzin5np incubation resulted in a 35 per cent decrease in the cell viability.

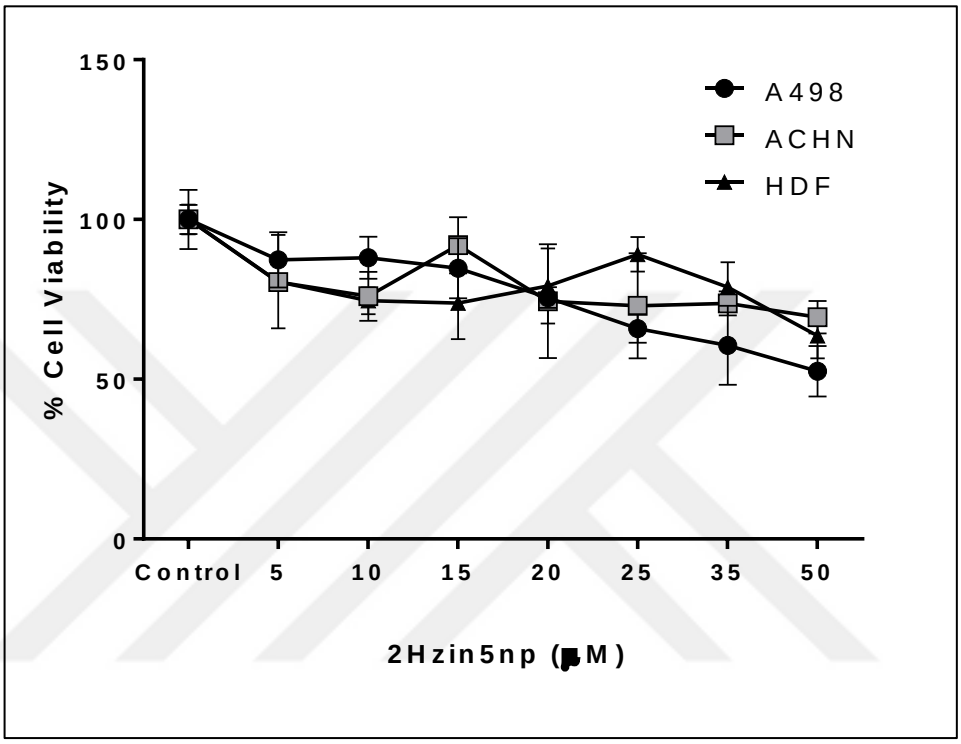

Figure 4.14. Cytotoxic effect of 2Hzin5np on ACHN, A498 and HDF cell line. Cells were treated with 5 µM, 10 µM, 15 µM, 20 µM, 25 µM, and 50 µM 2Hzin5np for 30 minutes and then incubated with standard DMEM for 24 hours. Percentage of cell survival was calculated by conversion of absorbance values into percentage of control group. The error deviations were obtained from a representative experiment.

4.2.2. Optimization of Hydrogen Peroxide Concentration

Hydrogen peroxide induced oxidative stress level was determined by visualizing the morphological changes of live cells, as mentioned in Section 3.3.1. When A498 and ACHN cells were treated with different concentration of H_2O_2 at different time points, cell morphologies were disturbed, and cells were detached from the tissue culture plate surface. The maximum level of oxidative stress, which caused the maximum morphological change without causing cell death was chosen for the later experiments. Figure 4.15 demonstrated that 1 mM, 2 mM and 2.5 mM H_2O_2 treatment did not cause any morphological change on

A498 while 3 mM and concentrations more than 3 mM H_2O_2 led to not only morphological changes and but also reduction in cell viability. In order to obtain maximum nontoxic oxidative stress on A498 cell line, 2.5 mM H_2O_2 treatment for 120 minutes was used in the later experimental setups.

Figure 4.16 demonstrated that after 120 minutes, change in the ACHN cell morphology was obvious at 2.5 mM – 4 mM H_2O_2 concentrations. After 2.5 mM H_2O_2 treatment for 180 minutes, cell aggregates were formed as cells detached from their substratum. In order to prevent H_2O_2 toxicity, the conditions of H_2O_2 treatment was set as 2 mM H_2O_2 for 2 hours.

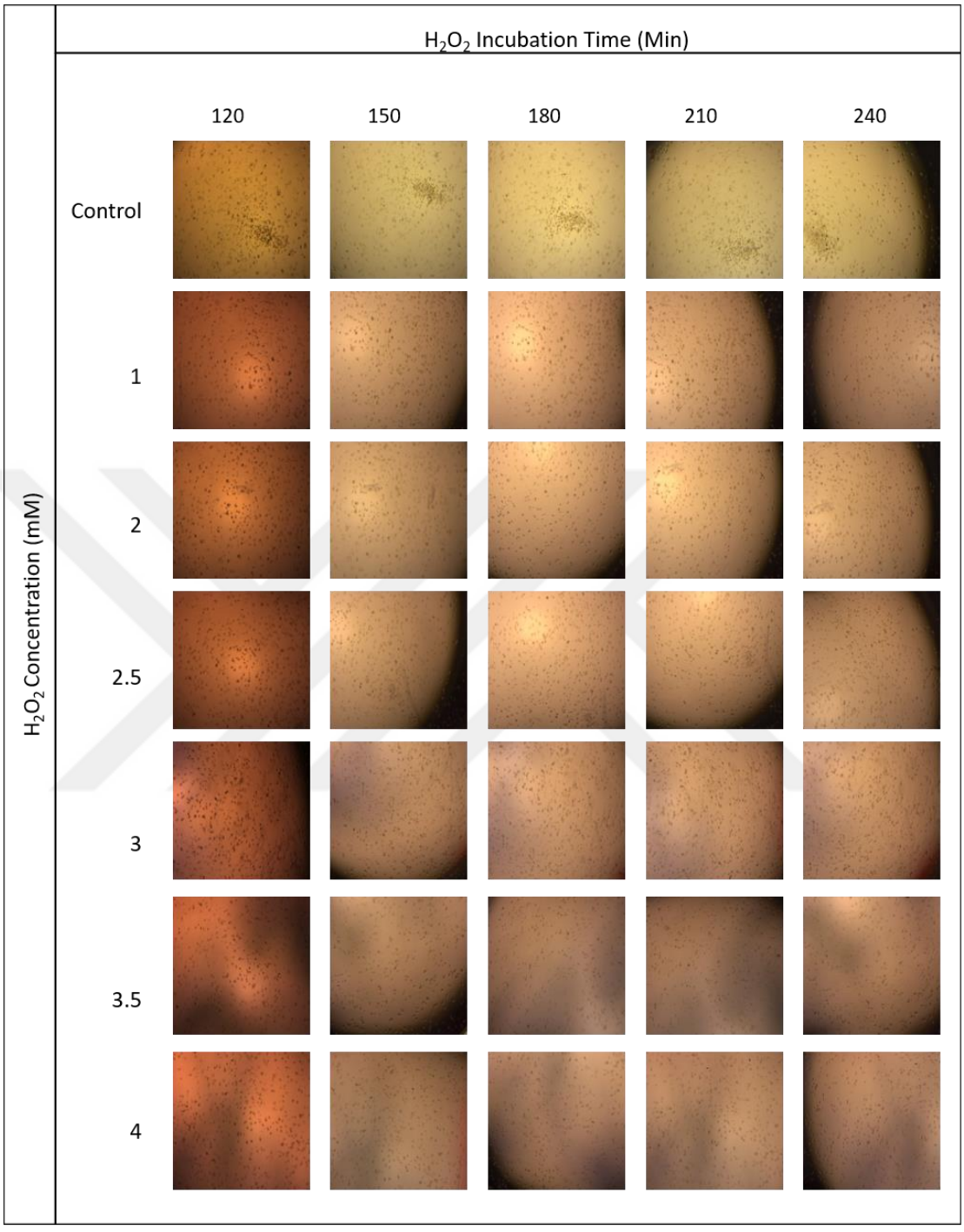

Figure 4.15. Optimization of H_2O_2 concentration and incubation time for A498 cell line. A498 cells were treated with 1 mM, 2 mM, 2.5 mM, 3 mM, 3.5 mM and 4 mM H_2O_2 concentration at five different incubation periods (120, 150, 180, 210 and 240 minutes). Images were captured at each H_2O_2 concentration and time point using 4x objective. The scale bar is equal to 200 µm.

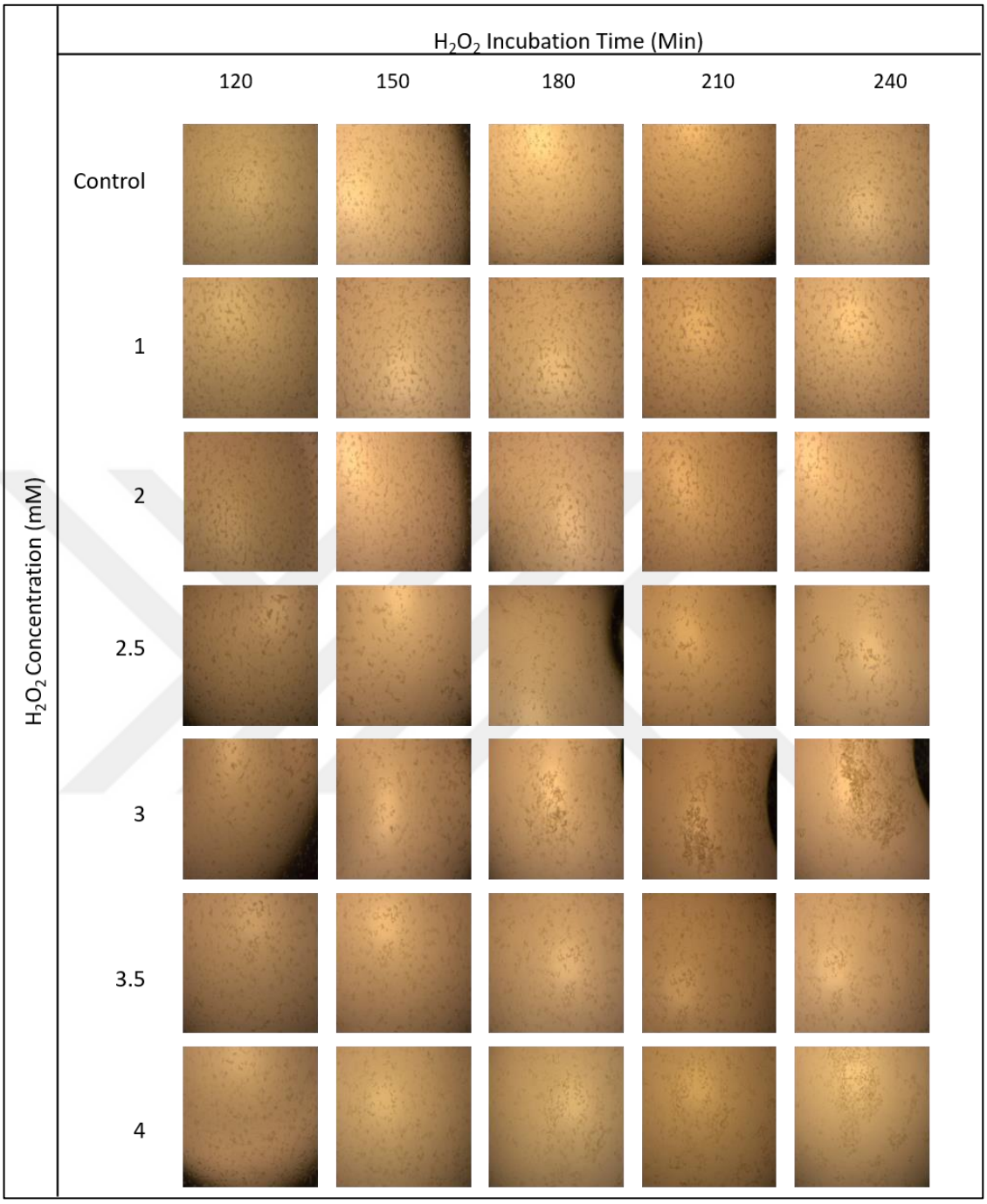

Figure 4.16. Optimization of H_2O_2 concentration and incubation time for ACHN cell line. ACHN cells were treated with six different H_2O_2 concentration (1 mM, 2 mM, 2.5 mM, 3 mM, 3.5 mM, and 4 mM) at five different time points (120, 150, 180, 210 and 240 minutes). Cells were imaged at each H_2O_2 concentration and time point using 4x objective. Scale bar was set to 200 µm.

In order to determine H_2O_2 induced ROS generation, DCFDA assay was employed. All cells were labeled with DCFH-DA as described in Section 3.3.2. In presence of the cellular esterases, DCFH-DA is deacetylated into a non-fluorescent molecule H_2DCF. In the presence of ROS, the H_2DCF is then oxidized into the highly fluorescent molecule DCF, which is therefore serve as an indicator of ROS levels in live cells. In order to analyze whether 2.5 mM H_2O_2 treatment could evoke oxidative response in A498 cells, DCFH-DA assay was employed for A498 cells. As can be seen from Figure 4.17, 2.5 mM H_2O_2 treated A498 cells were positively stained with DCF. DMSO treated group served as negative control and indicated that the death cells could not oxidized H_2DCF into DCF to yield in green fluorescence emission.

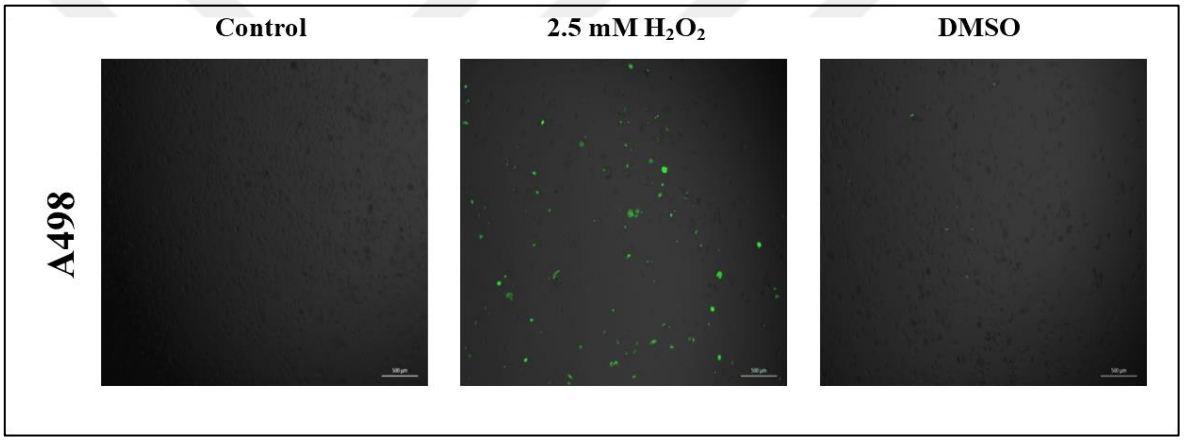

Figure 4.17. DCFDA labeling of A498 cell line for ROS detection. A498 cells were treated with 2.5 mM H_2O_2 and non-treated A498 cells serve as the control. Cells were imaged.

Figure 4.18 showed that 2 mM H_2O_2 treatment of ACHN cells led to an increase in ROS level, which was indicated by the conversion of DCFH-DA dye into DCF, which resulted in florescence emission at 529 nm, when compared to the non-treated control group. In the negative control, cells were treated with DMSO at toxic levels leading to cell solubilization did not yield in green fluorescence emission.

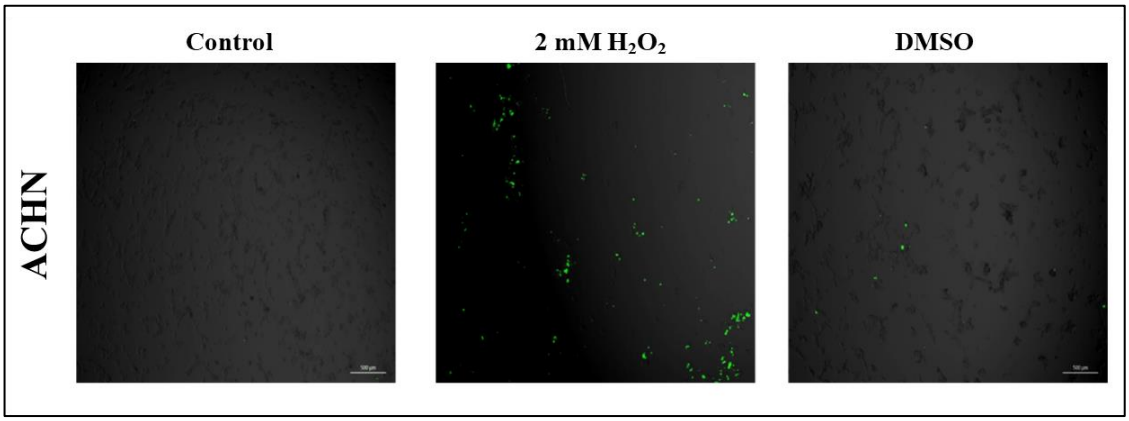

Figure 4.18. DCFH-DA Labeling of ACHN cell line for ROS detection. ACHN cells were treated with 2 mM H2O2 for 120 minutes, while the control group was incubated in standard DMEM and the negative control cells were treated with 10 per cent DMSO to achieve 100 per cent cell death. The bar is equal to 500 µm.

4.2.3. Determination of 2-Hydrazine-5-nitrophenol Concentration Optimization

H_2O_2 induced carbonylation was labeled with different concentrations of 2-Hydrazine-5-nitrophenol for the different incubation periods. 2Hzin5np is a bioorthogonal fluorescent probe which is specific for carbonyl moieties on biomolecules. Carbonylated biomolecules were labeled with 2Hzin5np. In order to determine the level of biomolecule carbonylation in A498 cells, 2Hzin5np labeling was employed for non-treated control cells and H_2O_2-treated cells. Figure 4.19 indicated that A498 cells were fluorescently labeled when treated with 15 and 20 µM 2Hzin5np for 30 minutes. The most efficient labeling condition of carbonylated biomolecules was obtained by incubation of A498 cells with 20 µM 2Hzin5np for 30 minutes. Figure 4.20 demonstrated that the non-treated control group did not show fluorescence emission at 506 nm, which is the maximum fluorescence peak of the 2Hzin5np. H_2O_2 treatment of ACHN cells induced carbonylation as these cells demonstrated the fluorescence emission after 10, 15 and 20 µM 2Hzin5np labeling for 30 minutes incubation. However, the maximum green fluorescence intensity was obtained by labeling H_2O_2 treated ACHN cells with 15µM 2Hzin5np for 30 minutes. When the fluorescence intensity of the H_2O_2-treated ACHN and A498 cells were compared ACHN cells were stained with a wider concentration range of 2Hzin5np labeling while the carbonylation of A498 cells could only be labeled at higher 2Hzin5np concentration.

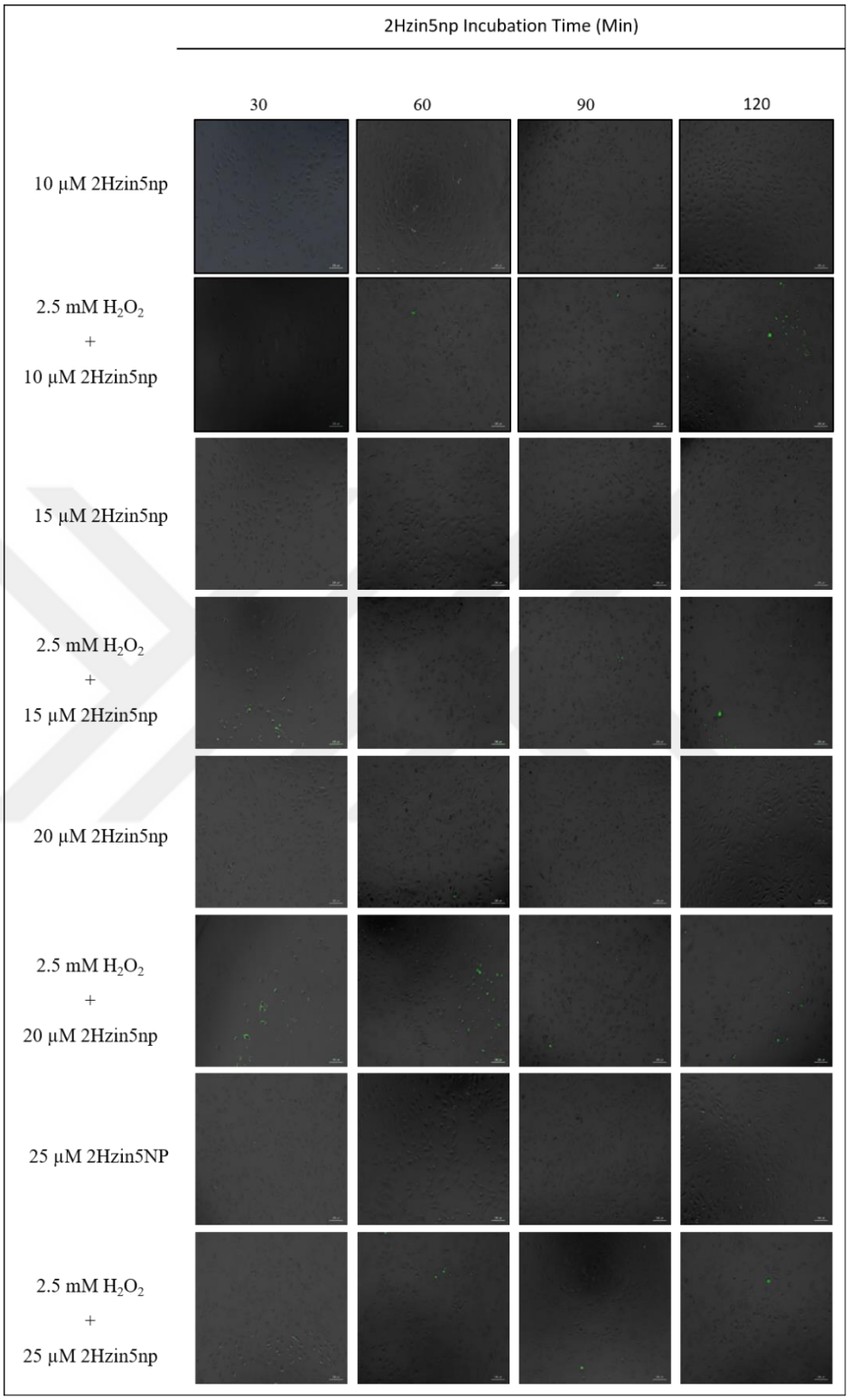

Figure 4.19. Optimization of concentration and incubation period of 2Hzin5np labeling in A498 cell line. Non-treated control and 2.5 mM H_2O_2 treated cells were labeled with 10, 15, 20 and 25 µM 2Hzin5np for 30, 60, 90 and 120 minutes. Scale bar was set to 200 µm.

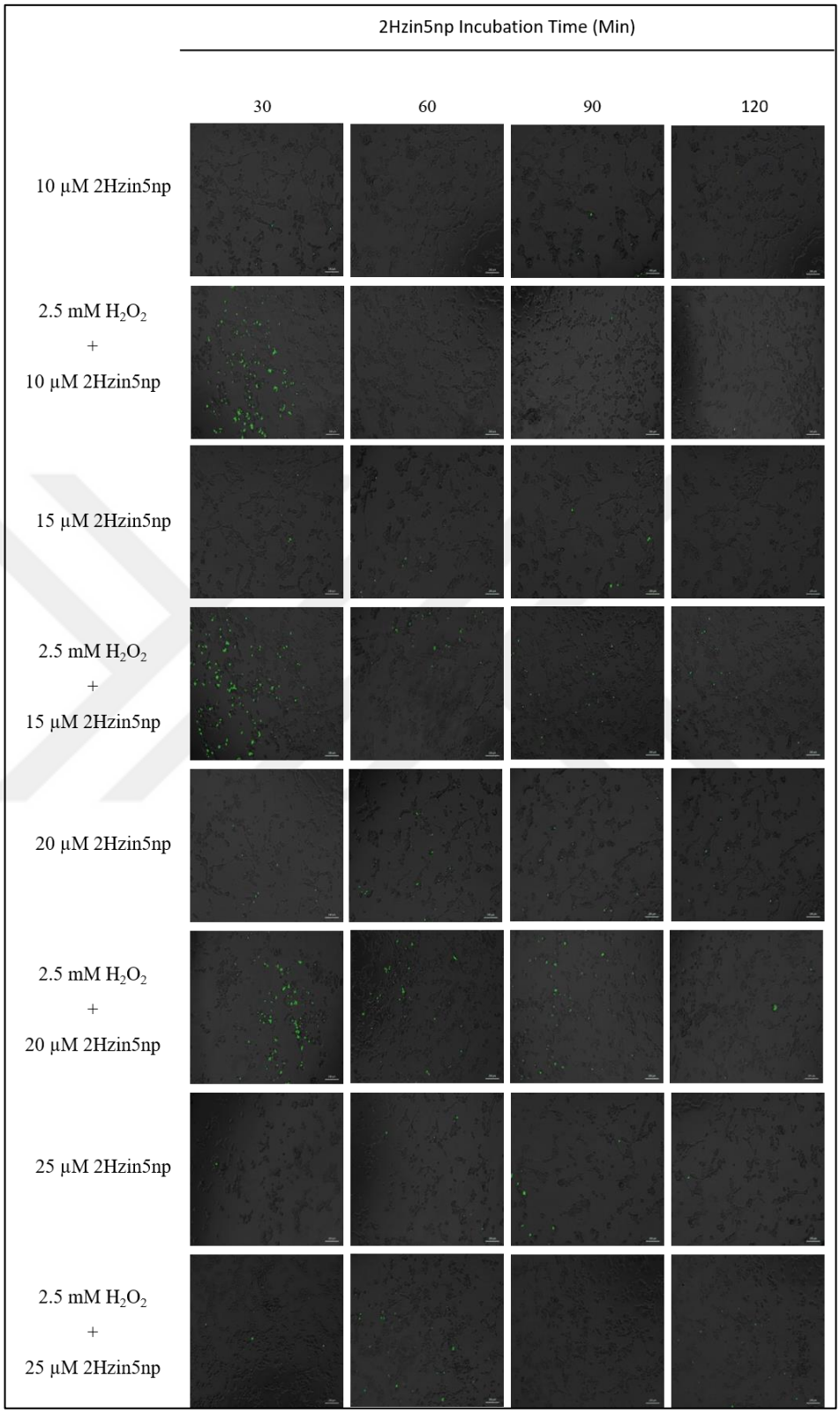

Figure 4.20. Optimization of concentration and incubation period for 2Hzin5np labeling in ACHN cell line. Non-treated and 2.5 mM H_2O_2 pretreated cells were labeled with 10, 15, 20 and 25µM 2Hzin5np for 30, 60, 90 and 120 minutes. Scale bar was set to 200 µm.

4.2.4. Fluorescence Labeling of H_2O_2 Induced Carbonylation

H_2O_2 induced carbonylation of biomolecules in A498, ACHN, and HDF cells were examined by confocal microscopy. H_2O_2 treatment and 2Hzin5np labeling strategies were described in Sec. 3.3.4-5.

As it can be seen in Figure 4.21, A498 cells treated with 2 mM H_2O_2 were effectively labeled with 20 µM 2Hzin5np. Non-treated control group was labeled with 20 µM 2Hzin5np gave a weak background fluorescence intensity. H_2O_2 treated-2Hzin5np labeled A498 cells showed dot-like fluorescence signals around nucleus with an even distribution in the cellular cytoplasm. In addition, while 2Hzin5np labeling provided a fluorescent response in the cytoplasm, nucleus did not show any fluorescent staining.

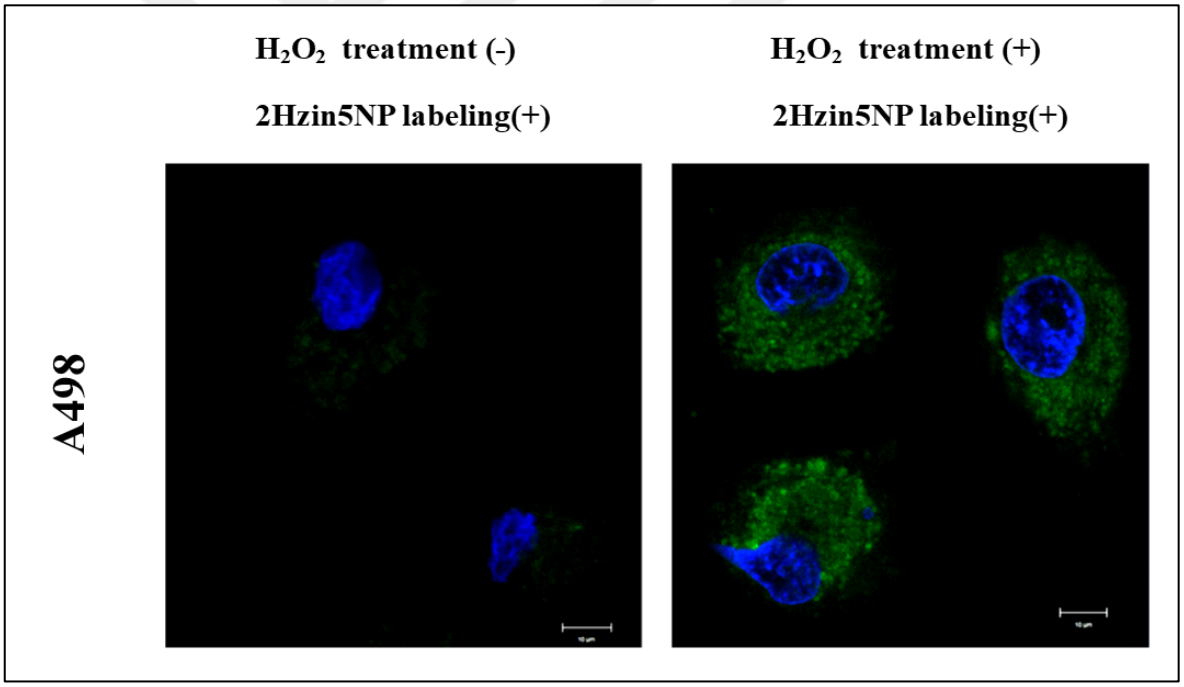

Figure 4.21. 2Hzin5np labeling of H_2O_2 induced carbonylation in A498 cells. Cells grown in standard DMEM containing 1 mM sodium pyruvate, were treated with 2 mM H2O2 for 2 hours. Carbonylation was visualized by 20 µM 2Hzin5np labelling for 30 minutes. 405 nm and 488 nm diode lasers were used for excitation and the emission was monitored using LP 435 and 518 filters in Zeiss LSM 800 confocal microscope. Scale bar was equal to 10 µm.

Given that pyruvate acts a ROS scavenger and inhibits H_2O_2 induced oxidative damages on live cells [176]. In order to intensify the fluorescence intensity of H_2O_2 induced carbonylated biomolecules, DMEM without pyruvate was used in cell culture.

Figure 4.22 demonstrated that the increasing concentration of pyruvate in the medium led to decrease in the fluorescence intensity of H_2O_2 treated and 2Hzin5np labeled A498 cells. The most effective 2Hzin5np labeling was performed by decreasing the pyruvate concentration in the medium. So that pyruvate free DMEM incubated and H_2O_2 treated A498 cells resulted in the highest fluorescent intensity. When non-treated 2Hzin5np labeled control group was incubated with 2 mM sodium pyruvate contained DMEM, A498 cells demonstrated the minimum level of background fluorescence intensity.

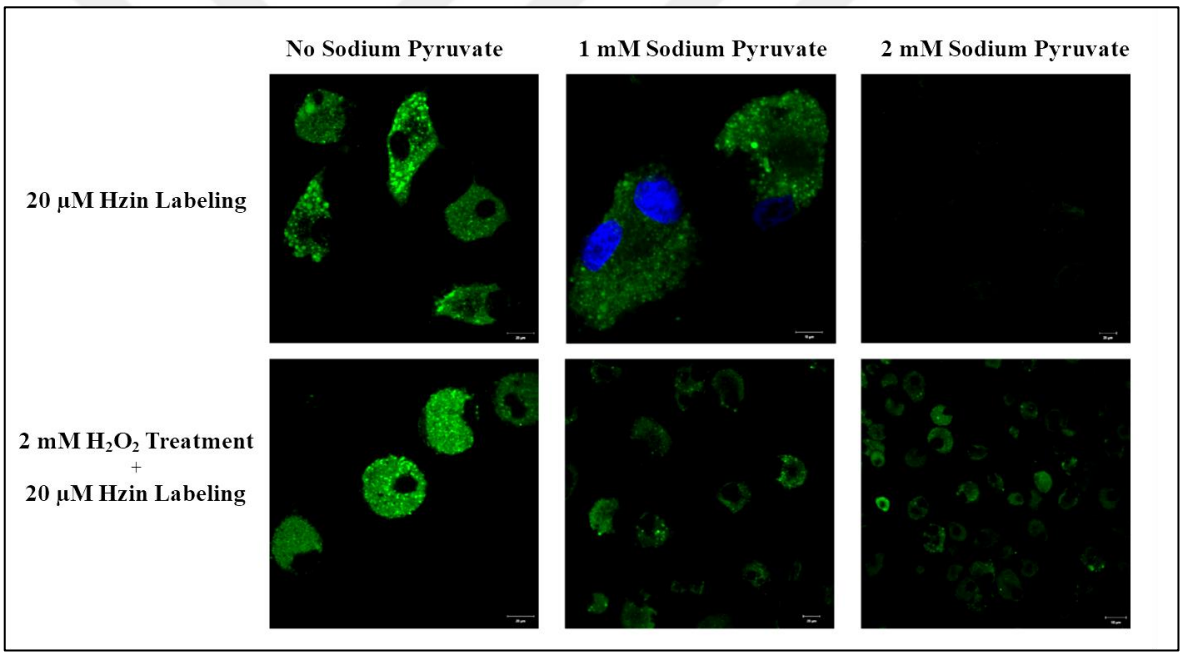

Figure 4.22. Effects of pyruvate concentration dependent inhibition of carbonylation level in A498 cells. A498 cells were incubated DMEM with (1 and 2 mM) without sodium pyruvate prior to 2 mM H_2O_2 treatment and 15 µM 2Hzin5np labeling. 405 nm and 488 nm diode lasers were used for excitation and the emission was monitored using LP 435 and 518 filters in Zeiss LSM 800 confocal microscope. Scale bar was equal to 10 µm.

In Figure 4.23, the use of DMEM without pyruvate in the experimental set up led to an increased fluorescent 2Hzin5np labelling of carbonylation in ACHN cells treated with H_2O_2. As expected, fluorescence intensity of 2Hzin5np labeled cells was decreased by increasing the concentration of pyruvate in the medium. In confirmation to these results, the non-treated

2Hzin5np labeled control cells also gave a stronger background fluorescence intensity in pyruvate free medium, which got weaker by the addition of pyruvate in the culture media.

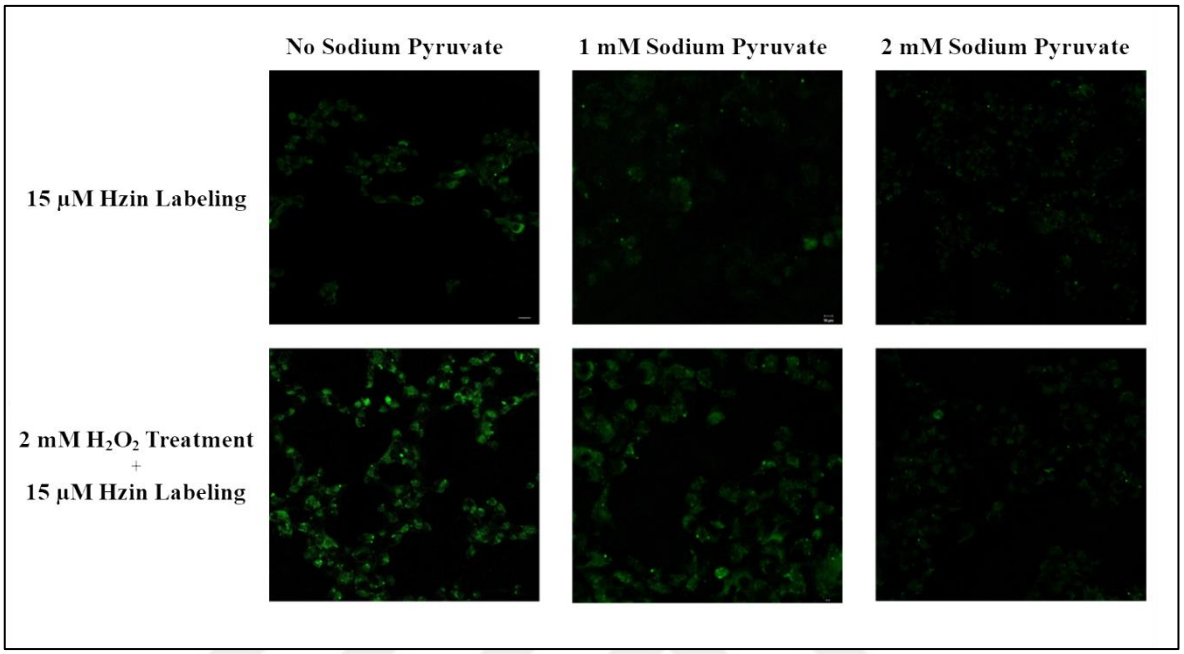

Figure 4.23. Effect of pyruvate on 2Hzin5np labelling of carbonylation in ACHN cells. Cells were incubated DMEM with (1 and 2 mM) without sodium pyruvate prior to 2 mM H_2O_2 treatment and 15 µM 2Hzin5np labeling. 488 nm diode laser was used for excitation and the emission was monitored using LP 518 filter in Zeiss LSM 800 confocal microscope. Scale bar was equal to 10 µm. Images were captured using 10x objective lens.

The presented results of A498 and ACHN demonstrated that the experimental set up of pyruvate free DMEM incubation and H_2O_2 treatment resulted in the maximum fluorescent intensity of 2Hzin5np labeling.

HDF cell line was used as a healthy control group and the optimal H_2O_2 treatment was used as described by Shostak *et al.* [162]. In order to demonstrate H_2O_2 induced carbonylation level of healthy cells, H_2O_2 treated and 2Hzin5np labeled HDF cells were examined by confocal microscopy. As shown below in Figure 4.24, H_2O_2 treated HDF cells indicated a significant increase in fluorescence intensity which provides information about carbonylation level of biomolecules.

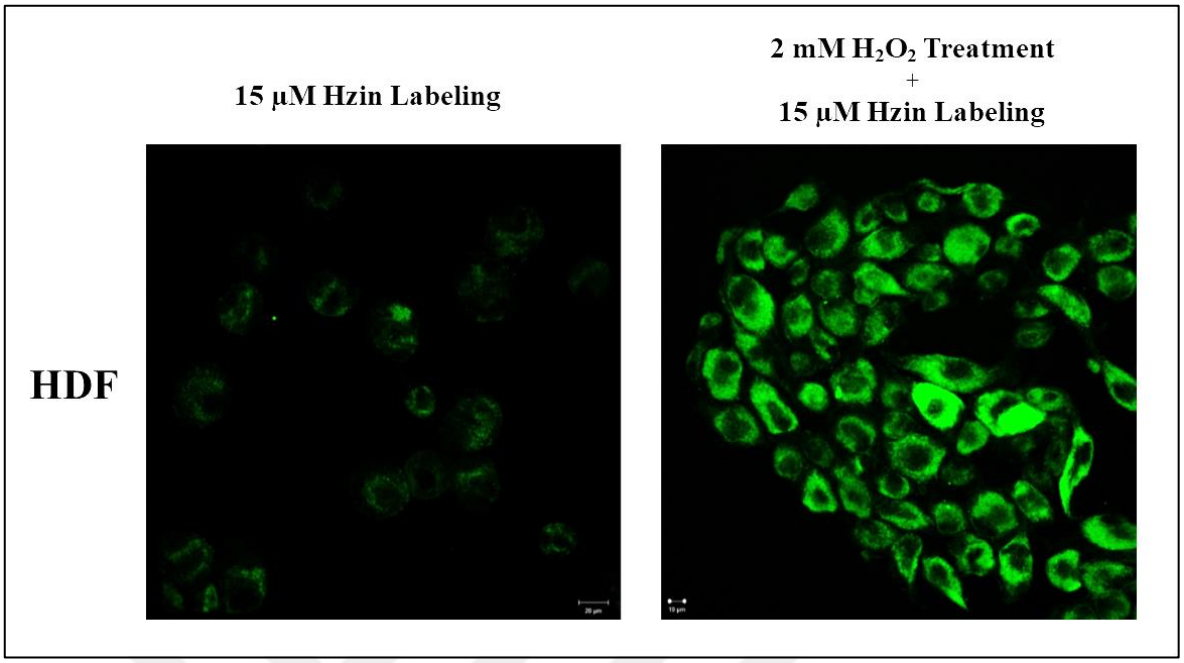

Figure 4.24. 2Hzin5np labeling of H_2O_2 induced carbonylation in HDF cells. Cells grown in standard DMEM without sodium pyruvate, were treated with 2 mM H2O2 for 2 hours. Carbonylation was visualized by 15 µM 2Hzin5np labelling for 30 minutes. 488 nm diode laser was used for excitation and the emission was monitored using 518 filter in Zeiss LSM 800 confocal microscope. Representative image was taken on a confocal microscope by the usage of 40x objective.

4.2.5. 2-Hydrazin-5-nitrophenol Labeling of Serum Starvation Induced Carbonylation

Serum starvation induced ROS generation was introduced by Troppmair and co-workers [177]. In order to detect the effects of endogenous ROS generation on carbonylation of biomolecules, A498 and ACHN cells were serum starved and 2Hzin5np labeled as mentioned Sec. 3.3.6. As shown in Figure 4.25, when cells were incubated with standard DMEM a background fluorescence was detected for both A498 and ACHN cell lines. However, serum starvation led to an induction in carbonylation as increase in fluorescence intensity for both A498 and ACHN cells was evident after 2Hzin5np labelling. Similar to results with obtained for H_2O_2 induced carbonylation labeling, serum starved A498 and ACHN cells did not show any fluorescence emission in the nuclei.

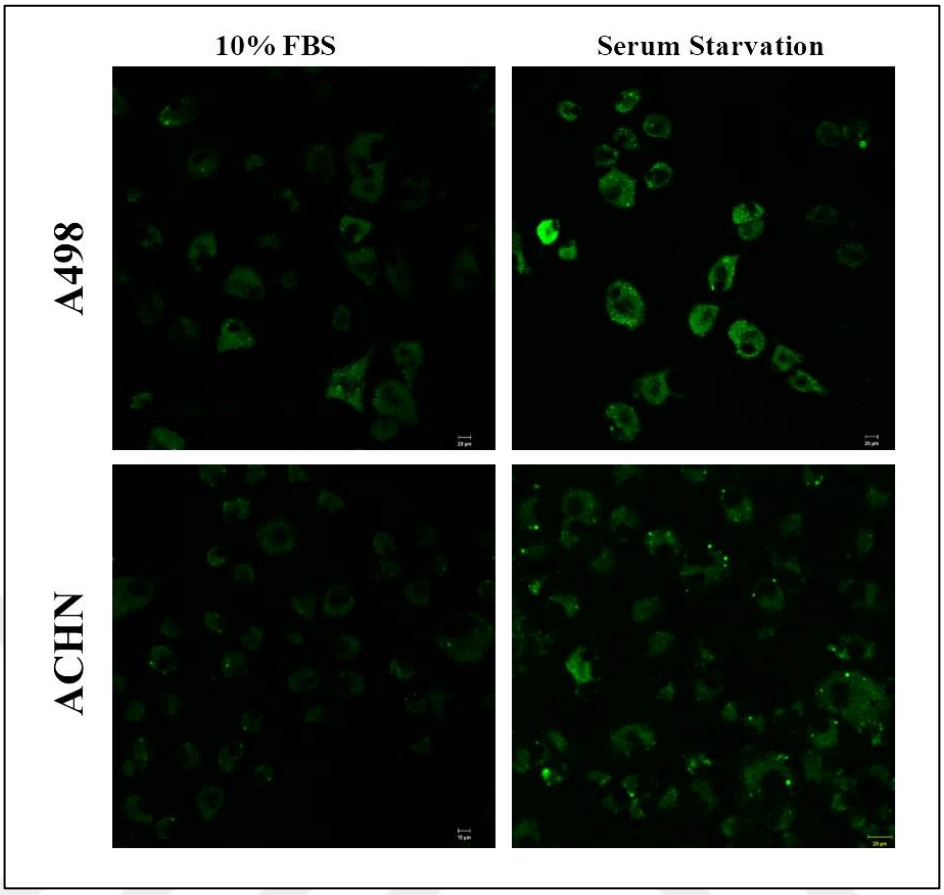

Figure 4.25. Detection of serum starvation induced carbonylation in A498 and ACHN cells. Cells were incubated with and without 10 per cent FBS in DMEM for 16 hours. While A498 cells were labeled with 20 µM, ACHN cells were labeled with 15 µM 2Hzin5np for 30 minutes. Representative image was taken on a confocal microscope using 40x objective. A 488 nm diode laser was used for excitation and LP 518 filter was used for emission.

4.2.6. Quantitative Analysis of Protein Carbonylation

H_2O_2 induced and serum starvation induced protein carbonylation were determined by measuring the fluorescent intensity of 2Hzin5np labeling via Varioskan Lux Microplate Reader.

In order to analyze H_2O_2 induced protein carbonylation in A498, ACHN, and HDF cell lines, cells were treated and labeled as described in Sec. 3.3.5. and total cell lysates were obtained by described method in Sec.3.3.8. Fluorescence intensity of 2Hzin5np labeled cell's lysate

was recorded for each experimental set up. In Figure 4.26. (A), 2Hzin5np labeling of pyruvate free DMEM incubated and H_2O_2 treated A498 cells showed 1.5-fold increase in the fluorescence intensity. On the other hand, 2 mM pyruvate DMEM incubated and H_2O_2 treated A498 cells demonstrated the fluorescence intensity increase in 2-fold. In Figure 4.26. (B), in the absence of the pyruvate, H_2O_2 treated and 2Hzin5np labeled ACHN cells indicated 2-fold increase in fluorescence intensity while 2 mM pyruvate pre-incubated ACHN cells resulted in 2.5-fold increase in fluorescent intensity.

2Hzin5np labeling of non-treated control groups which were incubated with pyruvate free DMEM demonstrated that A498 cell line exhibited 1.8-fold more protein carbonylation compared to ACHN cell line. In addition, H_2O_2 treated A498 cells demonstrated 1.5-fold higher protein carbonylation level in comparison to ACHN cells in absence of pyruvate.

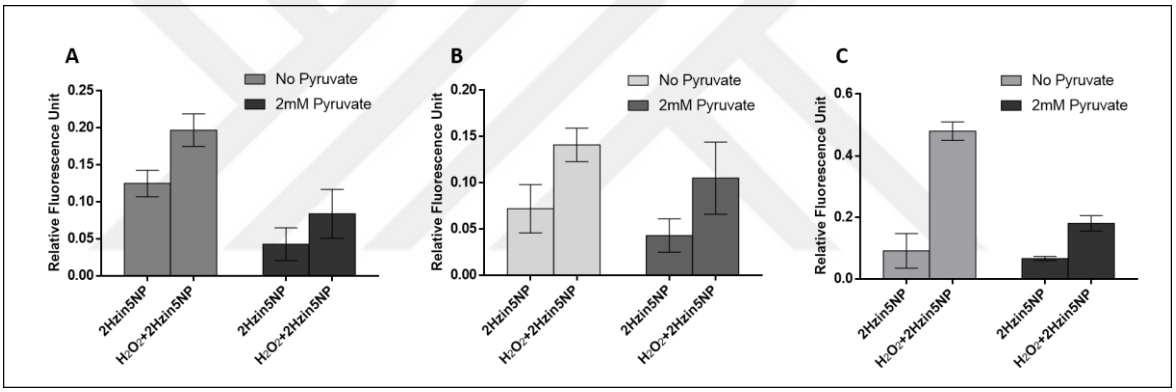

Figure 4.26. Effects of pyruvate concentration dependent inhibition of carbonylation level in (a) A498, (b) ACHN, and (c) HDF cells. Cells were incubated DMEM with and without 2 mM sodium pyruvate prior to 2 mM H_2O_2 treatment and 15 µM 2Hzin5np labeling. Cells were then lysed by six freeze-thaw cycles in lysis buffer (0.05 mM PMSF, 1 per cent PI). Cell lysates loaded into black 96-well plate and fluorescence intensities were measured by Varioskan Multimode Plate Reader. 2Hzin5np labeled A498 ACHN, and HDF cells lysates were excited at 396 nm and emitted at 506 nm. The autofluorescence intensity of control groups were respectively subtracted from all experimental groups. Each data point represents to the mean of fluorescence intensity of at least three separate experiments performed for each cell. (P<0.05)

HDF cell was used a healthy experimental group. 2Hzin5np labeling of pyruvate free DMEM incubated HDF cells showed 5.3-fold increase in fluorescent response. 2 mM

pyruvate containing DMEM incubated HDF cells demonstrated 1.1-fold greater fluorescence intensity in H_2O_2 induced carbonylation of HDF cell line (In Figure 4.26. (C)). In order to detect serum starvation induced carbonylation levels in A498 and ACHN cell lines, cells were either serum starved or incubated in 10 per cent FBS containing DMEM and then labeled with 2-Hzin5np as described in Section 4.2.5. The relative fluorescence was detected using a Varioskan Multimode Plate reader. Serum starved A498 cells demonstrated 2.5-fold fluorescent intensity than 10 per cent FBS containing DMEM incubated A498 cells. Serum starved ACHN cells showed 1.7-fold enhanced protein carbonylation level from 10 per cent FBS containing DMEM incubated ACHN cells. In addition, carbonylated protein level of serum starved ACHN cell line was 1.7 times higher than carbonylation level of serum starved A498 cell line. Comparison between of A498 and ACHN cell lines incubated with 10 per cent FBS supplemented standard DMEM demonstrated that ACHN cells showed 2.5-fold higher carbonylation levels than A498 cells.

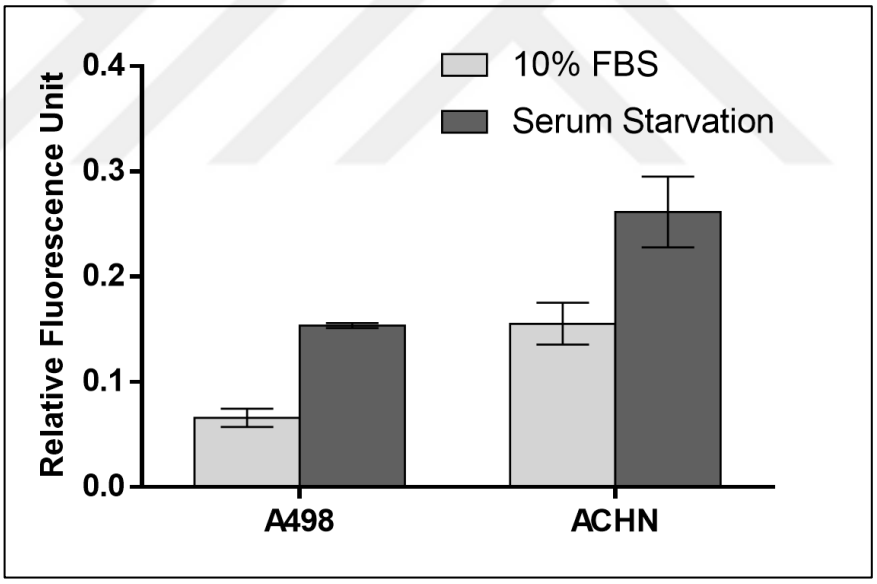

Figure 4.27. Detection of serum starvation induced carbonylation in A498 and ACHN cells. Cells were incubated with and without 10 per cent FBS in DMEM for 16 hours. While A498 cells were labeled with 20 µM, ACHN cells were labeled with 15 µM 2Hzin5np for 30 minutes. Cells were then lysed by six freeze-thaw cycles in lysis buffer (0.05 mM PMSF, 1 per cent PI). Cells lysates were excited at 396 nm and emitted at 506 nm. The autofluorescence intensity of control groups were respectively subtracted from all experimental groups Error bars indicate the standard deviation from a representative experiment in triplicate. (P<0.05)

5. DISCUSSION

Bioorthogonal chemistry is a click reaction concept which relies on the ligation between a chemical probe and a chemical reporter on biomolecules. Drug discovery and live cell imaging are the major applications of bioorthogonal chemistry. Recent developments in bioorthogonal chemistry have heightened the need for the site specific labeling of biomolecules *in vitro* and *in vivo*. There has been an increasing trend of literature on investigating novel fluorescent probes in order to perform accelerated and selective bioorthogonal reactions. Recent studies focused on PTM specific labeling [163, 167] and also multi-color labeling of biomolecules [178].

PTM specific bioorthogonal labeling provides either detection of specific moieties on biomolecules [62] or enzyme activities in live cells [90]. Bane and co-workers developed a coumarin based hydrazine molecule which was specific for aldehyde group in live cells [163]. They investigated an aldehyde-hydrazine reaction in order to detect the oxidative stress induced carbonylation in cancer cells. Fluorescence analysis of coumarin hydrazine which had emission maximum at 450 nm with excitation at 360 nm was performed. The past ten years have seen increasingly rapid advances in the field of designing red shifted (NIR) probes in order to decrease excitation energy of the probe to eliminate phototoxicity of the labeling and reduce autofluorescence level [179].

In this thesis, coumarin hydrazine was derivatized into azacoumarin by introducing nitrogen at coumarin's 4-position to provide the red stoke shift absorption and maximum emission. Introduction of electronegative nitrogen decreases the energy of the LUMO which results in HOMO-LUMO energy gap causing the red shift in the spectrum [180]. Mukherjee *et al.* demonstrated that coumarin hydrazone resulted in 101 nm shift in red range on the emission maximum, while here in this study we showed that 3-Methyl-7-hydrazone azacoumarin provided a 141 nm red shift giving a higher emission (Table 4.1) [62]. Our results indicated that bathochromic effect of nitrogen in azacoumarin and increased the molecular conjugation due to hydrazone formation resulting in red shift of the emission spectrum. In order to increase molecular conjugation, a phenyl group was introduced in third carbon methyl of the 3-Methyl-7-hydrazone azacoumarin, which resulted in 3-Phenyl-7-hydrazone azacoumarin with a higher red shift on the absorption and emission spectra. However, a blue shift was also observed in absorption spectra. Addition of phenyl group may break the conjugation

and cause an increase in the band gap between the HOMO and LUMO which is demonstrated by Outlaw as protonation of 6-Amino-8-cyanobenzo[1, 2-b]indolizines to be a new class of photoluminescent [181]. Imines exhibit two major peaks in the absorption spectrum because of $\pi \rightarrow \pi^*$ and $n \rightarrow \pi^*$ transitions. Imine formations reversible due to transfer of the phenolic proton to the imino nitrogen with formation of the corresponding *o*-quinoid forms [182]. Neither 3-Methyl-7-amino azacoumarin nor 3-Phenyl-7-amino azacoumarin were applicable probes for labeling of live cells due to reversibility of imine reaction. Syntheses of 3-Methyl-7-hydrazine azacoumarin and 3-Phenyl-7-hydrazine azacoumarin were failed due to high reactivity of amino group on azacoumarin scaffold.

During organic syntheses, all reactions were followed by thin layer chromatography (TLC) which provided Rf value for each sample, which was not enough in order to determine the reaction process. For this reason, the reaction confirmations were performed by spectrophotometric and spectrofluorometric analysis and structural conformation of product were demonstrated with NMR spectroscopy. NMR spectra indicated that unexpected peaks belonged to impurities in the products. NMR spectrum of 3-Methyl-7-hydrazine azacoumarin indicated a byproduct formation which was called as 2-Hydrazine-5-nitrophenol. 2-Hydrazine-5-nitrophenol demonstrated high fluorescence quenching ability in methanol and phosphate buffered saline. So, 2-Hydrazine-5-nitrophenol was preferred as a site-specific bioorthogonal probe for carbonylation labeling because of its stability and mild reaction steps.

Imbalance between reactive oxygen species (ROS) and antioxidant metabolism causes oxidative stress in live cells. High level of ROS leads to the oxidation of micro- and macro-biomolecules. Carbonylation of biomolecules is one of the consequences of ROS damage in live cells, which happens with the addition of aldehyde, ketone or lactam moieties giving rise to the lipid peroxidation, glycation and protein carbonylation. These are oxidative stress biomarkers detected with biochemical and analytical techniques. Carbonyl groups on biomolecules are utilized as a chemical reporter for the bioorthogonal labeling. Thereby, this study focused on the site specific labeling of carbonylation via bioorthogonal chemistry with design and synthesis of a fluorescent probe 2-Hydrazine-5-nitrophenol.

Renal cell adenocarcinoma (RCC) is a subtype of kidney cancer. Clear cell renal cell carcinoma (ccRCC) is the most abundant histological subtypes of RCC that accounts 70-75

percent of all histological subtypes of RCC [183]. Genetic characterization of 90 per cent of ccRCC indicates a defection in the short arm of the third chromosome [184], which comprises a tumor suppressor gene called Von Hippel-Lindau (VHL). Mutated VHL gene was observed in 60 per cent of the ccRCC [185].

Hypoxia induced factor (HIF) is a heterodimeric transcription factor consisting of an alpha subunit (HIF-1α) and a beta subunit (HIF-β). HIF-1α subunit is substrate of proline and asparagine hydroxylases. Under normoxic conditions, Pro^{402} and Pro^{564} of HIF-1α subunit is hydroxylated by prolyl hydroxylases (PHD) in the presence of molecular oxygen, ferrous iron (Fe^{2+}) and 2-oxoglutarate. Hydroxylated HIF-1α becomes the target of E3 ubiquitin ligase which is also called VHL protein (pVHL) [186]. pVHL is responsible for the regulation of HIF-1α via ubiquitin-mediated degradation by 26S proteasome [187].

Under hypoxic conditions, mitochondrial ROS generation is induced by the electron transport chain at complexes I, II, and III. Whereas, complexes I and II are responsible for producing ROS only into the mitochondrial matrix, complex III produces ROS on both sides of the mitochondrial inner membrane, this process is called as Q-cycle. During hypoxia, increased mitochondrial ROS generation inhibits the activity of PHDs and accumulated HIF-1α translocates to the nucleus, where it binds to HIF-β to induce the expression of hypoxia-response elements (HRE) such as platelet-derived growth factor (PDGF), vascular endothelial growth factor (VEGF), hepatocyte growth factor receptor (c-MET), transforming growth factor alpha (TGF-a), glucose transporters (e.g. GLUT-1), epidermal growth factor receptor (EGFR), and other receptors involved in energy and iron metabolism [188].

Binding between growth factors such as VEGF and PDGF to their receptor tyrosine kinases activates PI3K/AKT/mTOR pathway, one of the main intracellular signal transduction pathways coordinating cell survival, proliferation, angiogenesis, and migration [189]. PIP3 (phosphatidylinositol-3,4,5-triphosphate) is produced by the phosphorylation of PIP2 (phosphatidylinositol-4,5-biphosphate) via PI3K. PIP3 promotes the translocation of AKT from cytoplasm kinase the cell membrane, where it is activated through phosphorylation by PDK1 and mTOR. Phosphorylated and activated AKT inactivates proapoptotic proteins through phosphorylation, which results in the inhibition of apoptosis [190]. VEGF and PDGF signaling through AKT activates mTOR (rapamycin) pathway. mTOR is consist of two different complexes. First of them is rapamycin sensitive TORC1 regulating protein

synthesis and cell cycle, the second complex is rapamycin insensitive TORC2 coordinating cell polarity and dynamic remodeling through actin cytoskeleton. The TORC2 complex of mTOR induces AKT activation via phosphorylation [191].

In order to clarify relative contribution of oxidative stress and cancerogenesis, A498 and ACHN cell lines were examined in this study. A498 primary site is a VHL mutated while ACHN metastatic site is a VHL wildtype cell model of ccRCC. Although ACHN cell line is a histologically subtype of ccRCC, its genetic composition harbors deficiency in proto-oncogene c-MET (mesenchymal-epithelial transition factor) seen in the type 1 papillary RCC [192].

The proto-oncogene MET is located on human chromosome 7, the gene encodes hepatocyte growth factor (HGF)-specific cell surface tyrosine kinase. MET deficiency is observed as trisomy 7^{th}, 16^{th}, and 17^{th} chromosome [193], or overexpression of MET gene. HGF/MET pathway drives tumorigenesis signaling. Overexpression of c-MET was accompanying with increased metastatic potential and poor prognosis in RCC [194]. c-MET expression is upregulated with hypoxic conditions. Hypoxia-induced overexpression of c-MET increases the HGF sensitivity which induces cell motility and invasion [195]. Phosphorylated MET activation is suppressed by wild-type VHL gene. VHL mutation induces phosphorylation of MET protein and triggers the cell growth freed from the contact inhibition [196].

In recent studies, Mukherjee *et al*. and Vemula *et al*. demonstrated that coumarin based hydrazine labeling of H_2O_2 and serum starvation induced carbonylation in live cells [62, 167]. In our study, 2-Hydrazine-5-nitrophenol was used to detect H_2O_2 induced carbonylation and serum starvation induced carbonylation in live cells. Cytotoxicity assay of H_2O_2 on A498, ACHN and HDF cell lines demonstrated that the A498 primary site ccRCC cell line could tolerate higher concentrations of H_2O_2 compared to the ACHN metastatic site ccRCC cell line. Since A498 cell line has mutated VHL gene these cells have HIF-1α accumulation., which would lead to the activation of PI3 Kinase/Akt and mTOR pathways resulting in enhanced cell survival against H_2O_2 treatment [197]. On the other hand, HDF cells endured higher concentrations of H_2O_2 when compared to the cancer cell lines. This observation may be due to entrance of HDF into the transition shock state. Shock state is defined as increase in BCL-2 levels that causes a delay apoptosis to provide enough time for reversal of cell damage [198].

Healthy and cancer cells present principal differences in their carbonylation responses to oxidative stress. In redox homeostasis, healthy cells maintain a low level of ROS production and possess antioxidant defenses which are enough to prevent the oxidative damage. Under oxidative stress conditions, detoxification process is triggered in order to prevent oxidative damage in healthy cells by neutralizing the high level of ROS. Whereas, cancer cells are continuously exposed to the elevated levels of oxidative stress, which cause the steady-state upregulation of antioxidant defense in order to prevent ROS induced apoptosis [199].

In order to label carbonylation of biomolecules, non-toxic dose of 2Hzin5np was used to treat A498, ACHN and HDF cells. Cytotoxicity assay of 2-Hydrazine-5-nitrophenol on these cells demonstrated that the proliferation was inhibited by the increased concentration of 2Hzin5np. This finding was inconsistent with findings of the past study by Mukherjee *et al*., which demonstrated non-cytotoxic effect of benzocoumarin hydrazine on PC3 and A549 cell lines [163].

Sodium pyruvate is a natural scavenger which reacts with H_2O_2 to yield sodium acetate, carbon dioxide and water as byproducts [200]. Physiological concentrations of sodium pyruvate, present in cell culture medium also in serum, could alter the effective lifetime of exogenously added hydrogen peroxide and inhibits both oxidative stress damage and H_2O_2-induced carbonylation of biomolecules. In order to observe maximum fluorescence intensity of carbonylation level in live cells, cells were incubated with pyruvate free FBS containing DMEM. The result is consistent with the findings of past study by Salahudeen *et al.* The author examined pyruvate protection of H_2O_2 induced damages in renal tissue *in vivo* and *in vitro* [176]. Our quantitative analyses revealed that A498 primary site ccRCC demonstrated a higher level of H_2O_2 induced carbonylated protein when compared to ACHN and HDF. As mentioned above, this could be due to the VHL mutation resulting in accumulated HIF1α which transcriptionally upregulates glucose transporters GLUT1-GLUT4 [201]. GLUT-mediated glucose influx stimulates oxidative stress via disruption of cellular energy homeostasis and redox status [202].

Recently Aryal *et al.* (2018) demonstrated the difference in the carbonylation levels of HSP90β, filamin A and bifunctional glutamate/proline-tRNA ligase proteins by comparing the molecular weight alteration in these proteins isolated from the breast tumor tissues and healthy MCF12A breast epithelial cell line. The researcher confirmed greater protein

carbonylation level in the tumor tissue compared to the healthy cells [203]. In consistent with the afore mentioned study H_2O_2 treated healthy HDF cells demonstrated a dramatic increase in the carbonylation level due to imbalanced redox hemostasis.

Serum starvation induces endogenous ROS generation in live cells. In 2011, Kuznetsov *et al.* reported that serum starvation caused up to a 3.5 -fold increase in ROS generation in 32D myeloid cells, NIH3T3 mouse embryonic fibroblast cells and for HL-1 cardiac muscle cells [204]. Likewise, in our study, serum starvation led to an increased protein carbonylation levels in A-498 and albeit with higher levels in ACHN. This difference can be explained by the overexpression of MET gene in ACHN metastatic site ccRCC [205]. Overexpressed c-Met mediates PI3K/Akt activation which is involved in endogenous ROS generation and oxidative stress[206]. Activation of PI3K/Akt pathway stimulates expression of the redox-sensitive transcription factor nuclear factor-κB (NF-κB), which regulates antiapoptotic target genes [207]. Activated PI3K/Akt signaling through overexpression of c-met leads to higher oxidative stress in ACHN metastatic site when compared to c-MET wild-type primary site ccRCC.

Carbonylation is an irreversible post-translational modification that causes formation of misfolded proteins in the cytosol. High level of carbonyl moiety on proteins increase protein aggregation due to increased hydrophobicity at target proteins [208]. The confocal microscopy provided the evidence of carbonylated protein aggregation via dot-like fluorescence responses on the images (Section 4.2.4).

In summary, together with the results presented in this thesis, it was strongly proposed that 2-Hydrazine-5-nitrophenol was a carbonyl moiety specific bioorthogonal probe which is applicable for fluorescent labeling and detection of ROS induced carbonylation in live cells. Analysis of the computed results showed that oxidative damage caused by H_2O_2 treatment on VHL mutated A498 primary site ccRCC demonstrated a higher level of protein carbonylation. While, the serum starvation induced endogenously ROS generation promoted a higher level of protein carbonylation c-MET mutated ACHN metastatic site ccRCC.

6. CONCLUSION AND FUTURE PERSPECTIVE

Carbonylation is a biomarker of oxidative stress in live cells from neurogenerative diseases and cancer. Determination of carbonylation level may provide information about cancer staging. Bioorthogonal chemistry is a novel approach to determine the level of carbonylation via click reaction which gives quantitative and qualitative measurements.

2-Amino-5-nitrophenol is reduced to 2-Hydrazine-5-nitrophenol which reaction is called diazotization. 2Hzin5np is specific for carbonyl groups on aldehydes, ketones and lactams. In this study, 2Hzin5np was used a site-specific fluorescent probe for detection of oxidative stress induced carbonylation in ACHN, A498 and HDF cells. Primary site and metastatic site of RCC demonstrated different carbonylation responses due to exogenous or endogenous variability in ROS generation.

This site-specific bioorthogonal labeling may be announced as a potentially useful strategy that can be used as small molecule-based diagnostics for the molecular detection of oxidative damaged processes in biological systems. In future investigations, it might be possible to synthase and design bioorthogonal near-infrared fluorescent probes. It is therefore important that future probes should be have the specificity to define cancer aggressiveness and/or oxidative stress induced carbonylation of biomolecules *in vitro* and *in vivo.* Bioorthogonal labeling of carbonylation would allow us to determine the dynamics of oxidative stress induced carbonylation which have vital roles in diagnosis and determination of therapeutic targets for cancer staging.

REFERENCES

1. Zheng M, Zheng L, Zhang P, Li J, Zhang Y. Development of bioorthogonal reactions and their applications in bioconjugation. *Molecules*. 2015;20(2):3190-205.

2. Patterson DM, Nazarova LA, Prescher JA. Finding the right (bioorthogonal) chemistry. *ACS Chemical Biology*. 2014;9(3):592-605.

3. Ramil CP, Lin Q. Bioorthogonal chemistry: strategies and recent developments. *Chemical Communications*. 2013;49(94):11007-22.

4. Horisawa K. Specific and quantitative labeling of biomolecules using click chemistry. *Frontiers in Physiology*. 2014;5:457-462

5. Shieh P, Bertozzi CR. Design strategies for bioorthogonal smart probes. *Organic & Biomolecular Chemistry*. 2014;12(46):9307-20.

6. Sletten EM, Bertozzi CR. Bioorthogonal chemistry: fishing for selectivity in a sea of functionality. *Angewandte Chemie (International ed in English)*. 2009;48(38):6974-98.

7. Moses JE, Moorhouse AD. The growing applications of click chemistry. Chemical Society Reviews. 2007;36:1249-1262.

8. Huisgen R. 1,3- Dipolar cycloadditions. Past and future. *Angewandte Chemie International Edition in English*. 1963;2(10):565-98.

9. McKay CS, Finn MG. Click chemistry in complex mixtures: Bioorthogonal bioconjugation. *Chemistry & Biology*. 2014;21(9):1075-101.

10. Baskin JM, Bertozzi CR. Bioorthogonal click chemistry: covalent labeling in living systems. *QSAR & Combinatorial Science*. 2007;26(11- 12):1211-9.

11. Rostovtsev VV, Green LG, Fokin VV, Sharpless KB. A stepwise huisgen cycloaddition process: copper(I)-catalyzed regioselective "ligation" of azides and terminal alkynes. *Angewandte Chemie (International ed in English).* 2002;41(14):2596-9.

12. Tornoe CW, Christensen C, Meldal M. Peptidotriazoles on solid phase: [1,2,3]-triazoles by regiospecific copper(i)-catalyzed 1,3-dipolar cycloadditions of terminal alkynes to azides. *The Journal of Organic Chemistry*. 2002;67(9):3057-64.

13. Kolb HC, Sharpless KB. The growing impact of click chemistry on drug discovery. *Drug Discovery Today*. 2003;8(24):1128-37.

14. Himo F, Lovell T, Hilgraf R, Rostovtsev VV, Noodleman L, Sharpless KB, et al. Copper(I)-catalyzed synthesis of azoles. dft study predicts unprecedented reactivity and intermediates. *Journal of the American Chemical Society*. 2005;127(1):210-6.

15. Lang K, Chin JW. Cellular incorporation of unnatural amino acids and bioorthogonal labeling of proteins. *Chemical Reviews*. 2014;114(9):4764-806.

16. Hong V, Steinmetz NF, Manchester M, Finn MG. Labeling live cells by copper-catalyzed alkyne--azide click chemistry. *Bioconjugate Chemistry*. 2010;21(10):1912-6.

17. Soriano Del Amo D, Wang W, Jiang H, Besanceney C, Yan AC, Levy M, et al. Biocompatible copper(I) catalysts for in vivo imaging of glycans. *Journal of the American Chemical Society*. 2010;132(47):16893-9.

18. Kennedy DC, McKay CS, Legault MC, Danielson DC, Blake JA, Pegoraro AF, et al. Cellular consequences of copper complexes used to catalyze bioorthogonal click reactions. *Journal of the American Chemical Society*. 2011;133(44):17993-8001.

19. Brotherton WS, Michaels HA, Simmons JT, Clark RJ, Dalal NS, Zhu L. Apparent copper(II)-accelerated azide-alkyne cycloaddition. *Organic Letters*. 2009;11(21):4954-7.

20. Uttamapinant C, Tangpeerachaikul A, Grecian S, Clarke S, Singh U, Slade P, et al. Fast, cell-compatible click chemistry with copper-chelating azides for biomolecular labeling. *Angewandte Chemie (International ed in English)*. 2012;51(24):5852-6.

21. Agard NJ, Prescher JA, Bertozzi CR. A strain-promoted [3 + 2] azide-alkyne cycloaddition for covalent modification of biomolecules in living systems. *Journal of the American Chemical Society*. 2004;126(46):15046-7.

22. Codelli JA, Baskin JM, Agard NJ, Bertozzi CR. Second-generation difluorinated cyclooctynes for copper-free click chemistry. *Journal of the American Chemical Society*. 2008;130(34):11486-93.

23. Sivakumar K, Xie F, Cash BM, Long S, Barnhill HN, Wang Q. A Fluorogenic 1,3-dipolar cycloaddition reaction of 3-azidocoumarins and acetylenes. *Organic Letters*. 2004;6(24):4603-6.

24. Beatty KE, Liu JC, Xie F, Dieterich DC, Schuman EM, Wang Q, et al. Fluorescence visualization of newly synthesized proteins in mammalian cells. *Angewandte Chemie (International ed in English)*. 2006;45(44):7364-7.

25. Bharathi MV, Chhabra M, Paira P. Development of surface immobilized 3-azidocoumarin-based fluorogenic probe via strain promoted click chemistry. *Bioorganic & medicinal chemistry Letters*. 2015;25(24):5737-42.

26. Rong L, Zhang C, Lei Q, Qin SY, Feng J, Zhang XZ. A two- photon excitation based fluorogenic probe for sialome imaging in living systems. *Advanced Science*. 2016;3(1):1500211.

27. Horner A, Volz D, Hagendorn T, Furniss D, Greb L, Ronicke F, et al. Switchable fluorescence by click reaction of a novel azidocarbazole dye. *RSC Advances*. 2014;4(23):11528-34.

28. Herner A, Nikic I, Kallay M, Lemke EA, Kele P. A new family of bioorthogonally applicable fluorogenic labels. *Organic & Biomolecular Chemistry*. 2013;11(20):3297-306.

29. Albrecht M, Lippach A, Exner MP, Jerbi J, Springborg M, Budisa N, et al. Site-specific conjugation of 8-ethynyl-BODIPY to a protein by [2 + 3] cycloaddition. *Organic & Biomolecular Chemistry*. 2015;13(24):6728-36.

30. Sustmann R, Huisgen R, Huber H. 1.3- Dipolare Cycloadditionen, XXX. substituenteneffekte in den kernresonanzspektren von 1.3- Diphenyl- Δ2- pyrazolinen und 3- Phenyl- Δ2- isoxazolinen. *Chemische Berichte*. 1967;100(6):1802-13.

31. Lim RKV, Lin Q. Azirine ligation: fast and selective protein conjugation via photoinduced azirine-alkene cycloaddition. *Chemical Communications*. 2010;46(42):7993-5.

32. An P, Yu Z, Lin Q. Design of oligothiophene-based tetrazoles for laser-triggered photoclick chemistry in living cells. *Chemical Communications*. 2013;49(85):9920-2.

33. Yu Z, Ohulchanskyy TY, An P, Prasad PN, Lin Q. Fluorogenic, two-photon-triggered photoclick chemistry in live mammalian cells. *Journal of the American Chemical Society*. 2013;135(45):16766-9.

34. Blackman ML, Royzen M, Fox JM. Tetrazine ligation: fast bioconjugation based on inverse-electron-demand diels−alder reactivity. *Journal of the American Chemical Society*. 2008;130(41):13518-9.

35. Devaraj NK, Upadhyay R, Haun JB, Hilderbrand SA, Weissleder R. Fast and sensitive pretargeted labeling of cancer cells via tetrazine/trans-cyclooctene cycloaddition. *Angewandte Chemie (International ed in English)*. 2009;48(38):7013-6.

36. Karver MR, Weissleder R, Hilderbrand SA. Synthesis and evaluation of a series of 1,2,4,5-tetrazines for bioorthogonal conjugation. *Bioconjugate Chemistry*. 2011;22(11):2263-70.

37. Yang J, Šečkutė J, Cole CM, and Devaraj NK. Live- cell imaging of cyclopropene tags with fluorogenic tetrazine cycloadditions. *Angewandte Chemie*. 2012;124(30): 7476-7479.

38. Patterson DM, Nazarova LA, Xie B, Kamber DN, Prescher JA. Functionalized cyclopropenes as bioorthogonal chemical reporters. *Journal of the American Chemical Society*. 2012;134(45):18638-43.

39. Sachdeva A, Wang K, Elliott T, Chin JW. Concerted, rapid, quantitative, and site-specific dual labeling of proteins. *Journal of the American Chemical Society*. 2014;136(22):7785-8.

40. Eggert F, Kath-Schorr S. A cyclopropene-modified nucleotide for site-specific RNA labeling using genetic alphabet expansion transcription. *Chemical Communications*. 2016;52(45):7284-7.

41. Spate AK, Schart VF, Schollkopf S, Niederwieser A, Wittmann V. Terminal alkenes as versatile chemical reporter groups for metabolic oligosaccharide engineering. *Chemistry*. 2014;20(50):16502-8.

42. Staudinger H, Meyer J. Über neue organische phosphorverbindungen III. phosphinmethylenderivate und phosphinimine. *Helvetica Chimica Acta*. 1919;2(1):635-646.

43. Lin FL, Hoyt HM, van Halbeek H, Bergman RG, Bertozzi CR. Mechanistic investigation of the staudinger ligation. *Journal of the American Chemical Society*. 2005;127(8):2686-95.

44. Saxon E, Bertozzi CR. Cell surface engineering by a modified Staudinger reaction. *Science (New York, NY)*. 2000;287(5460):2007-10.

45. Saxon E, Armstrong JI, Bertozzi CR. A "Traceless" Staudinger ligation for the chemoselective synthesis of amide bonds. *Organic Letters*. 2000;2(14):2141-3.

46. Nilsson BL, Kiessling LL, Raines RT. Staudinger ligation: a peptide from a thioester and azide. *Organic Letters*. 2000;2(13):1939-41.

47. Qin L-H, Hu W, Long Y-Q. Bioorthogonal chemistry: Optimization and application updates during 2013–2017. *Tetrahedron Letters*. 2018;59(23):2214-28.

48. Lemieux GA, De Graffenried CL, Bertozzi CR. A fluorogenic dye activated by the staudinger ligation. *Journal of the American Chemical Society*. 2003;125(16):4708-9.

49. Hangauer MJ, Bertozzi CR. A FRET-based fluorogenic phosphine for live cell imaging with the Staudinger ligation. *Angewandte Chemie (International ed in English)*. 2008;47(13):2394-7.

50. Plass T, Schultz C. Covalent labeling of biomolecules in living cells. *Advanced fluorescence reporters in chemistry and biology iii: applications in sensing and imaging*. 2011: 225-61.

51. Chen X, Wu Y-W. Selective chemical labeling of proteins. *Organic & Biomolecular Chemistry*. 2016;14(24):5417-39.

52. Lin YA, Chalker JM, Floyd N, Bernardes GJ, Davis BG. Allyl sulfides are privileged substrates in aqueous cross-metathesis: application to site-selective protein modification. *Journal of the American Chemical Society*. 2008;130(30):9642-3.

53. Chalker JM, Wood CS, Davis BG. A convenient catalyst for aqueous and protein Suzuki-Miyaura cross-coupling. *Journal of the American Chemical Society.* 2009;131(45):16346-7.

54. Kodama K, Fukuzawa S, Nakayama H, Kigawa T, Sakamoto K, Yabuki T, et al. Regioselective carbon-carbon bond formation in proteins with palladium catalysis; new protein chemistry by organometallic chemistry. *Chembiochem : A European Journal of Chemical Biology*. 2006;7(1):134-9.

55. Chalker JM, Wood CSC, Davis BG. A convenient catalyst for aqueous and protein suzuki−miyaura cross-coupling. *Journal of the American Chemical Society*. 2009;131(45):16346-7.

56. Kodama K, Fukuzawa S, Nakayama H, Sakamoto K, Kigawa T, Yabuki T, et al. Site-specific functionalization of proteins by organopalladium reactions. *Chembiochem : A European Journal Of Chemical Biology*. 2007;8(2):232-8.

57. Jencks WP. Studies on the mechanism of oxime and semicarbazone formation. *Journal of the American Chemical Society*. 1959;81(2):475-81.

58. Sander EG, Jencks WP. Equilibria for additions to the carbonyl group. *Journal of the American Chemical Society*. 1968;90(22):6154-62.

59. Rideout D. Self-assembling cytotoxins. *Science*. 1986;233(4763):561-3.

60. de Silva AP, Gunaratne HQN, Gunnlaugsson T, Huxley AJM, McCoy CP, Rademacher JT, et al. Signaling recognition events with fluorescent sensors and switches. *Chemical Reviews*. 1997;97(5):1515-66.

61. Dilek O, Bane SL. Synthesis and spectroscopic characterization of fluorescent boron dipyrromethene-derived hydrazones. *Journal of Fluorescence*. 2011;21(1):347-54.

62. Mukherjee K, Chio TI, Sackett DL, Bane SL. Detection of oxidative stress-induced carbonylation in live mammalian cells. *Free Radical Biology & Medicine*. 2015;84:11-21.

63. Zeng Y, Ramya TNC, Dirksen A, Dawson PE, Paulson JC. High efficiency labeling of glycoproteins on living cells. *Nature Methods*. 2009;6(3):207-9.

64. Liu J, Wu S, Li Z. Recent advances in enzymatic oxidation of alcohols. *Current Opinion in Chemical Biology*. 2018;43:77-86.

65. Hermanson GT. The Reactions of bioconjugation. *Bioconjugate techniques*. 2013:229-58.

66. Chen D, Disotuar MM, Xiong X, Wang Y, Chou DH-C. Selective N-terminal functionalization of native peptides and proteins. *Chemical Science*. 2017;8(4):2717-22.

67. Mahal LK, Yarema KJ, Bertozzi CR. Engineering chemical reactivity on cell surfaces through oligosaccharide biosynthesis. *Science*. 1997;276(5315):1125-8.

68. Zhang Z, Smith BAC, Wang L, Brock A, Cho C, Schultz PG. A new strategy for the site-specific modification of proteins in vivo. *Biochemistry*. 2003;42(22):6735-46.

69. Nauman DA, Bertozzi CR. Kinetic parameters for small-molecule drug delivery by covalent cell surface targeting. *Biochimica et Biophysica Acta*. 2001;1568(2):147-54.

70. Anouk D, M. HT, E. DP. Nucleophilic catalysis of oxime ligation. *Angewandte Chemie International Edition*. 2006;45(45):7581-4.

71. Dirksen A, Dirksen S, Hackeng TM, Dawson PE. Nucleophilic catalysis of hydrazone formation and transimination: Implications for dynamic covalent chemistry. *Journal of the American Chemical Society*. 2006;128(49):15602-3.

72. Dirksen A, Dawson PE. Rapid oxime and hydrazone ligations with aromatic aldehydes for biomolecular labeling. *Bioconjugate Chemistry*. 2008;19(12):2543-8.

73. Blanden AR, Mukherjee K, Dilek O, Loew M, Bane SL. 4-aminophenylalanine as a biocompatible nucleophilic catalyst for hydrazone ligations at low temperature and neutral pH. *Bioconjugate Chemistry*. 2011;22(10):1954-61.

74. Rashidian M, Mahmoodi MM, Shah R, Dozier JK, Wagner CR, Distefano MD. A highly efficient catalyst for oxime ligation and hydrazone–oxime exchange suitable for bioconjugation. *Bioconjugate Chemistry*. 2013;24(3):333-42.

75. Agarwal P, van der Weijden J, Sletten EM, Rabuka D, Bertozzi CR. A Pictet-Spengler ligation for protein chemical modification. *Proceedings of the National Academy of Sciences of the United States of America*. 2013;110(1):46-51.

76. Albers AE, Garofalo AW, Drake PM, Kudirka R, de Hart GW, Barfield RM, et al. Exploring the effects of linker composition on site-specifically modified antibody-drug conjugates. *European Journal of Medicinal Chemistry*. 2014;88:3-9.

77. Link AJ, Mock ML, Tirrell DA. Non-canonical amino acids in protein engineering. *Current Opinion in Biotechnology*. 2003;14(6):603-9.

78. Kiick KL, Saxon E, Tirrell DA, Bertozzi CR. Incorporation of azides into recombinant proteins for chemoselective modification by the Staudinger ligation. *Proceedings of the National Academy of Sciences of the United States of America*. 2002;99(1):19-24.

79. Kent K, S. CI, A. TD. Biosynthesis of proteins incorporating a versatile set of phenylalanine analogues. *Chembiochem: a European Journal of Chemical Biology*. 2002;3(2- 3):235-7.

80. Prescher JA, Bertozzi CR. Chemistry in living systems. *Nature Chemical Biology*. 2005;1:13.

81. Johnson JA, Lu YY, Van Deventer JA, Tirrell DA. Residue-specific incorporation of non-canonical amino acids into proteins: recent developments and applications. *Current Opinion in Chemical Biology*. 2010;14(6):774-80.

82. Wang L, Schultz PG. Expanding the genetic code. *Angewandte Chemie (International ed in English)*. 2004;44(1):34-66.

83. Kipper K, Lundius EG, Curic V, Nikic I, Wiessler M, Lemke EA, et al. Application of noncanonical amino acids for protein labeling in a genomically recoded escherichia coli. *ACS synthetic Biology*. 2017;6(2):233-55.

84. Praveschotinunt P, Dorval Courchesne N-M, den Hartog I, Lu C, Kim JJ, Nguyen PQ, et al. Tracking of engineered bacteria in vivo using nonstandard amino acid incorporation. *ACS Synthetic Biology*. 2018;7(6):1640-50.

85. Li N, Ramil CP, Lim RK, Lin Q. A genetically encoded alkyne directs palladium-mediated protein labeling on live mammalian cell surface. *ACS Chemical Biology*. 2015;10(2):379-84.

86. Shang X, Song X, Faller C, Lai R, Li H, Cerny R, et al. Fluorogenic protein labeling using a genetically encoded unstrained alkene. *Chemical Science*. 2017;8(2):1141-5.

87. Ellman J, Mendel D, Anthony-Cahill S, Noren CJ, Schultz PG. Biosynthetic method for introducing unnatural amino acids site-specifically into proteins. *Methods in Enzymology*. 1991;202:301-36.

88. Yin J, Liu F, Li X, Walsh CT. Labeling proteins with small molecules by site-specific posttranslational modification. *Journal of the American Chemical Society*. 2004;126(25):7754-5.

89. Chen I, Howarth M, Lin W, Ting AY. Site-specific labeling of cell surface proteins with biophysical probes using biotin ligase. *Nature Methods*. 2005;2(2):99-104.

90. Banerjee A, Panosian TD, Mukherjee K, Ravindra R, Gal S, Sackett DL, et al. Site-Specific orthogonal labeling of the carboxy terminus of α-tubulin. *ACS Chemical Biology*. 2010;5(8):777-85.

91. Haltiwanger RS, Lowe JB. Role of glycosylation in development. *Annual Review of Biochemistry*. 2004;73:491-537.

92. Varki A. Biological roles of glycans. *Glycobiology*. 2017;27(1):3-49.

93. Dube DH, Bertozzi CR. Glycans in cancer and inflammation--potential for therapeutics and diagnostics. *Nature Reviews Drug Discovery*. 2005;4(6):477-88.

94. Palaniappan KK, Bertozzi CR. Chemical glycoproteomics. *Chemical Reviews*. 2016;116(23):14277-306.

95. Yoon HY, Koo H, Kim K, Kwon IC. Molecular imaging based on metabolic glycoengineering and bioorthogonal click chemistry. *Biomaterials*. 2017;132:28-36.

96. Prescher JA, Dube DH, Bertozzi CR. Chemical remodelling of cell surfaces in living animals. *Nature*. 2004;430(7002):873-7.

97. Salic A, Mitchison TJ. A chemical method for fast and sensitive detection of DNA synthesis in vivo. *Proceedings of the National Academy of Sciences of the United States of America*. 2008;105(7):2415-20.

98. George JT, Srivatsan SG. Posttranscriptional chemical labeling of RNA by using bioorthogonal chemistry. *Methods*. 2017;120:28-38.

99. Thirumurugan P, Matosiuk D, Jozwiak K. Click chemistry for drug development and diverse chemical-biology applications. *Chemical Reviews*. 2013;113(7):4905-79.

100. Resh MD. Trafficking and signaling by fatty-acylated and prenylated proteins. *Nature Chemical Biology*. 2006;2(11):584-90.

101. Hang HC, Geutjes EJ, Grotenbreg G, Pollington AM, Bijlmakers MJ, Ploegh HL. Chemical probes for the rapid detection of fatty-acylated proteins in Mammalian cells. *Journal of the American Chemical Society*. 2007;129(10):2744-5.

102. Neef AB, Schultz C. Selective fluorescence labeling of lipids in living cells. *Angewandte Chemie International Edition*. 2009;48(8):1498-500.

103. Gopalan, B. and Balasubramanian, K. K. Applications of click chemistry in drug discovery and development. *Click Reactions in Organic Synthesis.* 2016: 25-76.

104. Thirumurugan P, Matosiuk D, Jozwiak K. Click chemistry for drug development and diverse chemical–biology applications. *Chemical Reviews*. 2013;113(7):4905-79.

105. de Kloe GE, Bailey D, Leurs R, de Esch IJP. Transforming fragments into candidates: small becomes big in medicinal chemistry. *Drug Discovery Today*. 2009;14(13):630-46.

106. Schmidt MF, Rademann J. Dynamic template-assisted strategies in fragment-based drug discovery. *Trends in Biotechnology*. 2009;27(9):512-21.

107. Meghani NM, Amin HH, Lee BJ. Mechanistic applications of click chemistry for pharmaceutical drug discovery and drug delivery. *Drug Discovery Today*. 2017;22(11):1604-19.

108. Fili N, Toseland CP. Fluorescence and labelling: how to choose and what to do. *Exs*. 2014;105:1-24.

109. Toseland CP. Fluorescent labeling and modification of proteins. *Journal of Chemical Biology*. 2013;6(3):85-95.

110. Shanker N, Bane SL. Basic aspects of absorption and fluorescence spectroscopy and resonance energy transfer methods. *Methods in Cell Biology*. 2008;84:213-42.

111. Lukinavičius G, Umezawa K, Olivier N, Honigmann A, Yang G, Plass T, et al. A near-infrared fluorophore for live-cell super-resolution microscopy of cellular proteins. *Nature Chemistry*. 2013;5(2):132-9.

112. Kiley PJ, Storz G. Exploiting thiol modifications. *PLOS Biology*. 2004;2(11):e400.

113. Finkel T. Signal transduction by reactive oxygen species. *The Journal of Cell Biology*. 2011;194(1):7-15.

114. Dickinson BC, Chang CJ. Chemistry and biology of reactive oxygen species in signaling or stress responses. *Nature Chemical Biology*. 2011;7(8):504-11.

115. Sabharwal SS, Schumacker PT. Mitochondrial ROS in cancer: initiators, amplifiers or an Achilles' heel? *Nature Reviews Cancer*. 2014;14(11):709-21.

116. Halliwell B, Gutteridge JM. Role of free radicals and catalytic metal ions in human disease: an overview. *Methods in Enzymology*. 1990;186:1-85.

117. Bedard K, Krause K-H. The NOX family of ROS-generating nadph oxidases: physiology and pathophysiology. *Physiological Reviews*. 2007;87(1):245-313.

118. Brand MD. Mitochondrial generation of superoxide and hydrogen peroxide as the source of mitochondrial redox signaling. *Free Radical Biology and Medicine*. 2016;100:14-31.

119. Cairns RA, Harris IS, Mak TW. Regulation of cancer cell metabolism. *Nature Reviews Cancer*. 2011;11(2):85-95.

120. Schieber M, Chandel NS. ROS function in redox signaling and oxidative stress. *Current biology : CB*. 2014;24(10):R453-R62.

121. Brunet A, Bonni A, Zigmond MJ, Lin MZ, Juo P, Hu LS, et al. Akt promotes cell survival by phosphorylating and inhibiting a Forkhead transcription factor. *Cell*. 1999;96(6):857-68.

122. Gao P, Zhang H, Dinavahi R, Li F, Xiang Y, Raman V, et al. HIF-dependent antitumorigenic effect of antioxidants in vivo. *Cancer Cell*. 2007;12(3):230-8.

123. Reddy KB, Glaros S. Inhibition of the MAP kinase activity suppresses estrogen-induced breast tumor growth both in vitro and in vivo. *International Journal of Oncology*. 2007;30(4):971-5.

124. Mazzio EA, Soliman KF. Glioma cell antioxidant capacity relative to reactive oxygen species produced by dopamine. *Journal of Applied Toxicology : JAT*. 2004;24(2):99-106.

125. Dikalov SI, Harrison DG. Methods for detection of mitochondrial and cellular reactive oxygen species. *Antioxidants & Redox Signaling*. 2014;20(2):372-82.

126. Finkelstein E, Rosen GM, Rauckman EJ. Spin trapping of superoxide and hydroxyl radical: Practical aspects. *Archives of Biochemistry and Biophysics*. 1980;200(1):1-16.

127. Yasui H, Sakurai H. Chemiluminescent detection and imaging of reactive oxygen species in live mouse skin exposed to UVA. *Biochemical and Biophysical Research Communications*. 2000;269(1):131-6.

128. Xiqian J, Lingfei W, L. CS, Jianwei C, C. WM, Jin W. Challenges and opportunities for small-molecule fluorescent probes in redox biology applications. *Antioxidants & Redox Signaling*. 2018;29(6):518-540.

129. Hempel SL, Buettner GR, O'Malley YQ, Wessels DA, Flaherty DM. Dihydrofluorescein diacetate is superior for detecting intracellular oxidants: comparison with 2',7'-dichlorodihydrofluorescein diacetate, 5(and 6)-carboxy-2',7'-

dichlorodihydrofluorescein diacetate, and dihydrorhodamine 123. *Free Radical Biology & Medicine*. 1999;27(1-2):146-59.

130. Zhao H, Kalivendi S, Zhang H, Joseph J, Nithipatikom K, Vasquez-Vivar J, et al. Superoxide reacts with hydroethidine but forms a fluorescent product that is distinctly different from ethidium: potential implications in intracellular fluorescence detection of superoxide. *Free Radical Biology & Medicine*. 2003;34(11):1359-68.

131. Gill JG, Piskounova E, Morrison SJ. Cancer, oxidative stress, and metastasis. *Cold Spring Harbor Symposia on Quantitative Biology*. 2017:81:163-175

132. Kim GH, Kim JE, Rhie SJ, Yoon S. The role of oxidative stress in neurodegenerative diseases. *Experimental Neurobiology*. 2015;24(4):325-40.

133. Schaich KM, Shahidi F, Zhong Y, Eskin NAM. Chapter 11 - Lipid oxidation. *Biochemistry of foods.*; 2013:419-78.

134. Khoubnasab Jafari M, Ansarin K, Jouyban A. Comments on "Use of malondialdehyde as a biomarker for assesing oxidative stress in different disease pathologies: a review". *Iranian Journal of Public Health*. 2015;44(5):714-5.

135. Bono R, Romanazzi V. Isoprostanes as biomarkers of disease and early biological effect. *General methods in biomarker research and their applications*. 2015:383-404.

136. Poli G, Biasi F, Leonarduzzi G. 4-Hydroxynonenal-protein adducts: A reliable biomarker of lipid oxidation in liver diseases. *Molecular Aspects of Medicine*. 2008;29(1-2):67-71.

137. Sultana R, Cenini G, Butterfield DA. Biomarkers of oxidative stress in neurodegenerative diseases. *Molecular basis of oxidative stress*. 2013:359-76.

138. Young IS, McEneny J. Lipoprotein oxidation and atherosclerosis. *Biochemical Society Transactions*. 2001;29(2):358-62.

139. Poulsen HE, Prieme H, Loft S. Role of oxidative DNA damage in cancer initiation and promotion. *European Journal of Cancer Prevention (ECP)*. 1998;7(1):9-16.

140. Schulz WA, Obendorf MS, Sies H. Localization of strand breaks in plasmid DNA treated with reactive oxygen species. *Methods in Enzymology*. 1994;234:45-51.

141. Ames BN. Endogenous oxidative DNA damage, aging, and cancer. *Free Radical Research Communications*. 1989;7(3-6):121-8.

142. Steenken S, Jovanovic SV. How easily oxidizable is DNA? One-electron reduction potentials of adenosine and guanosine radicals in aqueous solution. *Journal of the American Chemical Society*. 1997;119(3):617-8.

143. Helbock HJ, Beckman KB, Ames BN. 8-Hydroxydeoxyguanosine and 8-hydroxyguanine as biomarkers of oxidative DNA damage. *Methods in Enzymology*. 1999;300:156-66.

144. Aust AE, Eveleigh JF. Mechanisms of DNA oxidation. *Proceedings of the Society for Experimental Biology and Medicine Society for Experimental Biology and Medicine*. 1999;222(3):246-52.

145. Markkanen E. Not breathing is not an option: How to deal with oxidative DNA damage. *DNA Repair*. 2017;59:82-105.

146. Bonnefont-Rousselot D. Glucose and reactive oxygen species. *Current Opinion in Clinical Nutrition and Metabolic Care*. 2002;5(5):561-8.

147. Garcia-Garcia A, Rodriguez-Rocha H, Madayiputhiya N, Pappa A, Panayiotidis MI, Franco R. Biomarkers of protein oxidation in human disease. *Current Molecular Medicine*. 2012;12(6):681-97.

148. Breusing N, Grune T. Biomarkers of protein oxidation from a chemical, biological and medical point of view. *Experimental Gerontology*. 2010;45(10):733-7.

149. Santos AL, Lindner AB. Protein posttranslational modifications: roles in aging and age-related disease. *Oxidative Medicine and Cellular Longevity*. 2017;2017:5716409.

150. Weng S-L, Huang K-Y, Kaunang FJ, Huang C-H, Kao H-J, Chang T-H, et al. Investigation and identification of protein carbonylation sites based on position-specific amino acid composition and physicochemical features. *BMC Bioinformatics*. 2017;18(Suppl 3):66.

151. Dalle-Donne I, Rossi R, Giustarini D, Milzani A, Colombo R. Protein carbonyl groups as biomarkers of oxidative stress. *Clinica Chimica Acta; International Journal of Clinical Chemistry*. 2003;329(1-2):23-38.

152. Suzuki YJ, Carini M, Butterfield DA. Protein carbonylation. *Antioxidants & Redox Signaling*. 2010;12(3):323-5.

153. Wong CM, Bansal G, Marcocci L, Suzuki YJ. Proposed role of primary protein carbonylation in cell signaling. *Redox Report : Communications in Free Radical Research*. 2012;17(2):90-4.

154. Villamena FA. Reactive species in biological systems. *Reactive species detection in biology*. 2017:65-86.

155. Fedorova M, Bollineni RC, Hoffmann R. Protein carbonylation as a major hallmark of oxidative damage: update of analytical strategies. *Mass Spectrometry Reviews*. 2014;33(2):79-97.

156. Madian AG, Regnier, F. E. and Zeng, A. Analysis of protein carbonylation. *Protein carbonylation.* 2017;.

157. Mirzaei H, Regnier F. Protein:protein aggregation induced by protein oxidation. *Journal of Chromatography B: Analytical Technologies in the Biomedical and Life Sciences*. 2008;873(1):8-14.

158. Davies KJ. Degradation of oxidized proteins by the 20S proteasome. *Biochimie*. 2001;83(3-4):301-10.

159. Wong CM, Marcocci L, Liu L, Suzuki YJ. Cell signaling by protein carbonylation and decarbonylation. *Antioxidants & Redox Signaling*. 2010;12(3):393-404.

160. Ngo JK, Davies KJA. Mitochondrial Lon protease is a human stress protein. *Free Radical Biology & Medicine*. 2009;46(8):1042-8.

161. Aldini G, Dalle-Donne I, Facino RM, Milzani A, Carini M. Intervention strategies to inhibit protein carbonylation by lipoxidation-derived reactive carbonyls. *Medicinal Research Reviews*. 2007;27(6):817-68.

162. Shostak A, Gotloib L, Kushnier R, Wajsbrot V. Protective effect of pyruvate upon cultured mesothelial cells exposed to 2 mM hydrogen peroxide. *Nephron*. 2000;84(4):362-6.

163. Mukherjee K, Chio TI, Gu H, Banerjee A, Sorrentino AM, Sackett DL, et al. Benzocoumarin hydrazine: a large stokes shift fluorogenic sensor for detecting carbonyls in isolated biomolecules and in live cells. *ACS Sensors*. 2017;2(1):128-34.

164. Pandey S, Lopez C, Jammu A. Oxidative stress and activation of proteasome protease during serum deprivation-induced apoptosis in rat hepatoma cells; inhibition of cell death by melatonin. *Apoptosis : an International Journal on Programmed Cell Death*. 2003;8(5):497-508.

165. Fedorova M. Diversity of protein carbonylation pathways. *Protein Carbonylation*. 2017:48-82.

166. Villamena FA. Electrochemical, mass spectroscopic, immunochemical, and nuclear magnetic resonance techniques. *Reactive species detection in biology*. 2017:253-322.

167. Vemula V, Ni Z, Fedorova M. Fluorescence labeling of carbonylated lipids and proteins in cells using coumarin-hydrazide. *Redox Biology*. 2015;5:195-204.

168. Sanchez DJ, Celeste Simon M. Genetic and metabolic hallmarks of clear cell renal cell carcinoma. *Biochimica et Biophysica Acta*. 2018: 23-31.

169. Rini BI, Campbell SC, Escudier B. Renal cell carcinoma. *The Lancet*. 2009;373(9669):1119-32.

170. Hunt JD, van der Hel OL, McMillan GP, Boffetta P, Brennan P. Renal cell carcinoma in relation to cigarette smoking: meta-analysis of 24 studies. *International Journal of Cancer*. 2005;114(1):101-8.

171. van Dijk BA, Schouten LJ, Kiemeney LA, Goldbohm RA, van den Brandt PA. Relation of height, body mass, energy intake, and physical activity to risk of renal cell carcinoma: results from the Netherlands Cohort Study. *American Journal of Epidemiology*. 2004;160(12):1159-67.

172. McLaughlin JK, Chow WH, Mandel JS, Mellemgaard A, McCredie M, Lindblad P, et al. International renal-cell cancer study. VIII. Role of diuretics, other anti-hypertensive medications and hypertension. *International Journal of Cancer*. 1995;63(2):216-21.

173. Moffett RB. 2H-1,4-Benzoxazin-2-ones. *Journal of Medicinal Chemistry*. 1966;9(4):475-8.

174. Li L, Han J, Nguyen B, Burgess K. Syntheses and spectral properties of functionalized, water-soluble BODIPY derivatives. *The Journal of Organic Chemistry*. 2008;73(5):1963-70.

175. Portoghese PS, Sultana M, Takemori AE. Design of peptidomimetic .delta. opioid receptor antagonists using the message-address concept. *Journal of Medicinal Chemistry*. 1990;33(6):1714-20.

176. Salahudeen AK, Clark EC, Nath KA. Hydrogen peroxide-induced renal injury. A protective role for pyruvate in vitro and in vivo. *The Journal of Clinical Investigation*. 1991;88(6):1886-93.

177. Kuznetsov AV, Kehrer I, Kozlov AV, Haller M, Redl H, Hermann M, et al. Mitochondrial ROS production under cellular stress: comparison of different detection methods. *Analytical and Bioanalytical Chemistry*. 2011;400(8):2383-90.

178. Alamudi SH, Su D, Lee KJ, Lee JY, Belmonte-Vázquez JL, Park H-S, et al. A palette of background-free tame fluorescent probes for intracellular multi-color labelling in live cells. *Chemical Science*. 2018;9(8):2376-83.

179. Zhu S, Yang Q, Antaris AL, Yue J, Ma Z, Wang H, et al. Molecular imaging of biological systems with a clickable dye in the broad 800- to 1,700-nm near-infrared window. *Proceedings of the National Academy of Sciences of the United States of America*. 2017;114(5):962-7.

180. Karlsson JKG, Harriman A. Origin of the red-shifted optical spectra recorded for Aza-BODIPY dyes. *The Journal of Physical Chemistry A*. 2016;120(16):2537-46.

181. Outlaw VK, Zhou J, Bragg AE, Townsend CA. Unusual blue-shifted acid-responsive photoluminescence behavior in 6-Amino-8-cyanobenzo[1,2-b]indolizines. *RSC Advances*. 2016;6(66):61249-53.

182. Pratt AC. The photochemistry of imines. *Chemical Society Reviews*. 1977;6(1):63-81.

183. Brodaczewska KK, Szczylik C, Fiedorowicz M, Porta C, Czarnecka AM. Choosing the right cell line for renal cell cancer research. *Molecular Cancer*. 2016;15:83.

184. Nickerson ML, Jaeger E, Shi Y, Durocher JA, Mahurkar S, Zaridze D, et al. Improved identification of von Hippel-Lindau gene alterations in clear cell renal tumors. *Clinical Cancer Research : An Official Journal of the American Association for Cancer Research*. 2008;14(15):4726-34.

185. Gnarra JR, Tory K, Weng Y, Schmidt L, Wei MH, Li H, et al. Mutations of the VHL tumour suppressor gene in renal carcinoma. *Nature Genetics*. 1994;7(1):85-90.

186. Taylor Cormac T. Mitochondria and cellular oxygen sensing in the HIF pathway. *Biochemical Journal*. 2008;409(1):19-26.

187. Huang C, Park CC, Hilsenbeck SG, Ward R, Rimawi MF, Wang YC, et al. beta1 integrin mediates an alternative survival pathway in breast cancer cells resistant to lapatinib. *Breast Cancer Research : BCR*. 2011;13(4):R84.

188. Monteiro MS, Carvalho M, de Lourdes Bastos M, de Pinho PG. Biomarkers in renal cell carcinoma: a metabolomics approach. *Metabolomics*. 2014;10(6):1210-22.

189. LoPiccolo J, Blumenthal GM, Bernstein WB, Dennis PA. Targeting the PI3K/Akt/mTOR pathway: effective combinations and clinical considerations. *Drug Resistance Updates : Reviews and Commentaries in Antimicrobial and Anticancer Chemotherapy*. 2008;11(1-2):32-50.

190. Banumathy G, Cairns P. Signaling pathways in renal cell carcinoma. *Cancer Biology & Therapy*. 2010;10(7):658-64.

191. Makhov P, Joshi S, Ghatalia P, Kutikov A, Uzzo RG, Kolenko VM. Resistance to systemic therapies in clear cell renal cell carcinoma: Mechanisms and Management Strategies. *Molecular Cancer Therapeutics*. 2018;17(7):1355-64.

192. Giubellino A, Linehan WM, Bottaro DP. Targeting the Met signaling pathway in renal cancer. *Expert Review of Anticancer Therapy*. 2009;9(6):785-93.

193. Furge KA, Dykema K, Petillo D, Westphal M, Zhang Z, Kort EJ, et al. Combining differential expression, chromosomal and pathway analyses for the molecular characterization of renal cell carcinoma. *Canadian Urological Association Journal*. 2007;1(2 Suppl):S21-S7.

194. Granito A, Guidetti E, Gramantieri L. c-MET receptor tyrosine kinase as a molecular target in advanced hepatocellular carcinoma. *Journal of Hepatocellular Carcinoma*. 2015;2:29-38.

195. Pennacchietti S, Michieli P, Galluzzo M, Mazzone M, Giordano S, Comoglio PM. Hypoxia promotes invasive growth by transcriptional activation of the met protooncogene. *Cancer Cell*. 2003;3(4):347-61.

196. Nakaigawa N, Yao M, Baba M, Kato S, Kishida T, Hattori K, et al. Inactivation of von Hippel-Lindau gene induces constitutive phosphorylation of MET protein in clear cell renal carcinoma. *Cancer Research*. 2006;66(7):3699-705.

197. Hudson CC, Liu M, Chiang GG, Otterness DM, Loomis DC, Kaper F, et al. Regulation of hypoxia-inducible factor 1alpha expression and function by the mammalian target of rapamycin. *Molecular and Cellular Biology*. 2002;22(20):7004-14.

198. Bladier C, Wolvetang E, Hutchinson P, de Haan J, Kola I. Response of a primary human fibroblast cell line to H2O2: senescence-like growth arrest or apoptosis? *Cell Growth Differentiation:* 1997;8(5):589-98.

199. Benfeitas R, Uhlen M, Nielsen J, Mardinoglu A. New challenges to study heterogeneity in cancer redox metabolism. *Frontiers in Cell and Developmental Biology*. 2017;5(65).

200. Giandomenico AR, Cerniglia GE, Biaglow JE, Stevens CW, Koch CJ. The importance of sodium pyruvate in assessing damage produced by hydrogen peroxide. *Free Radical Biology & Medicine*. 1997;23(3):426-34.

201. Srinivasan R, Ricketts CJ, Sourbier C, Linehan WM. New strategies in renal cell carcinoma: targeting the genetic and metabolic basis of disease. *Clinical Cancer Research : An Official Journal of The American Association for Cancer Research*. 2015;21(1):10-7.

202. Liemburg-Apers DC, Willems PH, Koopman WJ, Grefte S. Interactions between mitochondrial reactive oxygen species and cellular glucose metabolism. *Archives of Toxicology*. 2015;89(8):1209-26.

203. Aryal B, Rao VA. Specific protein carbonylation in human breast cancer tissue compared to adjacent healthy epithelial tissue. *PLOS one*. 2018;13(3):e0194164.

204. Kuznetsov AV, Kehrer I, Kozlov AV, Haller M, Redl H, Hermann M, et al. Mitochondrial ROS production under cellular stress: comparison of different detection methods. *Analytical and Bioanalytical Chemistry*. 2011;400(8):2383-90.

205. Schmidt L, Junker K, Nakaigawa N, Kinjerski T, Weirich G, Miller M, et al. Novel mutations of the MET proto-oncogene in papillary renal carcinomas. *Oncogene*. 1999;18:2343.

206. Ozaki M, Haga S, Zhang HQ, Irani K, Suzuki S. Inhibition of hypoxia/reoxygenation-induced oxidative stress in HGF-stimulated antiapoptotic signaling: role of PI3-K and Akt kinase upon rac1. *Cell Death and Differentiation*. 2003;10(5):508-15.

207. Gloire G, Legrand-Poels S, Piette J. NF-κB activation by reactive oxygen species: Fifteen years later. *Biochemical Pharmacology*. 2006;72(11):1493-505.

208. Tanase M, Urbanska AM, Zolla V, Clement CC, Huang L, Morozova K, et al. Role of carbonyl modifications on aging-associated protein aggregation. *Scientific Reports*. 2016;6:19311-19324.